

D-A101 307

RADIATION RESEARCH ASSOCIATES INC FORT WORTH TEX  
E-O SENSOR SIGNAL RECOGNITION SIMULATION: COMPUTER CODE SPOT I. (U)  
OCT 78 C M LAMPLEY, W G BLATTNER

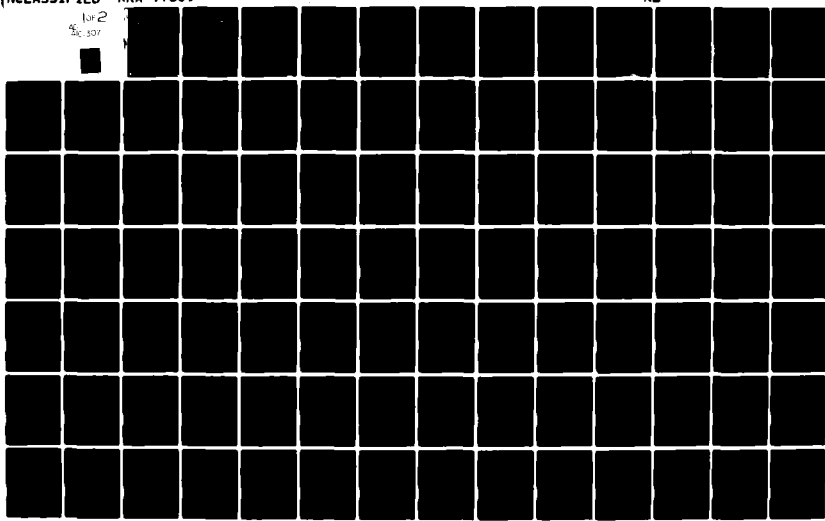
F6 20/6  
F08606-77-C-0008

NL

? (INCLASSIFIED)

RRA-T7809

10P2  
42c 507



RRA-T7809

11  
#

0

**RRA** RADIATION RESEARCH ASSOCIATES

Fort Worth, Texas

AD A101307

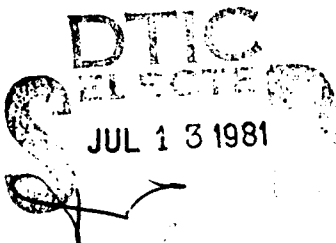
E-O SENSOR SIGNAL RECOGNITION  
SIMULATION: COMPUTER CODE SPOT I

BY  
C. M. LAMPLEY AND W. G. M. BLÄTTNER

CONTRACT No. F08606-77-C-0008  
TASK 4.4.6

FINAL TECHNICAL REPORT

1 OCTOBER 1978



APPROVED FOR PUBLIC RELEASE, DISTRIBUTION UNLIMITED.

FILE COPY

PREPARED FOR  
ATMOSPHERIC SCIENCES LABORATORY (ASL)  
WHITE SANDS MISSILE RANGE, NM 88002

81 7 10 115

Unclassified

SECURITY CLASSIFICATION OF THIS PAGE (When Data Entered)

REPORT DOCUMENTATION PAGE		READ INSTRUCTIONS BEFORE COMPLETING FORM
1. REPORT NUMBER RRA-T7809	2. GOVT ACCESSION NO. AD-A 101307	3. RECIPIENT'S CATALOG NUMBER
4. TITLE (and Subtitle) E-O SENSOR SIGNAL RECOGNITION SIMULATION: COMPUTER CODE SPOT I		5. TYPE OF REPORT & PERIOD COVERED FINAL 14 March 1978 - 30 Sept 1978
7. AUTHOR(s) C. M. Lampley and W. G. M. Blättner		6. PERFORMING ORG. REPORT NUMBER [REDACTED]
9. PERFORMING ORGANIZATION NAME AND ADDRESS Radiation Research Associates, Inc. 3550 Hulen Street Fort Worth, Texas 76107		10. PROGRAM ELEMENT, PROJECT, TASK AREA & WORK UNIT NUMBERS Task 4.4.6
11. CONTROLLING OFFICE NAME AND ADDRESS Air Force Technical Applications Center (TFR) Patrick Air Force Base, FL 32925		12. REPORT DATE 1 October 1978
14. MONITORING AGENCY NAME & ADDRESS (if different from Controlling Office) Atmospheric Sciences Laboratory DRSEL-BL-MS White Sands Missile Range, NM 88002		13. NUMBER OF PAGES 118
15. SECURITY CLASS. (of this report) Unclassified		
15a. DECLASSIFICATION/DOWNGRADING SCHEDULE		
16. DISTRIBUTION STATEMENT (of this Report) Approved for public release; distribution unlimited		
17. DISTRIBUTION STATEMENT (of the abstract entered in Block 20, if different from Report)		
18. SUPPLEMENTARY NOTES		
19. KEY WORDS (Continue on reverse side if necessary and identify by block number) Aerosol Models Path Radiance Rayleigh Scattering Sunlight Transmission Aerosol Scattering Atmospheric Emission Molecular Absorption Terrain Emission		
20. ABSTRACT (Continue on reverse side if necessary and identify by block number) This report describes a preliminary version of an engineering-type predictive users' code developed to simulate the radiative energy (signal) reaching an electro-optical sensor operating within the atmosphere. The computer code, designated SPOT, allows for the definition of a point monodirectional receiver located within a plane parallel atmosphere. Sunlight, moonlight, and the thermal radiation emitted by the atmosphere and the ground surface characterize the natural radiative environment. In addition, SPOT allows for the definition of a plane reflective/emissive target arbitrarily oriented at a specified distance from the sensor along the sensor's line.		

DD FORM 1 JAN 73 1473 EDITION OF 1 NOV 68 IS OBSOLETE

Unclassified  
SECURITY CLASSIFICATION OF THIS PAGE (When Data Entered)

UNCLASSIFIED

SECURITY CLASSIFICATION OF THIS PAGE(When Data Entered)

**20. ABSTRACT (Continued)**

of-sight. Primary components of the radiative environment are treated in this version of the code. In particular, this includes; direct and single-scattered sunlight (or moonlight), target (or ground) reflection of direct sunlight (or moonlight), uncollided atmospheric emission, and uncollided target (or ground) emission. Data bases for the extraterrestrial spectral irradiance, along with the compilation of various aerosol phase matrices are used in order to provide adequate computational details. In addition, the LOWTRAN 4 atmospheric transmittance/radiance code is utilized as an integral part of the program. Various computational options provide the user with a sufficient degree of flexibility in order to perform spectral analyses of sensors operating within a variety of atmospheric conditions.

UNCLASSIFIED

SECURITY CLASSIFICATION OF THIS PAGE(When Data Entered)

#### ACKNOWLEDGMENTS

The authors wish to express their appreciation to Doug Jones of the RRA staff for providing valuable assistance in the development of the SPOT computer code described herein. Special thanks go to Richard Gomez, project monitor from the Atmospheric Sciences Laboratory, whose cooperation and assistance throughout the project are gratefully acknowledged. The performance of the work described in this report was under the technical direction of M. B. Wells, Vice President of Radiation Research Associates, Inc.

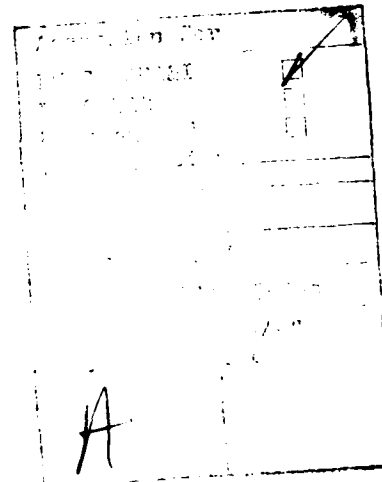


## TABLE OF CONTENTS

	<u>Page</u>
ACKNOWLEDGMENTS	
LIST OF FIGURES	
LIST OF TABLES	
I. INTRODUCTION	1
II. THE RADIATIVE ENVIRONMENT	5
2.1 Sunlight and Moonlight	8
2.2 Electromagnetic Emission	13
III. THE SPOT COMPUTER CODE	18
3.1 Computational Methods	19
3.1.1 Atmospheric Transmittance	19
3.1.2 Direct Sunlight or Moonlight	21
3.1.3 Path Radiance	21
3.1.4 Target (or Ground) Reflection of Direct Sunlight or Moonlight	25
3.1.5 Uncollided Atmospheric Emission	26
3.1.6 Uncollided Target (or Ground) Emission	27
3.2 Data Base	28
3.2.1 Extraterrestrial Solar Spectrum	28
3.2.2 Extraterrestrial Lunar Spectrum	28
3.2.3 Atmospheric Models (LOWTRAN 4)	31
3.2.4 Aerosol Data Base (HAZESDATA)	34
3.3 Program Logic	47
3.3.1 Input	47

TABLE OF CONTENTS (Continued)

	<u>Page</u>
3.3.2 Output	52
3.4 Validation	60
3.5 Future Improvements	62
IV. AN EXAMPLE PROBLEM: E-O SENSOR SCAN	66
V. UTILIZATION INSTRUCTIONS FOR THE SPOT COMPUTER CODE	99
REFERENCES	106

LIST OF FIGURES

<u>Figure</u>	<u>Page</u>
1. Source-Receiver Geometry for Plane Parallel Atmosphere	6
2. Geometry for Reflectance Calculations with Sensor Viewing an Object	7
3. Geometry for Calculation of Single Scattered Path Radiance	22
4. Standard Values for the Extraterrestrial Solar Spectral Irradiance (watts $m^{-2} \mu m^{-1}$ )	29
5. Extraterrestrial Solar Spectral Irradiance (watts $m^{-2} \mu m^{-1}$ ) for UV and Visible Regions	30
6. Geometrical Albedo versus Wavelength for the Moon	33
7. Size Distribution for the Rural Aerosol Model used in LOWTRAN 4. Also shown are the Modified Haze C Model and the Individual Log Normal Distribution which make up the Rural Model.	40
8. Size Distribution for the Maritime Aerosol Model used in LOWTRAN 4. Also shown are the Individual Distributions for the Aerosols of Continental Origin and the Sea Spray Produced Aerosols.	41
9. Extinction Coefficients for the Four Aerosol Models used in LOWTRAN 4 as a Function of Wavelength. The Extinction at 0.55 microns corresponds to a Meteorological Range of 23 km.	42
10. Attenuation Coefficients for Modified Haze C Aerosol Distribution as a Function of Wavelength	44
11. Phase Function for Modified Haze C Aerosol Distribution as a Function of Wavelength, Scattering Angles of 0, 30, 90 and 180°	45
12. FLOWCHART for the SPOT Computer Code	54
13. Comparison of Results from FLASH, LOWTRAN 4, and SPOT Spectral Calculations of Ground Emission and Total Emission (including Uncollided Atmospheric Emission): Ground Emissivity = 1.0	61

LIST OF FIGURES (Continued)

<u>Figure</u>		<u>Page</u>
14.	Total Target and Background Radiance (wavelength-integrated) versus Sensor Polar Angle	67
15.	Target and Background Radiance Components (wavelength-integrated) due to Sunlight versus Sensor Polar Angle	68
16.	Target and Background Radiance Components (wavelength-integrated) due to Thermal Emission vs Sensor Polar Angle	69
17.	Contrast Ratio (wavelength-integrated) versus Sensor Polar Angle	70
18.	Target Radiance Components versus Frequency for Sensor Polar Angle of $60^{\circ}$	74
19.	Background Radiance Components versus Frequency for Sensor Polar Angle of $60^{\circ}$	75
20.	Spectral Source Strength for Sunlight and Target Emission: Target Temperature = $295^{\circ}\text{K}$ , Emissivity = .95	76
21.	Atmospheric Transmittance from Sensor to Target and from Sensor to Top of Atmosphere, for Sensor Polar Angle of $60^{\circ}$	77
22.	Uncollided Sunlight Flux versus Frequency for Sensor Polar Angle of $60^{\circ}$	80
23.	Target Radiance Components versus Frequency for Sensor Polar Angle of $140^{\circ}$	81
24.	Background Radiance Components versus Frequency for Sensor Polar Angle of $140^{\circ}$	82
25.	Spectral Source Strength for Ground Emission: Ground Temperature = $288.1^{\circ}\text{K}$ , Emissivity = 1.0	83
26.	Atmospheric Transmittance from Sensor to Target and from Sensor to Ground Surface, for Sensor Polar Angle of $140^{\circ}$	84
27.	Spectral Contrast Ratio for Sensor Polar Angles of $60^{\circ}$ and $140^{\circ}$	86
28.	Page One of the SPOT Printed Output	89

LIST OF FIGURES (Continued)

<u>Figure</u>		<u>Page</u>
29.	Page Two of the SPOT Printed Output	90
30.	Page Three of the SPOT Printed Output	91
31.	Page Four of the SPOT Printed Output	92
32.	Page Five of the SPOT Printed Output	93
33.	Page Six of the SPOT Printed Output	94
34.	Page Seven of the SPOT Printed Output	95
35.	Page Eight of the SPOT Printed Output	96
36.	Page Nine of the SPOT Printed Output	97
37.	Page Ten of the SPOT Printed Output	98
38.	Sample Run Stream for Execution of the SPOT Program on the WSMR UNIVAC-1108	105

LIST OF TABLES

<u>TABLE</u>		<u>Page</u>
I.	THE INTEGRATED PHASE-CURVE OF THE MOON	32
II.	TROPICAL ( $15^{\circ}$ N) MODEL ATMOSPHERE	35
III.	MIDLATITUDE SUMMER ( $45^{\circ}$ N, JULY) MODEL ATMOSPHERE	36
IV.	MIDLATITUDE WINTER ( $45^{\circ}$ N, JANUARY) MODEL ATMOSPHERE	37
V.	SUBARCTIC SUMMER ( $60^{\circ}$ N, JULY) MODEL ATMOSPHERE	38
VI.	SUBARCTIC WINTER ( $60^{\circ}$ N, JANUARY) MODEL ATMOSPHERE	39
VII.	WAVELENGTHS ( $\mu$ m) CHOSEN FOR DATA BASE HAZESDATA	46
VIII.	SPECTRAL APPLICABILITY OF SPOT DATA BASES	50
IX.	SUMMARY OF PROBLEM DESCRIPTION INPUT DATA FOR THE SPOT COMPUTER CODE	53
X.	FORMAT OF THE INPUT DATA FOR THE SPOT COMPUTER CODE	101
XI.	FORMAT OF THE AEROSOL PHASE FUNCTION DATA BASE	104

## I. INTRODUCTION

The ability of an electro-optical (E-O) sensor operating within the atmosphere to accurately distinguish between the signal received from a reflective/emissive target within its field-of-view and that portion of the signal attributable to natural (background) sources is dependent upon many parameters. Basicly, the problem of signal recognition may be subdivided into three major areas: 1) the reflective/emissive properties of the object being viewed by the detector, 2) the transmittance of the atmosphere, and 3) the characteristics of the natural radiative environment. In addition to the natural environment, various man-made obscurants such as smokes, dust and debris may be present within the atmosphere, causing a perturbation of the atmospheric transmittance. Hence, the designer and user of such sensing devices must be acutely aware of the properties which characterize the radiative energy (signal) incident upon the detector during its operation in order to determine its performance capabilities. It is to this end, characterization of the incident radiative energy, that the work described within this report was dedicated.

Much work has been directed toward the development of the capability to simulate optical signatures indicative of any combination of natural and/or man-made features on the ground under illumination conditions resulting from sunlight, moonlight, and the thermal radiation emitted by the atmosphere, the ground, and any man-made features either on the ground or within the atmosphere (Ref. 1). Preliminary investigations into the importance of multiple scattering have utilized the sophisticated Monte Carlo codes FLASH and BRITE, developed by Radiation Research Associates (Refs. 2,3). The results of this study, as presented at the "First CSL Scientific Conference on Obscuration and Aerosol Research," are reported in Ref. 4. Two additional Monte Carlo codes have recently been completed, and are expected to provide further insight into the question of multiple scattering. The first code, THARTL, simulates a monodirectional source embedded within a homogeneous atmosphere (Ref. 5). It is anticipated that the THARTL program will prove useful in assessing the spectral regions

and atmospheric conditions for which multiple scattering of radiation emitted by surface-sources, especially blackbody-type radiators, will contribute significantly to the radiative energy perceived by an electro-optical sensor. The additional Monte Carlo code represents an extensive modification of an earlier code, TPART-3, developed by RRA (Ref. 6). In the new program, provisions have been made for the incorporation of three-dimensional models of clouds or other obscurants which might be present within the atmosphere (Ref. 7). Due to the geometrical flexibility of the new program, the user will have the capability to study such problems as the detectability of objects by a reflected laser beam in an environment containing clouds of smoke and dust. In particular, it will be of interest to determine the scattering conditions under which a localized target cannot be distinguished from its surroundings because of degradation of the collimated beam.

A special effort has been directed toward the development of an aerosol phase matrix data base to be used in investigating the influence of multiple scattering (Ref. 8). Continental aerosol size distributions, approximated by a model similar to Deirmendjian's Haze C model (Ref. 9), have been employed in conjunction with several MIE calculations (Ref. 10) in order to produce a collection of phase matrices applicable to the spectral region from 0.1585 to 40.0  $\mu\text{m}$ . MIE3 calculations in the spectral region from 0.4 to 15.0  $\mu\text{m}$  were performed for a number of size distributions that were measured by the Atmospheric Sciences Laboratory at Fort A. P. Hill. These data were collected on a day characterized by low-visibility conditions. In addition, MIE calculations have been performed for another six aerosol models representing size distributions of haze and fog layers. Each model was assumed to be defined by a number of log normal distributions. The results from these various calculations should add a degree of authenticity to future Monte Carlo analyses of aerosol scattering, and to the SPOT code discussed below.

The primary purpose of this report is to describe a preliminary version of an engineering-type predictive users' code developed to simulate the radiative energy (signal) reaching an electro-optical sensor operating

within the atmosphere. This computer code, designated SPOT, allows for the definition of a point monodirectional receiver located within a plane parallel atmosphere. Sunlight, moonlight, and the thermal radiation emitted by the atmosphere and the ground surface characterize the natural radiative environment. In addition, SPOT allows for the definition of a plane reflective/emissive target arbitrarily oriented at a specified distance from the sensor along the sensor's line-of-sight. Primary components of the radiative environment are treated in this version of the code. In particular, this includes: direct and single-scattered sunlight (or moonlight), target (or ground) reflection of direct sunlight (or moonlight), uncollided atmospheric emission, and uncollided target (or ground) emission. Data bases for the extraterrestrial spectral irradiance, along with the compilation of various aerosol phase matrices previously discussed, are used in order to provide adequate computational details. In addition, the LOWTRAN4 atmospheric transmittance/radiance code (Ref. 11) is utilized as an integral part of the program. Various computational options provide the user with a sufficient degree of flexibility in order to perform spectral analyses of sensor's operating within a variety of atmospheric conditions.

A technical discussion of the radiative environment is presented in section II. In this section, the various components which define the radiative energy incident at a sensor are outlined and analytical expressions are given which describe the contribution of each to the incident signal. In section III, the SPOT computer code is described in detail. The computational methods employed by the program in the evaluation of the radiative components are presented in subsection 3.1. Subsection 3.2 describes the various data bases employed by the program while subsection 3.3 contains a description of the program logic, including a discussion of the input requirements. Validation of the SPOT code is given in subsection 3.4, where several comparisons are made with data obtained from the FLASH Monte Carlo code. Future improvements to the code are discussed in subsection 3.5. Finally, in section IV an example problem

is shown in which the signal received by a sensor scanning the atmosphere from the zenith to the nadir is analyzed. In order to demonstrate the capabilities of the program, a target is placed within the sensor's line-of-sight, in an atmosphere characterized by low-visibility conditions.

It is anticipated that the SPOT program will provide a very useful tool in the analysis and prediction of sensor performance and capabilities operating within a wide variety of illumination and atmospheric conditions. It is planned that future extensions of the SPOT code will include different atmospheric models, atmospheric obscurants such as smokes and debris and the effects of multiple scattering. Such extensions to SPOT would enhance the capability of the program to a most useful level.

## II. THE RADIATIVE ENVIRONMENT

The radiative energy incident upon a sensor is produced primarily by a combination of three sources: sunlight, moonlight, and emitted electromagnetic radiation. The radiative environment produced by these sources may be categorized into various components which in turn may be described by computerized mathematical models. In the following text, a description of the various radiative components vital to the E-O (electro-optical) sensor signal recognition problem will be presented. In order to simplify the discussion in this report, unless stated otherwise, we shall assume a plane-parallel atmospheric model.

The geometrical features pertinent to the analysis of the radiative environment are shown in Figs. 1 and 2. Shown in Fig. 1 is a simplified configuration in which a point monodirectional detector is located at an altitude  $h$ , with a line-of-sight defined by the standard polar angles  $(\theta, \phi)$  intersecting the ground surface. A broad beam source, indicative of sunlight or moonlight, oriented along a zenith angle given by  $\theta_0$ , is incident upon the top of the plane parallel atmosphere. A more complex configuration is shown in Fig. 2 in which the detector's line-of-sight is incident upon an object located at an altitude  $h'$ . The object being viewed is described as a plane reflective/emissive surface whose orientation is defined by a unit vector  $\vec{n}$  normal to the surface. Radiation propagating along a zenith angle  $\theta'$  which impinges upon the object, is described by the angle of incidence  $\beta$  measured with respect to the normal  $\vec{n}$ . In addition, the angle subtended by the receivers' line-of-sight and the normal vector  $\vec{n}$  is given by  $\gamma$ .

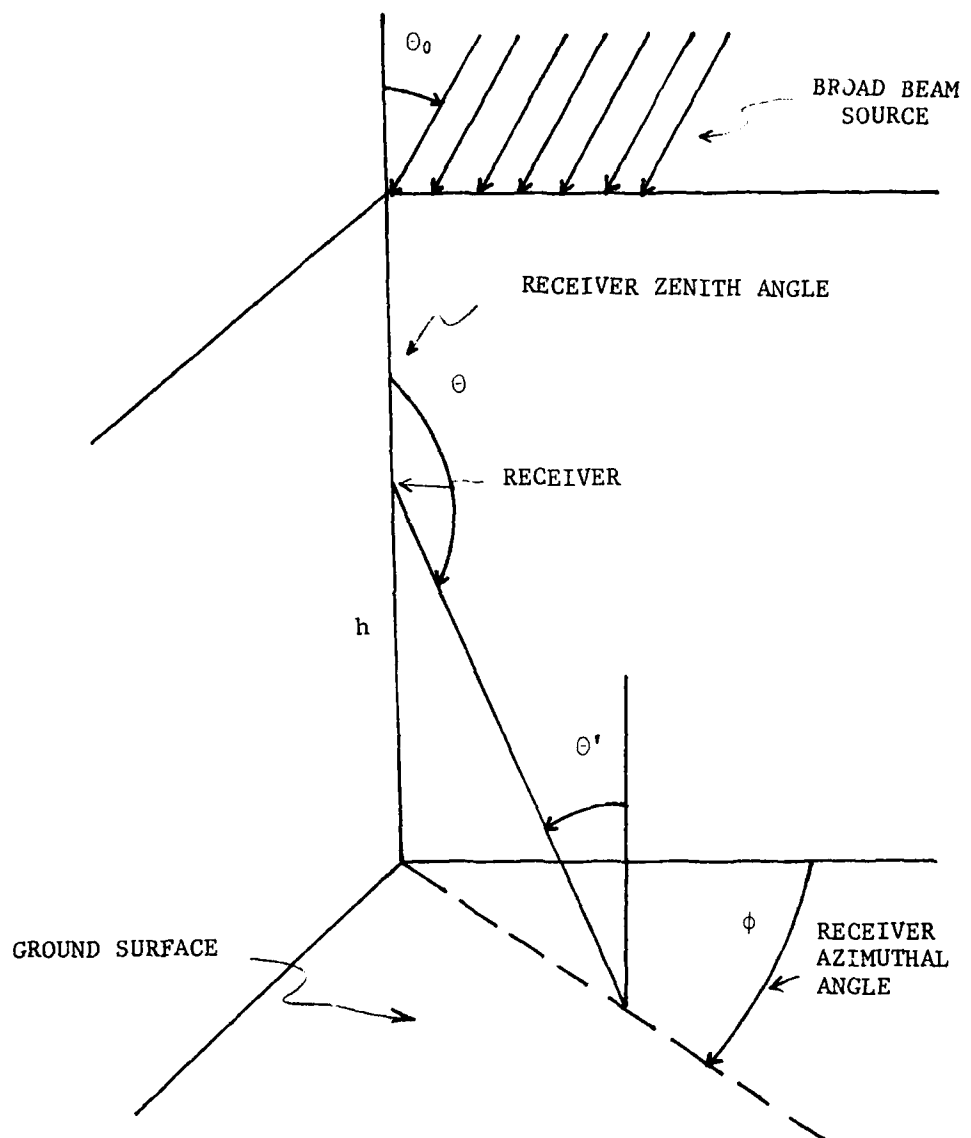


Fig. 1. Source-Receiver Geometry for Plane Parallel Atmosphere

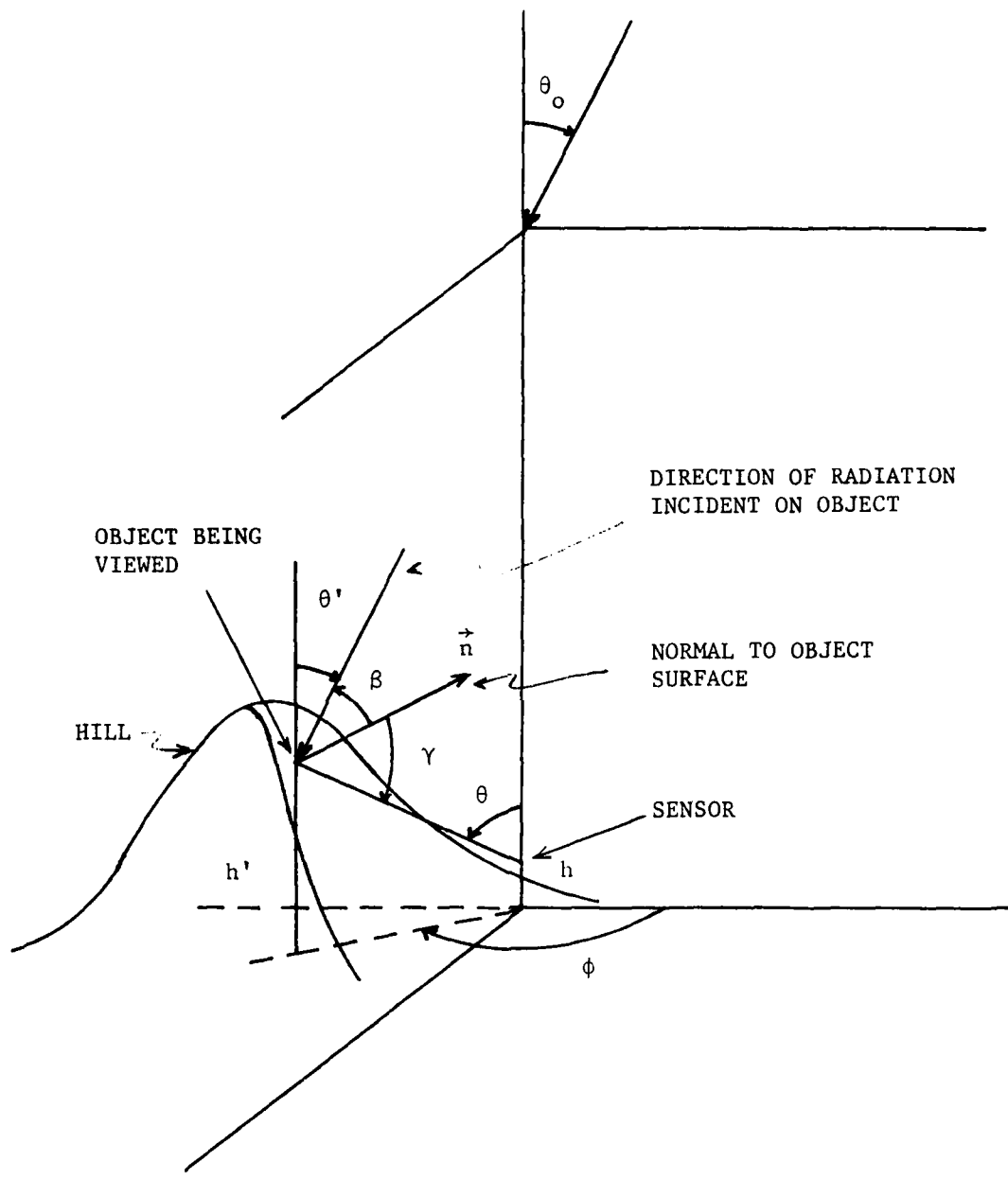


Fig. 2. Geometry for Reflectance Calculations with Sensor Viewing an Object

## 2.1 Sunlight and Moonlight

In the event that the position of the sun or moon lies within a detector's line-of-sight, direct (uncollided) sunlight or moonlight may contribute significantly to the signal received by the sensor. Assuming a source strength for sunlight and moonlight sources of one photon/m<sup>2</sup> incident to the top of the atmosphere oriented along a zenith direction  $\theta_0$ , the uncollided flux (photons m<sup>-2</sup>/photon m<sup>-2</sup>) incident upon a point detector is given by

$$F_D(\lambda, \theta_0, h) = e^{-[\tau(h_{\max}) - \tau(h)] \sec \theta_0} \quad (1)$$

where  $\tau(h_{\max})$  is the optical thickness of the atmosphere,  $\tau(h)$  is the optical thickness from ground level to the sensor's altitude  $h$ ; both quantities defined at the wavelength of interest  $\lambda$ .

Similarly, the uncollided flux incident upon the ground is given by

$$F_D(\lambda, \theta_0, h=0) = e^{-\tau(h_{\max}) \sec \theta_0} \quad (2)$$

The total scattered flux incident upon the ground is given by

$$F_S(\lambda, \theta_0, h=0, \alpha_0) = \int_0^{2\pi} \int_0^{\pi/2} I(\lambda, \theta_0, h=0, \alpha_0, \theta, \phi) \cos \theta \sin \theta d\theta d\phi \quad (3)$$

where the quantity  $I(\lambda, \theta_0, h=0, \alpha_0, \theta, \phi)$  is the scattered intensity for sunlight or moonlight incident upon the ground surface in the zenith direction  $\theta$  and the azimuthal direction  $\phi$ . The scattered intensity results from atmospheric scattering and ground reflection of photons of wavelength  $\lambda$  that were incident at a zenith angle  $\theta_0$  at the top of an atmosphere bounded by a ground surface characterized by Lambertian reflection properties and an albedo  $\alpha_0$ .

If the line-of-sight of a point detector is oriented toward the ground, the intensity of the ground reflected direct sunlight or moonlight incident upon the sensor is given by

$$R_D(\lambda, \theta_o, h, \alpha_o, \theta) = e^{-\tau(h_{\max}) \sec \theta_o} \cdot \alpha_o \frac{|\cos \theta|}{\pi} \cdot e^{-\tau(h) \sec \theta'} \cdot \cos \theta_o \quad (4)$$

where  $\theta$  defines the zenith direction of the sensor's orientation and  $\alpha_o$  is the albedo of the ground surface (assuming Lambertian reflection) defined at the wavelength of interest  $\lambda$ . Referring to Fig. 1, the definition of the variable  $\theta'$  is given by

$$\theta' = 180 - \theta \text{ (degrees)} \quad .$$

All other variables are as previously described.

The total intensity incident upon the sensor resulting from the ground reflection of solar or lunar radiation is given by

$$R_T(\lambda, \theta_o, h, \alpha_o, \theta) = R_D(\lambda, \theta_o, h, \alpha_o, \theta) + F_S(\lambda, \theta_o, h=0, \alpha_o) \cdot \alpha_o \frac{|\cos \theta|}{\pi} \cdot e^{-\tau(h) \sec \theta'} \quad . \quad (5)$$

Hence, when the sensor is looking toward the ground surface, the difference between the total scattered intensity  $I(\lambda, \theta_o, h, \alpha_o, \theta, \phi)$  and the total ground reflected intensity  $R_T(\lambda, \theta_o, h, \alpha_o, \theta)$  is the path radiance  $P_G(\lambda, \theta_o, h, \alpha_o, \theta, \phi)$  due to atmospheric scattering of the extraterrestrial radiation.

If a point detector located at an altitude  $h$  is viewing (in the direction  $\theta, \phi$ ) an object on the ground surface that has an albedo  $\alpha$  different from the ground albedo  $\alpha_o$ , then the intensity at the sensor coming directly from the object is given by

$$R'_T(\lambda, \theta_o, h, \alpha_o, \alpha, \theta) = \alpha / \alpha_o \cdot R_T(\lambda, \theta_o, h, \alpha_o, \theta) \quad . \quad (6)$$

If the albedo  $\alpha$  is for a surface that does not reflect like a Lambert reflector, then the quantity  $\alpha / \alpha_o$  in the above equation should be replaced with the quantity  $\frac{\pi}{\alpha_o |\cos \theta|} \alpha(\theta')$  (7)

where  $\alpha(\theta')$  is the differential current albedo in the direction  $\theta'$  (Fig. 1). The total intensity at the sensor, when viewing an object on the ground, is then given by

$$I_T(\lambda, \theta_o, h, \alpha_o, \alpha, \theta, \phi) = P_G(\lambda, \theta_o, h, \alpha_o, \theta, \phi) + R_T(\lambda, \theta_o, h, \alpha_o, \alpha, \theta) \quad . \quad (8)$$

For a point detector viewing an object located either on the ground ( $h'=0$ ) or at some altitude  $h'$  (Fig. 2), the intensity of the target (object) reflected direct sunlight or moonlight at the sensor is given by

$$R_D(\lambda, \theta_o, h, \theta, \phi, h', \alpha, \vec{n}) = e^{-[\tau(h_{\max}) - \tau(h')]\sec\theta_o} \quad (9)$$

$$\cdot (\alpha |\cos\gamma|/\pi) \cdot \cos\beta \cdot e^{-|[\tau(h) - \tau(h')]\sec\theta|}$$

where  $\theta, \phi$  define the zenith and azimuthal directions, respectively, of the detector's line-of-sight,  $\alpha$  is the albedo of the object being viewed (assuming Lambertian reflection), defined at the wavelength of interest  $\lambda$ , and  $\vec{n}$  is a unit vector normal to the object, which describes its orientation in space. The angles  $\beta$  and  $\gamma$  (Fig. 2) define, respectively, the angle of incidence and the reflection angle with respect to the object normal  $\vec{n}$ . Note, the object being viewed is characterized as a flat plate.

The total scattered flux incident upon the object is given by

$$F_{OS}(\lambda, \theta_o, h', \alpha_o) = \int_0^{2\pi} \int_0^{\pi/2} I(\lambda, \theta_o, h', \alpha_o, \beta, \delta) \cos\beta \sin\beta d\beta d\delta \quad (10)$$

where the quantity  $I(\lambda, \theta_o, h', \alpha_o, \beta, \delta)$  is the scattered intensity for sunlight or moonlight incident upon the object in the zenith direction  $\beta$  and the azimuthal direction  $\delta$ . Note, the zenith and azimuthal angles  $\beta, \delta$  are with respect to the normal vector  $\vec{n}$ . Once again, the scattered intensity is the result of the atmospheric scattering and ground reflection of photons of wavelength  $\lambda$  that were incident along a zenith angle  $\theta_o$  at the top of the atmosphere bounded by a ground surface characterized by Lambertian reflection properties and an albedo  $\alpha_o$ .

The total intensity incident upon the point detector resulting from the reflection of solar or lunar radiation by the object being viewed is given by

$$R'_T(\lambda, \theta_o, h, \theta, \phi, h', \alpha_o, \alpha, \vec{n}) = R_D(\lambda, \theta_o, h, \theta, \phi, h', \alpha, \vec{n}) + F_{OS}(\lambda, \theta_o, h', \alpha_o) \\ \cdot (\alpha |\cos\gamma|/\pi) \cdot \cos\beta \cdot e^{-|[\tau(h)-\tau(h')] \sec\theta|} \quad . \quad (11)$$

As with the ground reflection, it is assumed the object being viewed by the sensor possesses the reflection properties of a Lambertian surface with albedo  $\alpha$ . Otherwise, the quantity  $\alpha \cdot |\cos\gamma|/\pi$  appearing in both the direct and scattered components given above must be replaced by  $\alpha(\gamma)$ , which is the differential current albedo.

The path radiance at the sensor resulting from extraterrestrial radiation undergoing scattering along the path between the object being viewed and the sensor is given by

$$P_o(\lambda, \theta_o, h, \theta, \phi, h', \alpha_o) = I(\lambda, \theta_o, h, \alpha_o, \theta, \phi) - I(\lambda, \theta_o, h', \alpha_o, \theta, \phi) \\ \cdot e^{-|[\tau(h)-\tau(h')] \sec\theta|} \quad . \quad (12)$$

The radiative component described by the above equation neglects any radiation resulting from collisions for which the object being viewed lies between the sensor and the location of the last collision. Therefore, the total intensity at the sensor in the direction toward the object  $(\theta, \phi)$ , neglecting background contributions, is given by the sum

$$I_o(\lambda, \theta_o, h, \theta, \phi, h', \alpha) = R'_T(\lambda, \theta_o, h, \theta, \phi, h', \alpha_o, \alpha, \vec{n}) + \\ P_o(\lambda, \theta_o, h, \theta, \phi, h', \alpha_o) \quad . \quad (13)$$

A few points of clarification are in order concerning the radiative components resulting from interactions with the object being viewed by the

sensor. With respect to the reflection of solar or lunar radiation by the object in question, it should be noted that the total reflected intensity  $R'_T(\lambda, \theta_o, h, \theta, \phi, h', \alpha_o, \alpha, \vec{n})$ , (Eq. 11), does not account for atmospheric scattering or ground reflection of the radiation subsequent to its reflection by the object. In addition, the quantity  $I(\lambda, \theta_o, h, \alpha_o, \theta, \phi)$ , which appears in various forms in a number of the radiative components discussed, is indicative of a plane parallel atmosphere bounded by a plane ground surface. Multiple interactions with the object in question are not accounted for, i.e., the presence of an object within the line-of-sight of the sensor is evident only through the single reflection of either uncollided or multiple scattered radiation toward the sensor.

## 2.2 Electromagnetic Emission

All substances continuously emit electromagnetic radiation by virtue of the molecular and atomic agitation associated with the internal energy of the material (Ref. 12). In the equilibrium state, this internal energy is directly proportional to the temperature of the substance. The emitted radiant energy can range from radio waves, which can have wavelengths of several kilometers, to cosmic rays with wavelengths of less than  $10^{-10}$  centimeters. In this report, only that radiation which is detected as heat or light will be considered. Therefore, this radiative component will be referred to as thermal radiation.

Thermal radiation is often discussed in terms of an ideal radiating surface, i.e. a blackbody. In particular, a blackbody is defined as a body that is a perfect absorber of incident electromagnetic radiation. This is true of radiation for all wavelengths and for all angles of incidence. If there exists a state of equilibrium between the blackbody and its local environment (i.e., local thermodynamic equilibrium), then the blackbody in question must radiate exactly as much energy as it absorbs in order to preserve the second law of thermodynamics. It follows then that because the blackbody is by definition a perfect absorber, it must also be a perfect emitter of thermal radiation. In addition, the radiation is isotropic; the radiation received or emitted in any direction by the blackbody, per unit projected area normal to that direction, must be equal. The properties of perfect emission and absorption characteristic of a blackbody are true for each wavelength. The characteristics of the surrounding media do not affect the emissive behavior of the blackbody. Hence, the total radiant energy emitted by a blackbody is a function only of its temperature.

Planck's Radiation law or more specifically, Planck's spectral distribution of emissive power (Ref. 12), describes the spectral distribution of the radiant intensity for a blackbody in a vacuum, and is given as a function of absolute temperature and wavelength by

$$I_B(\lambda, T) = \frac{2\pi c^2 h}{\lambda^5} \frac{1}{[\exp(hc/k\lambda T) - 1]} \quad (14)$$

where  $c$  = the speed of light in a vacuum

$h$  = Planck's constant

$k$  = the Boltzmann constant

$T$  = the absolute temperature of the blackbody

$\lambda$  = the wavelength of the emitted radiation.

The following equation, often referred to as the blackbody function,

$$B(\lambda, T) = \frac{1}{\pi} I_B(\lambda, T) \quad (15)$$

indicates the directional emissive power normal to the radiating surface per steradian - per unit area - per unit wavelength.

If a point detector is positioned at an altitude  $h$  such that the ground surface lies within the sensor's line-of-sight, the uncollided thermal radiation emitted by the ground and incident upon the sensor is given by

$$I_{UGE}(\lambda, h, \theta, T_g, E_g) = E_g \cdot \cos\theta' \cdot B(\lambda, T_g) \cdot e^{-\tau(h) \sec\theta'} \quad (16)$$

where  $E_g$  and  $T_g$  are the emissivity and absolute temperature respectively of the ground surface,  $\theta$  defines the zenith direction of the sensor's line-of-sight (Fig. 1) and the other parameters are as described earlier. In addition to the uncollided thermal radiation emitted by the ground, there is radiation emitted by the atmosphere which impinges upon the sensor uncollided. This component is given by

$$I_{UAE}(\lambda, h, \theta) = \int_0^1 B(\lambda, T_a) \cdot TR_s \cdot dTR_a \quad (17)$$

$$TR_a(h \rightarrow 0, \theta)$$

where  $TR_s$  = the transmittance due to atmospheric scattering

$TR_a$  = the transmittance due to atmospheric absorption

$TR_a(h \rightarrow 0, \theta)$  = the total transmittance due to atmospheric absorption between the sensor and the ground along the zenith direction  $\theta$

$T_a$  = the absolute temperature of an atmospheric layer

$\lambda$  = the wavelength of the emitted radiation

$B(\lambda, T_a)$  = the blackbody function corresponding to a wavelength  $\lambda$   
and absolute temperature  $T_a$ .

The total uncollided thermal radiation incident upon a detector viewing the ground is then given by

$$I_{TUE}(\lambda, h, \theta, T_g, E_g) = I_{UGE}(\lambda, h, \theta, T_g, E_g) + I_{UAE}(\lambda, h, \theta) . \quad (18)$$

We shall denote the quantity  $I(\lambda, h, \theta, T_g, E_g, \alpha_o)$  as the total intensity incident at a sensor located at an altitude  $h$ , whose line-of-sight is defined by the zenith angle  $\theta$ , which results from the direct emission of thermal radiation by the ground and atmosphere plus the air-scattered/ground-reflected thermal radiation, where  $T_g$ ,  $E_g$  and  $\alpha_o$  are the absolute temperature, emissivity and albedo respectively of the ground surface (assuming Lambertian reflection), and the atmospheric temperature and pressure is a function of altitude. If the sensor is looking in a direction defined by  $\theta \leq 90^\circ$ , then there is no direct (uncollided) thermal radiation from the ground surface included in the total intensity. The difference between the total intensity  $I(\lambda, h, \theta, T_g, E_g, \alpha_o)$  and the uncollided ground emission reaching the sensor  $I_{UGE}(\lambda, h, \theta, T_g, E_g)$  is the path radiance  $P(\lambda, h, \theta, T_g, E_g, \alpha_o)$  due to thermal emission. Hence, the path radiance, as described herein, is the sum of the direct air emission along the detector's line-of-sight and the thermal radiation emitted by both the atmosphere and the ground outside of the detector's line-of-sight that undergoes at least one order of scattering (or ground reflection) such that the last collision of the scattered radiation occurs within the sensor's line-of-sight.

If an object positioned at an altitude  $h'$  lies within a sensor's line-of-sight, the uncollided thermal radiation emitted by the object and which is incident at the sensor is given by

$$I_{UDE}(\lambda, h, \theta, h', T_o, E_o, \vec{n}) = E_o \cdot \cos\gamma \cdot B(\lambda, T_o) \cdot e^{-|\tau(h)-\tau(h')|\sec\theta} \quad (19)$$

where  $E_o$  and  $T_o$  are the emissivity and absolute temperature of the object,  $\vec{n}$  is the unit vector normal to the radiating surface and the angle  $\gamma$  (Fig. 2) is the zenith angle defined by the sensor-object line-of-sight and the normal vector  $\vec{n}$ . The blackbody function  $B(\lambda, T_o)$  is indicative of the object's temperature  $T_o$  and the wavelength of interest  $\lambda$ . The uncollided thermal radiation emitted by the atmosphere along the sensor's line-of-sight, between the sensor and the object being viewed, is given by

$$I_{UAE}(\lambda, h, \theta, h') = \int_{TR_a(h \rightarrow h', \theta)}^1 B(\lambda, T_a) \cdot TR_s \cdot dTR_a \quad (20)$$

where  $TR_a(h \rightarrow h', \theta)$  is the total transmittance due to atmospheric absorption between the sensor and the object, along the sensor's line-of-sight defined by the zenith angle  $\theta$ .

The total intensity as previously described by the quantity  $I(\lambda, h, \theta, T_g, E_g, \alpha_o)$  does not include the radiation emitted by the object being viewed. The emissive path radiance defined as the sum of the uncollided air emission along the sensor's line-of-sight, between the sensor and the object, and the thermal radiation emitted by both the atmosphere and the ground outside of the sensor's line-of-sight which undergoes atmospheric scattering (or ground reflection) such that the last collision occurs within the sensor's line-of-sight and between the sensor and the object, is given by

$$P(\lambda, h, \theta, h', T_g, E_g, \alpha_o) = P(\lambda, h, \theta, T_g, E_g, \alpha_o) - P(\lambda, h', \theta, T_g, E_g, \alpha_o) \cdot TR_t(h \rightarrow h', \theta) \quad (21)$$

where  $TR_t(h \rightarrow h', \theta)$  is the total transmittance due to atmospheric absorption and scattering between the sensor and the object being viewed, along the sensor's line-of-sight.

If the object being viewed by the sensor is not an ideal blackbody (i.e. a perfect absorber), then a fraction of the thermal radiation emitted by the atmosphere and ground surface which is incident upon the object is reflected toward the sensor within its line-of-sight. This radiative component is given by

$$I_{ORE}(\lambda, h, \theta, h', \vec{n}, T_g, E_g, \alpha_o, \alpha) = 2\pi \cdot \int_0^{\pi/2} I(\lambda, h', \beta, T_g, E_g, \alpha_o) \cdot \cos\beta \sin\beta d\beta \cdot \frac{\alpha |\cos\gamma|}{\pi} \cdot e^{-|[\tau(h)-\tau(h')] \sec\theta|} \quad (22)$$

where  $\alpha$  is the albedo of the object (assuming Lambertian reflection),  $\beta$  is the zenith angle which the incident radiation makes with respect to the object normal vector  $\vec{n}$ ,  $\gamma$  is the zenith angle that the reflected radiation makes with respect to  $\vec{n}$  (Fig. 2), and all other parameters are as previously described.

It should be noted that the radiation reflected into the sensor, as described above, does not undergo further scattering or reflection subsequent to its reflection by the object being viewed. In addition, the total intensity described by the quantity  $I(\lambda, h, \theta, T_g, E_g, \alpha_o)$  does not include the thermal radiation emitted by the object, nor does it account for any interactions (absorption or reflection) which might occur between the radiation emitted by the atmosphere and the ground surface and the object in question.

## III. THE SPOT COMPUTER CODE

In order to analyze the signal recognition problem encountered by electro-optical sensors operating within the atmosphere, a computer code simulation designated SPOT has been written. The SPOT code, in its preliminary form as described in this report, is designed to calculate the radiative energy (signal) incident upon a monodirectional point detector located either on the ground or at some altitude above the ground within a plane parallel atmosphere. The radiative environment within which the sensor is to operate may be characterized by sunlight, moonlight, and the thermal radiation emitted by the atmosphere and the ground. In addition to the natural sources of radiation just defined, the SPOT code allows for the definition of a plane reflectional/emissive target arbitrarily oriented at a specified distance from the sensor along the sensor's line-of-sight. As previously described in Section II, the radiative environment produced by these sources may be categorized into various components. This version of the SPOT code will address primary components of the radiative environment, in particular:

- A. Sunlight or Moonlight Sources
  - 1. Direct sunlight or moonlight
  - 2. Single-scattered sunlight or moonlight
  - 3. Target (or ground) reflection of direct sunlight or moonlight
- B. Emission Sources
  - 1. Uncollided atmospheric emission
  - 2. Uncollided target (or ground) emission

In the following text, the computational methods employed in the SPOT code to evaluate the radiative components listed above are described.

## 3.1 Computational Methods

3.1.1 Atmospheric Transmittance

The parameter most difficult to define which appears in the analytical description of the radiative components outlined above is the atmospheric transmittance between two points within the atmosphere. Atmospheric transmittance of radiation is highly dependent upon a number of different physical properties of the atmosphere. In general, the monochromatic transmittance of radiation between two points located at altitudes  $h$  and  $h'$ , respectively, within a plane parallel atmosphere (Fig. 2) may be expressed as

$$TR_t(\lambda, h, h', \theta) = TR_s(\lambda, h, h', \theta) \cdot TR_a(\lambda, h, h', \theta) \quad (23)$$

where

$$TR_s(\lambda, h, h', \theta) = \exp\left[-\int_0^L \Sigma_s(\lambda, l) dl\right] \quad (24)$$

$$TR_a(\lambda, h, h', \theta) = \exp\left[-\int_0^L K_a(\lambda, l) \rho(l) dl\right] \quad (25)$$

and

$$h = \left|\frac{h-h'}{\cos\theta}\right| \quad (26)$$

In the above expressions,  $TR_s$  is the transmittance due to atmospheric scattering while  $TR_a$  is the transmittance due to atmospheric absorption. The parameter  $\Sigma_s(\lambda, l)$  is the altitude-dependent scattering coefficient for the scattering of electromagnetic radiation by molecules and aerosol particles distributed within the atmosphere, defined at the wavelength of interest  $\lambda$ . This parameter is dependent upon the number density of molecules and aerosol particulates found within the radiation path. The coefficient  $K_a(\lambda, l)$  is the altitude-dependent mass absorption coefficient, and  $\rho(l)$  is the absorber mass distributed along the path. Typically the molecular absorption of thermal radiation within the atmosphere is a highly oscillatory function of

wavelength due to the presence of numerous complex molecular absorption bands. It is this variable, the molecular absorption coefficient, which requires the most sensitive evaluation in order to accurately predict the transport of thermal radiation through the atmosphere.

The SPOT computer code utilizes the LOWTRAN 4 atmospheric transmittance/radiance computer program (Ref. 11) to calculate the transmittance of thermal radiation for a given atmospheric path at moderate spectral resolution. LOWTRAN 4 makes use of the band model technique in order to account for the absorption of thermal radiation by the molecular bands associated with:  $H_2O$ ,  $CO_2$ ,  $O_3$ ,  $N_2O$ ,  $CO$ ,  $O_2$ ,  $CH_4$ ,  $N_2$  and  $HNO_3$ . In general, LOWTRAN 4 is an empirical method, based upon the fit of an empirical formula to experimental data and data calculated from the AFCRL compilation of line parameters (Ref. 13). It should be noted that the LOWTRAN 4 code provides the average transmittance over a spectral interval  $\Delta\nu$  of  $20\text{ cm}^{-1}$  centered at the frequency of interest  $\nu$  (note that  $\nu(\text{cm}^{-1}) = 10^4/\lambda(\mu\text{m})$ ). Analytically, the average transmittance may be given by

$$\overline{TR}_t(\nu, h, h', \theta) = \frac{1}{\Delta\nu} \int_{\Delta\nu} \left\{ \exp \left[ - \int_0^L \sum_t(\lambda, l) \rho(l) dl \right] \right\} d\nu \quad (27)$$

The LOWTRAN 4 code is applicable to the spectral region from 0.2 to  $28.57\mu\text{m}$ .

It should be pointed out that there are numerous alternative methods available to obtain atmospheric transmittances. The FLASH and BRITE Monte Carlo radiation transport codes developed by RRA (Refs. 2,3) employ one such method which utilizes directly the AFCRL compilation of atmospheric absorption line parameters.

### 3.1.2 Direct Sunlight or Moonlight

The SPOT program calculates the spectral radiance incident at a sensor located within the atmosphere due to direct (uncollided) sunlight or moonlight (Eq. 1) by the expression

$$\text{DIR}(\lambda) = \text{TRANS}(\lambda) \cdot \text{SS}(\lambda) \quad (28)$$

where  $\text{TRANS}(\lambda)$  is the atmospheric transmittance from the top of the atmosphere to the detector along the detector's line-of-sight, as calculated by LOWTRAN 4. The quantity  $\text{SS}(\lambda)$  defines the extraterrestrial spectral irradiance for either sunlight or moonlight averaged over a small bandwidth centered at the wavelength of interest  $\lambda$ , in watts  $\text{m}^{-2} \mu\text{m}^{-1}$ . It should be remembered that the transmittances provided by LOWTRAN 4 are averaged over an interval of 20 wavenumbers ( $20\text{cm}^{-1}$ ).

### 3.1.3 Path Radiance

Assuming primary scattering, the path radiance obtained from sunlight or moonlight scattered into the line-of-sight of a detector D viewing an object O (Fig. 3) may be obtained through the integral

$$\text{PR}(\lambda) = \text{SS}(\lambda) \cdot \int_0^L \text{T}_1(\lambda, s) \cdot \text{T}_2(\lambda, s) \cdot \text{P}(\lambda, \psi, s) \cdot \Sigma_S(\lambda, s) \cdot ds \quad (29)$$

where

$\text{SS}(\lambda)$  = extraterrestrial spectral irradiance for sunlight or moonlight at wavelength  $\lambda$

$\text{T}_1(\lambda, s)$  = transmission along direction of incident radiation between top of atmosphere and collision point at position s from detector

$\text{T}_2(\lambda, s)$  = transmission along line-of-sight between detector D and object O

$\Sigma_S(\lambda, s)$  = scattering coefficient at position s

$\text{P}(\lambda, \psi, s)$  = value of normalized scattering function for scattering angle  $\psi$

$L$  = geometric distance between detector and object.

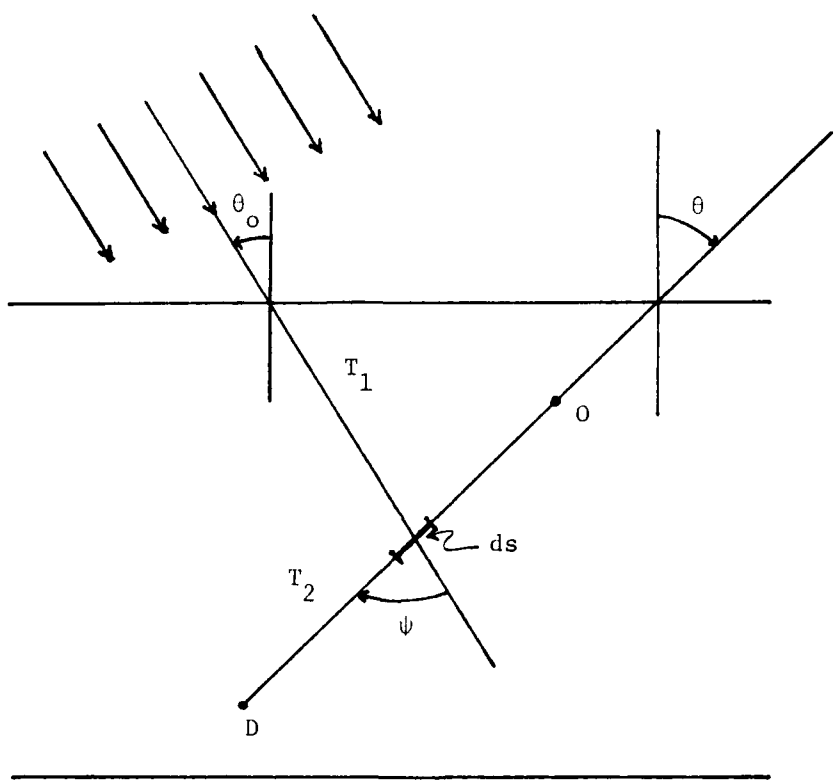


Fig. 3. Geometry for Calculation of Single Scattered Path Radiance

The background radiance obtained from single scattering may be computed by placing a hypothetical target on either the top of the atmosphere or on the ground surface, depending upon whether the sensor polar angle  $\theta$  is less than, or greater than  $90^\circ$ , respectively.

SPOT utilizes numerical methods in order to evaluate the integral in Eq. 29. The spectral transmission terms in Eq. 29 are obtained by two calls to LOWTRAN 4 for the atmospheric paths between the detector and collision point along the sensor's line-of-sight ( $T_2$ , see Fig. 3) and between the collision point and the top of the atmosphere in direction  $\theta_o(T_1)$ . Currently LOWTRAN 4 must be called for each collision point.

The scattering coefficient is calculated as the sum of the molecular and aerosol scattering coefficients

$$\Sigma_S(\lambda, s) = \Sigma_{RS}(\lambda, s) + \Sigma_{AS}(\lambda, s) \quad (30)$$

for each altitude for which the atmospheric layers are defined. An interpolation procedure is applied to give the value of the scattering coefficient at the altitude  $h$  that corresponds to position  $s$ . The necessary equations for the calculation of the coefficients are extracted from LOWTRAN 4.

The normalized phase function is obtained through the relation

$$P(\lambda, \psi, s) = \frac{1}{\Sigma_S(\lambda, s)} \cdot (\Sigma_{RS}(\lambda, s) \cdot P_R(\psi) + \Sigma_{AS}(\lambda, s) \cdot P_A(\lambda, \psi)) \quad (31)$$

where  $P_R$  and  $P_A$  denote the phase functions for Rayleigh and aerosol scattering, respectively. The aerosol phase function is obtained from the data base HAZESDATA (section 3.2.4) by an interpolation procedure with respect to wavelength, for each of the wavelengths considered. A second interpolation is applied with respect to angle in order to obtain the correct value of the aerosol phase function for the scattering angle  $\psi$ . The phase function for molecular (Rayleigh) scattering is obtained by use of the equation

$$P_R(\psi) = \frac{3}{16} \cdot \frac{1+\Delta}{1+\Delta/2} \cdot \left(1 + \frac{1-\Delta}{1+\Delta} \cos^2 \psi\right) \quad (32)$$

where  $\psi$  is the scattering angle and  $\Delta$  is the depolarization factor accounting

for the anisotropy of air molecules. Using Kasten's value of  $\Delta = 0.0295$  (Ref. 14), the phase function for Rayleigh scattering is then given by

$$P_R(\psi) = 0.03078 + 0.02854 \cdot \cos^2 \psi . \quad (32a)$$

Finally, the scattering angle  $\psi$  is obtained from a knowledge of the solar inclination angle  $\theta_o$ , and the polar and azimuthal angle  $\theta$  and  $\alpha$  defining the sensor's line-of-sight as

$$\cos \psi = \cos \theta \cdot \cos \theta_o + \sin \theta \cdot \sin \theta_o \cdot \cos \alpha . \quad (33)$$

In order to evaluate the integral given in Eq. 29, different methods must be used depending upon the geometry and whether the total background path radiance or the partial path radiance between the sensor and the target is to be calculated. For the partial path radiance, the line-of-sight is divided into equal increments less than 0.5 km in length. For the total path radiance, the same method is used if the observer's line-of-sight is directed towards the ground surface. If the line-of-sight is directed towards the top of the atmosphere, the total path radiance is obtained by placing the collision points at the midpoints of the atmospheric layers.

For the singularity in which both the sensor and target are at the same altitude  $h$  ( $\theta = 90^\circ$ ), the integral (Eq. 29) is replaced by the equation

$$PR(\lambda) = SS(\lambda) \cdot T_1(\lambda, h) \cdot \Sigma_S(\lambda, h) \cdot P(\lambda, h) \cdot \int_0^L T_2(\lambda, s) ds . \quad (29a)$$

When calculating the total background path radiance, the integral in Eq. 29a should be evaluated to an infinite distance  $L$ . In SPOT, the integral is solved by using equal increments of  $ds = 0.5$  km and by calculating the sum

$$SUM(s) = SUM(s) + 0.5 \sum_{i=1}^{NW} T_2(\lambda_i, s)$$

where the summation is terminated if either the value of  $SUM(s)$  does not change by more than 0.1 percent or if a distance of  $L = 40$  km is reached.

The computational procedure described herein provides the spectral path radiance incident at a point detector, normal to the direction of propagation, in units of watts  $m^{-2} \mu m^{-1} sr^{-1}$ . This method of evaluating the path radiance has been verified by comparing the total path radiance as calculated by SPOT with data obtained from the BRITE Monte Carlo program (Ref. 15) for similar atmospheric conditions and for sensor orientations defined for azimuthal angles of 0 and 180 degrees and polar angles between 0 and 85 degrees. Excellent agreement between the results from both calculational methods was achieved.

### 3.1.4 Target (or Ground) Reflection of Direct Sunlight or Moonlight

If a sensor is oriented such that its line-of-sight impinges upon a target (defined by the user), SPOT calculates the spectral radiance incident at the sensor due to the reflection of direct sunlight or moonlight (Eq. 9) by the target as

$$UTRF(\lambda) = SS(\lambda) \cdot (\alpha_t / \pi) \cos(\gamma) \cdot \cos(\beta) \cdot TRANS_1(\lambda) \cdot TRANS_2(\lambda) \quad (34)$$

where  $\beta$  and  $\gamma$  define the zenith angle, with respect to the target normal, of the incident and reflected radiation, respectively, (Fig. 2). The parameter  $TRANS_1(\lambda)$  defines the atmospheric transmittance for the line-of-sight between the target and the detector. The atmospheric transmittance from the top of the atmosphere to the target, along the solar inclination angle  $\theta_0$ , is given by  $TRANS_2(\lambda)$ . The source term  $SS(\lambda)$  is as described previously. This expression yields the spectral radiance incident upon a point detector as energy per unit time per unit area (normal to the direction of propagation) per unit spectral interval per unit solid angle, or more specifically as watts  $m^{-2} \mu m^{-1} sr^{-1}$ .

In the equation given above, the reflection surface was characterized as a Lambertian reflector with albedo  $\alpha_t$ . If the user so chooses, he may define the reflection properties of the target as isotropic, in which case the uncollided target reflection of direct sunlight (or moonlight) becomes

$$UTRF(\lambda) = SS(\lambda) \cdot (\alpha_t / 2\pi) \cos(\beta) \cdot TRANS_1(\lambda) \cdot TRANS_2(\lambda) \quad . \quad (35)$$

For situations in which the sensor's line-of-sight is directed toward the ground, the reflection of direct sunlight (or moonlight) by the ground (Eq. 4) is calculated by the expression

$$UERF(\lambda) = SS(\lambda) \cdot (\alpha_0 / \pi) \cos(\gamma) \cdot \cos(\beta) \cdot \text{TRANS}_1(\lambda) \cdot \text{TRANS}_2(\lambda) \quad (36)$$

for a Lambertian reflection surface, or by

$$UERF(\lambda) = SS(\lambda) \cdot (\alpha_0 / 2\pi) \cos(\beta) \cdot \text{TRANS}_1(\lambda) \cdot \text{TRANS}_2(\lambda) \quad (37)$$

for a surface characterized by isotropic reflection.

### 3.1.5 Uncollided Atmospheric Emission

LOWTRAN 4 calculates the spectral radiance due to uncollided thermal radiation produced by atmospheric emission along a given line-of-sight (Ref. 11). The numerical integration of the radiance (Eq. 20) along the line-of-sight is given by

$$\begin{aligned} UAE(\bar{v}) = \sum_{i=1}^{N-1} & \left( \overline{\text{TRANS}}_a(i) - \overline{\text{TRANS}}_a(i+1) \right) \cdot \text{BLACK} \left[ \bar{v}, \frac{\text{TEMP}(i) + \text{TEMP}(i+1)}{2} \right] \\ & \cdot \left[ \frac{\overline{\text{TRANS}}_s(i) + \overline{\text{TRANS}}_s(i+1)}{2} \right] \end{aligned} \quad (38)$$

for an atmosphere characterized by a series of isothermal layers. Contributions from each atmospheric layer along the line-of-sight are summed as shown by the expression given above, where

$\overline{\text{TRANS}}_a(i)$  = average transmittance due to atmospheric absorption in the  $i$ th layer along the line-of sight

$\overline{\text{TRANS}}_s(i)$  = average transmittance due to atmospheric scattering in the  $i$ th layer along the line-of-sight

$\text{TEMP}(i)$  = absolute temperature of the  $i$ th isothermal atmospheric layer

$\bar{v}$  = average frequency at which transmittances are calculated

$\text{BLACK}(\bar{v}, t)$  = blackbody function evaluated at the frequency  $\bar{v}$  and the absolute temperature  $t$  (Eq. 15).

The atmospheric radiance calculated by LOWTRAN 4 is an average (over a  $20 \text{ cm}^{-1}$  interval) centered at the frequency of interest  $\nu$ , the units of which are watts  $\text{m}^{-2} \mu\text{m}^{-1} \text{sr}^{-1}$ .

The SPOT code employs the LOWTRAN 4 evaluation of atmospheric radiance in order to calculate the spectral radiance incident at a sensor resulting from atmospheric emission of thermal radiation between the sensor and one of three points of interest:

- (1) a target which lies along the sensor's line-of-sight,
- (2) the ground surface if the sensor is looking downward, or
- (3) the top of the atmosphere if the sensor is looking upward.

### 3.1.6 Uncollided Target (or Ground) Emission

The SPOT program evaluates the uncollided spectral radiance incident at a sensor resulting from target (or ground) emission of thermal radiation (Eqs. 16 and 19) by the equation

$$\text{UTEM}(\lambda) = E_t \cdot \cos(\gamma) \cdot \text{BLACK}(\lambda, T_t) \cdot \text{TRANS}(\lambda) \quad (39)$$

where  $E_t$  and  $T_t$  define the emissivity and absolute temperature respectively of the emitting surface and  $\gamma$  defines the zenith angle of the emitted radiation (with respect to the surface normal). The directional emissive power normal to the surface is given by the blackbody function,  $\text{BLACK}(\lambda, T_t)$  (Eq. 15). LOWTRAN 4 is used to calculate the atmospheric transmittance  $\text{TRANS}(\lambda)$  along the line-of-sight between the sensor and the emitting surface. The expression cited above indicates the spectral radiance incident upon a point detector in units of watts  $\text{m}^{-2} \mu\text{m}^{-1} \text{sr}^{-1}$  (i.e., energy per unit time per unit area (normal to the direction of propagation) per unit spectral interval per unit solid angle).

## 3.2 Data Base

3.2.1 Extraterrestrial Solar Spectrum

Several of the radiative components evaluated by SPOT require values for the extraterrestrial solar spectral irradiance,  $SS(\lambda)$ . In order to provide sufficient detail to the calculations, these data are taken from a data base compiled by Thekaekara (Ref. 16). Two sets of data are utilized by the SPOT code. The first set represents standard values of the solar constant ( $1353 \text{ w m}^{-2}$ ) and extraterrestrial solar spectral irradiance. The spectral irradiance data represent values averaged over finite bandwidths centered at  $\lambda$ , in  $\text{watt m}^{-2} \mu\text{m}^{-1}$ , where  $\lambda$  ranges from .115 to 1000. ( $\mu\text{m}$ ). Bandwidths ranged from (all units in  $\mu\text{m}$ ) 0.01 for  $0.3 < \lambda < 0.75$ ; 0.05 for  $0.75 < \lambda < 1.0$ ; 0.1 for  $1.0 < \lambda < 5.0$ . Shown in Fig. 4 are the standard solar irradiance values as extracted from Ref. 16.

In the visible and near uv portions of the spectrum, the standard solar irradiance data are too widely spaced for many applications, such as atmospheric modeling, and transmittance/scattering in the atmosphere (Ref. 16). This inadequacy is due to the strong line absorption characteristic of the atmosphere in this spectral region. In order to circumvent this problem, Ref. 16 gives a more detailed spectrum obtained from solar scans made with a Perkin-Elmer, Model 112 monochromator. The new data, normalized to the standard curve described above, provides the extraterrestrial solar spectral irradiance at  $1\text{-}\text{\AA}$  intervals in the range  $3000\text{--}6100\text{ \AA}$ . SPOT makes use of the new, more detailed, data base whenever the wavelength of interest lies within the applicable range. The refined solar irradiance data, as taken from Ref. 16, are shown in Fig. 5.

3.2.2 Extraterrestrial Lunar Spectrum

The extraterrestrial lunar irradiance, considered by SPOT, incident at the top of the atmosphere is the result of lunar reflected sunlight. SPOT's calculation of the spectral irradiance is based upon Turner's derivation (Ref. 17) given by

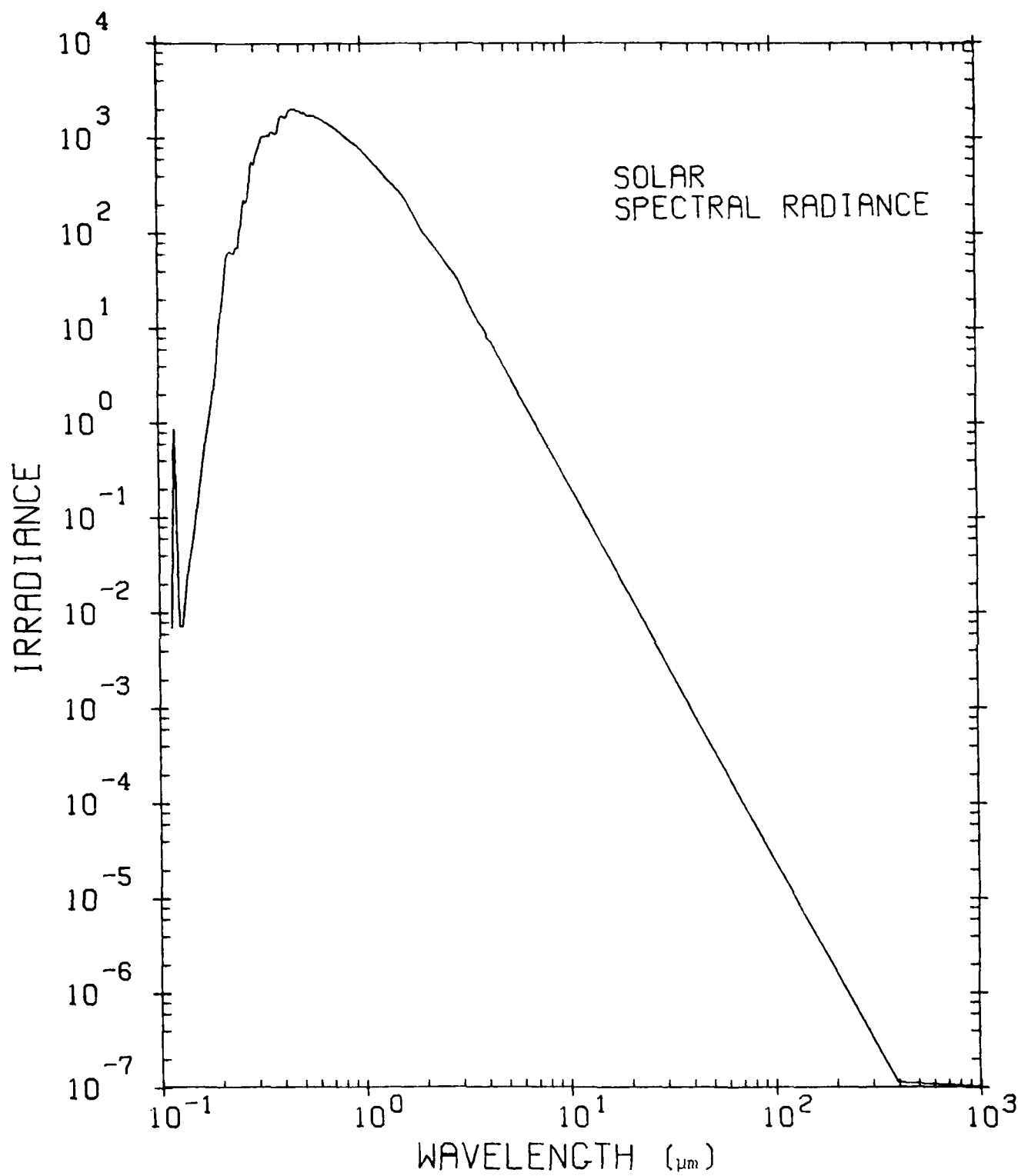


Fig. 4. Standard Values for the Extraterrestrial Solar Spectral Irradiance ( $\text{watts m}^{-2}\ \mu\text{m}^{-1}$ )

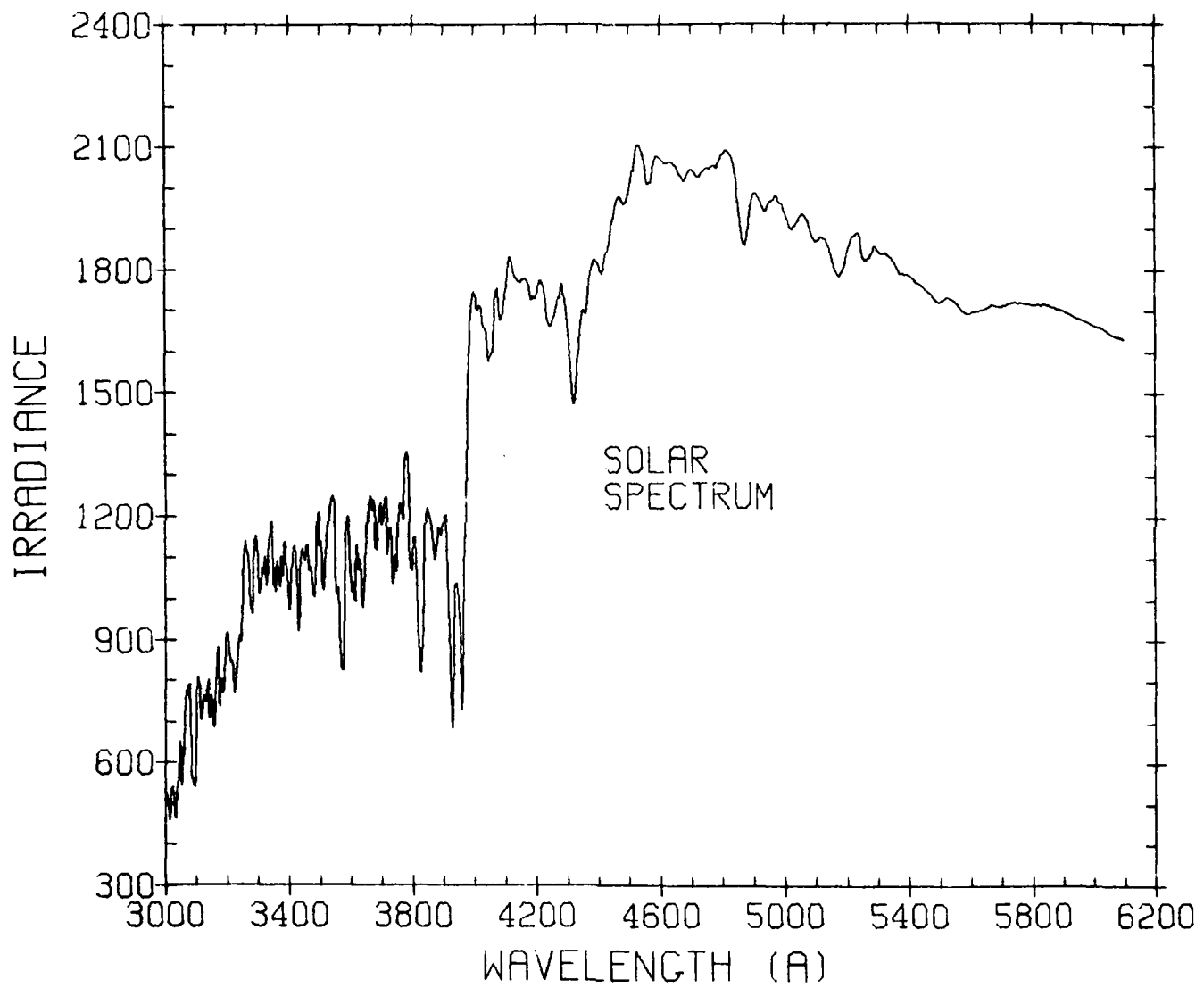


Fig. 5. Extraterrestrial Solar Spectral Irradiance ( $\text{watts m}^{-2} \mu\text{m}^{-1}$ ) for UV and Visible Regions

$$SMOON(\lambda) = 2.04472E-7 \cdot SOLARS(\lambda) \cdot ALBED(\lambda) \cdot PHAS(\chi) \quad (40)$$

where  $SOLARS(\lambda)$  is the extraterrestrial solar spectral irradiance (section 3.2.1),  $\chi$  is the phase angle for the moon,  $ALBED(\lambda)$  is the wavelength-dependent geometric albedo for the moon, and  $PHAS(\chi)$  is the phase function giving the relative intensity as a function of the phase angle. The lunar irradiance has the units  $\text{watts m}^{-2} \mu\text{m}^{-1}$ . Note that  $PHAS(\chi=0)=1$  for a full moon. Table I shows values of the phase function as obtained from measured data by Bullrich (Ref. 18). Values of the geometric albedo have been obtained from data of Candron, *et.al.* (Ref. 19) and of Lane and Irvine (Ref. 20). The geometric albedo is shown in Fig. 6 as a function of wavelength for the spectral region between  $0.2 \mu\text{m}$  and  $2.8 \mu\text{m}$ .

It should be noted that for wavelengths between  $0.1$  and  $0.2 (\mu\text{m})$ , SPOT employs a linear extrapolation of the geometric albedo data given between  $0.2$  and  $0.3 (\mu\text{m})$ . For wavelengths below  $0.1 (\mu\text{m})$ , a value of zero is assumed for the albedo. If the wavelength of interest is greater than or equal to  $5 (\mu\text{m})$ , an albedo of  $0.4$  is assumed. Finally, for wavelengths between  $2.8$  and  $5 (\mu\text{m})$ , an albedo equivalent to that for  $2.8 (\mu\text{m})$  is used. These computational limitations may restrict the validity of the lunar irradiance calculations to a spectral region given by  $0.2 - 2.8 (\mu\text{m})$ .

### 3.2.3 Atmospheric Models (LOWTRAN 4)

The atmospheric models utilized by the SPOT computer code are those which are available through LOWTRAN 4 (Ref. 11). In particular, they include the 1962 U.S. Standard Atmosphere (Ref. 21) and the five supplementary models:

- Tropical ( $15^{\circ}\text{N}$ )
- Midlatitude Summer ( $45^{\circ}\text{N}$ , July)
- Midlatitude Winter ( $45^{\circ}\text{N}$ , January)
- Subartic Summer ( $60^{\circ}\text{N}$ , July)
- Subartic Winter ( $60^{\circ}\text{N}$ , January).

Altitude-dependent data (pressure, temperature, water vapor density and ozone density) describing each of the models is provided in 1 km steps from 0 to 25 km, 5 km steps from 25 to 50 km, and at 70 km and 100 km. In addition to

TABLE I. THE INTEGRATED PHASE-CURVE OF THE MOON

Phase Angle (deg)	Relative Intensity
0	1.000
10	.732
20	.560
30	.423
40	.320
50	.233
60	.167
70	.124
80	.087
90	.067
100	.047
110	.036
120	.024
130	.012
140	.009
150	.004
160	.00002

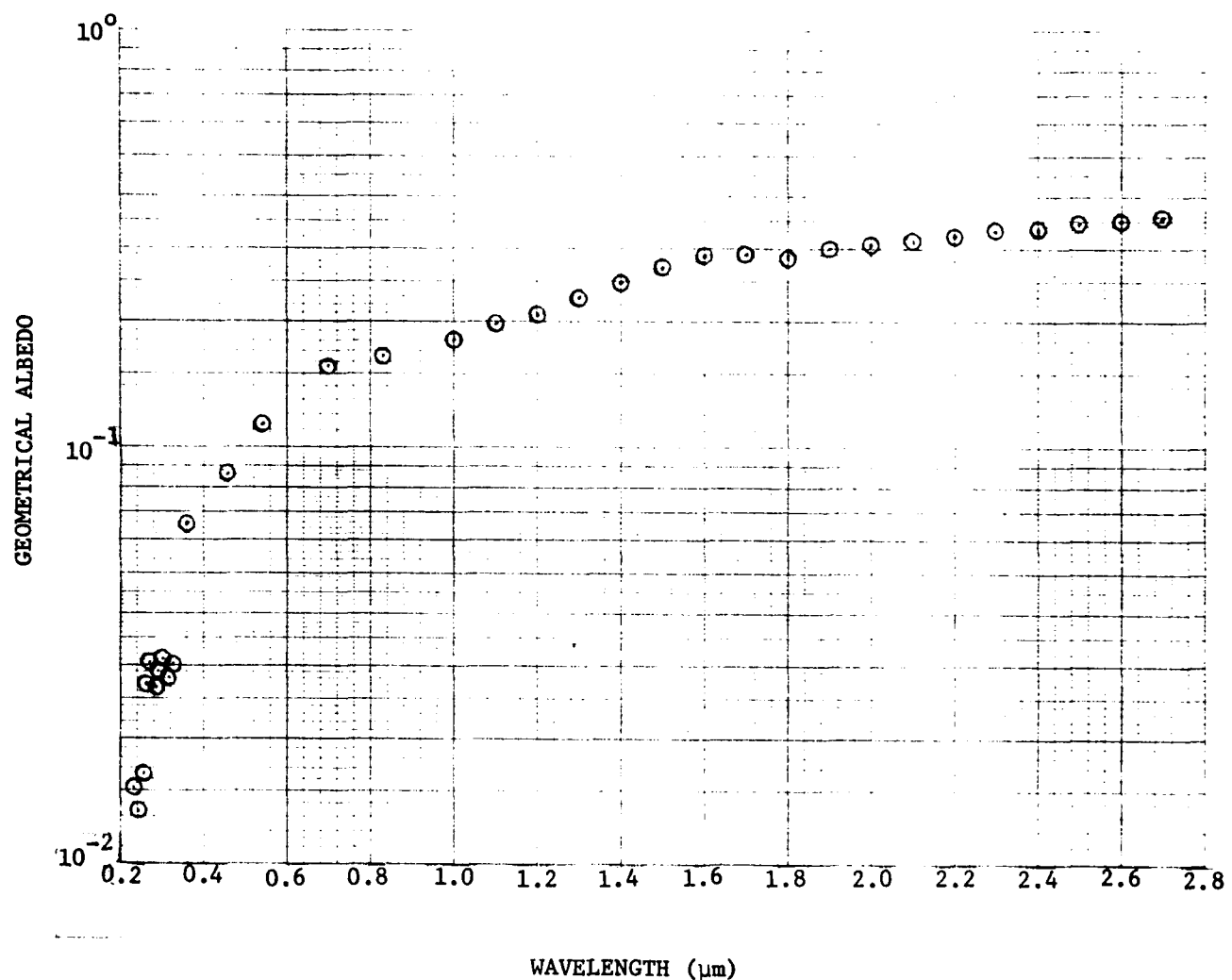


Fig. 6. Geometrical Albedo versus Wavelength for the Moon

the six models available in LOWTRAN 4, SPOT provides the user with the option of inserting his own model atmosphere (consistent with the format utilized by the LOWTRAN 4 data). Each of the five supplementary models described is shown in tabular form in TABLES II - VI (taken from Ref. 22).

Four aerosol models are available for use with the LOWTRAN 4 code. These data represent the wavelengths ( $\mu\text{m}$ ) and the extinction and absorption coefficients ( $\text{km}^{-1}$ ) for the maritime, urban, rural, and tropospheric aerosol models as developed by Shettle and Fenn (Ref. 23). Size distributions for the rural and maritime aerosol models are shown in Figs. 7 and 8 (taken from Ref. 23). The urban aerosol model has the same size distribution as the rural model. The tropospheric model has the same size distribution as the small particle portion of the urban and rural models, indicated by  $n_1(r)$  shown in Fig. 7. Also shown in Fig. 7 is the modified Haze C size distribution, indicated for comparative purposes. Extinction coefficients for each of the aerosol models is shown in Fig. 9 (taken from Ref. 23) as a function of wavelength for a ground level meteorological range of 23 km.

### 3.2.4 Aerosol Data Base (HAZESDATA)

A preliminary data base has been compiled that provides angular scattering data for atmospheric aerosols at a number of wavelengths. A model similar to Deirmendjian's Haze C model (Ref. 9) was chosen to describe the size distribution of the aerosol particles. The indices of refraction, as a function of wavelength, were taken from data provided by Volz (Ref. 24). It is assumed that the aerosols contain seventy per cent water solubles and thirty per cent dust-like aerosols.

This model was chosen mainly because a data base for the model already existed from previous RRA calculations for wavelengths less than 5  $\mu\text{m}$ . Therefore, only the data for larger wavelengths had to be computed. The model chosen is very similar to the aerosol model used in previous versions of LOWTRAN (Refs. 25,26). However, the upper limit of the size distribution was assumed to be 20  $\mu\text{m}$ ; the aerosol models in LOWTRAN 2 and LOWTRAN 3 use upper limits of 10 and 100  $\mu\text{m}$ , respectively.

The new versions of LOWTRAN (Refs. 27,11) use a total number of four

TABLE II. TROPICAL ( $15^{\circ}\text{N}$ ) MODEL ATMOSPHERE

TROPICAL					
Ht. (km)	Pressure (mb)	Temp. ( $^{\circ}\text{K}$ )	Density ( $\text{g}/\text{m}^3$ )	Water Vapor ( $\text{g}/\text{m}^3$ )	Ozone ( $\text{g}/\text{m}^3$ )
0	1.013E+03	300.0	1.167E+03	1.9E+01	5.6E-05
1	9.040E+02	294.0	1.064E+03	1.3E+01	5.6E-05
2	8.050E+02	288.0	9.689E+02	9.3E+00	5.4E-05
3	7.150E+02	284.0	8.756E+02	4.7E+00	5.1E-05
4	6.330E+02	277.0	7.951E+02	2.2E+00	4.7E-05
5	5.590E+02	270.0	7.199E+02	1.5E+00	4.5E-05
6	4.920E+02	264.0	6.501E+02	8.5E-01	4.3E-05
7	4.320E+02	257.0	5.855E+02	4.7E-01	4.1E-05
8	3.780E+02	250.0	5.258E+02	2.5E-01	3.9E-05
9	3.290E+02	244.0	4.708E+02	1.2E-01	3.9E-05
10	2.860E+02	237.0	4.202E+02	5.0E-02	3.9E-05
11	2.470E+02	230.0	3.740E+02	1.7E-02	4.1E-05
12	2.130E+02	224.0	3.316E+02	6.0E-03	4.3E-05
13	1.820E+02	217.0	2.929E+02	1.8E-03	4.5E-05
14	1.560E+02	210.0	2.578E+02	1.0E-03	4.5E-05
15	1.320E+02	204.0	2.260E+02	7.6E-04	4.7E-05
16	1.110E+02	197.0	1.972E+02	6.4E-04	4.7E-05
17	9.370E+01	195.0	1.676E+02	5.6E-04	6.9E-05
18	7.890E+01	199.0	1.382E+02	5.0E-04	9.0E-05
19	6.660E+01	203.0	1.145E+02	4.9E-04	1.4E-04
20	5.650E+01	207.0	9.515E+01	4.5E-04	1.9E-04
21	4.800E+01	211.0	7.938E+01	5.1E-04	2.4E-04
22	4.090E+01	215.0	6.645E+01	5.1E-04	2.8E-04
23	3.500E+01	217.0	5.618E+01	5.4E-04	3.2E-04
24	3.000E+01	219.0	4.763E+01	6.0E-04	3.4E-04
25	2.570E+01	221.0	4.045E+01	6.7E-04	3.4E-04
30	1.220E+01	232.0	1.831E+01	3.6E-04	2.4E-04
35	6.000E+00	243.0	8.600E+00	1.1E-04	9.2E-05
40	3.050E+00	254.0	4.181E+00	4.3E-05	4.1E-05
45	1.590E+00	265.0	2.097E+00	1.9E-05	1.3E-05
50	8.540E-01	270.0	1.101E+00	6.3E-06	4.3E-06
70	5.790E-02	219.0	9.210E-02	1.4E-07	8.6E-08
100	3.000E-04	210.0	5.000E-04	1.0E-09	4.3E-11

TABLE III. MIDLATITUDE SUMMER (45°N, JULY) MODEL ATMOSPHERE

MIDLATITUDE SUMMER					
Ht. (km)	Pressure (mb)	Temp. (°K)	Density (g/m <sup>3</sup> )	Water Vapor (g/m <sup>3</sup> )	Ozone (g/m <sup>3</sup> )
0	1.013E+03	294.0	1.191E+03	1.4E+01	6.0E-05
1	9.020E+02	290.0	1.080E+03	9.3E+00	6.0E-05
2	8.020E+02	285.0	9.757E+02	5.9E+00	6.0E-05
3	7.100E+02	279.0	8.846E+02	3.3E+00	6.2E-05
4	6.280E+02	273.0	7.998E+02	1.9E+00	6.4E-05
5	5.540E+02	267.0	7.211E+02	1.0E+00	6.6E-05
6	4.870E+02	261.0	6.487E+02	6.1E-01	6.9E-05
7	4.260E+02	255.0	5.830E+02	3.7E-01	7.5E-05
8	3.720E+02	248.0	5.225E+02	2.1E-01	7.9E-05
9	3.240E+02	242.0	4.669E+02	1.2E-01	8.6E-05
10	2.810E+02	235.0	4.159E+02	6.4E-02	9.0E-05
11	2.430E+02	229.0	3.693E+02	2.2E-02	1.1E-04
12	2.090E+02	222.0	3.269E+02	6.0E-03	1.2E-04
13	1.790E+02	216.0	2.882E+02	1.8E-03	1.5E-04
14	1.530E+02	216.0	2.464E+02	1.0E-03	1.8E-04
15	1.300E+02	216.0	2.104E+02	7.6E-04	1.9E-04
16	1.110E+02	216.0	1.797E+02	6.4E-04	2.1E-04
17	9.500E+01	216.0	1.535E+02	5.6E-04	2.4E-04
18	8.120E+01	216.0	1.305E+02	5.0E-04	2.8E-04
19	6.950E+01	217.0	1.110E+02	4.9E-04	3.2E-04
20	5.950E+01	218.0	9.453E+01	4.5E-04	3.4E-04
21	5.100E+01	219.0	8.056E+01	5.1E-04	3.6E-04
22	4.370E+01	220.0	6.872E+01	5.1E-04	3.6E-04
23	3.760E+01	222.0	5.867E+01	5.4E-04	3.4E-04
24	3.220E+01	223.0	5.014E+01	6.0E-04	3.2E-04
25	2.770E+01	224.0	4.288E+01	6.7E-04	3.0E-04
30	1.320E+01	234.0	1.322E+01	3.6E-04	2.0E-04
35	6.520E+00	245.0	6.519E+00	1.1E-04	9.2E-05
40	3.330E+00	258.0	3.330E+00	4.3E-05	4.1E-05
45	1.760E+00	270.0	1.757E+00	1.9E-05	1.3E-05
50	9.510E-01	276.0	9.512E-01	6.3E-06	4.3E-06
70	6.710E-02	218.0	6.706E-02	1.4E-07	8.6E-08
100	3.000E-04	210.0	5.000E-04	1.0E-09	4.3E-11

TABLE IV. MIDLATITUDE WINTER (45°N, JANUARY) MODEL ATMOSPHERE

MIDLATITUDE WINTER					
Ht. (km)	Pressure (mb)	Temp. (°K)	Density (g/m <sup>3</sup> )	Water Vapor (g/m <sup>3</sup> )	Ozone (g/m <sup>3</sup> )
0	1.018E+03	272.2	1.301E+03	3.5E+00	6.0E-05
1	8.973E+02	268.7	1.162E+03	2.5E+00	5.4E-05
2	7.897E+02	265.2	1.037E+03	1.8E+00	4.9E-05
3	6.938E+02	261.7	9.230E+02	1.2E+00	4.9E-05
4	6.081E+02	255.7	8.282E+02	6.6E-01	4.9E-05
5	5.313E+02	249.7	7.411E+02	3.8E-01	5.8E-05
6	4.627E+02	243.7	6.614E+02	2.1E-01	6.4E-05
7	4.016E+02	237.7	5.886E+02	8.5E-02	7.7E-05
8	3.473E+02	231.7	5.222E+02	3.5E-02	9.0E-05
9	2.992E+02	225.7	4.619E+02	1.6E-02	1.2E-04
10	2.568E+02	219.7	4.072E+02	7.5E-03	1.6E-04
11	2.199E+02	219.2	3.496E+02	6.9E-03	2.1E-04
12	1.882E+02	218.7	2.999E+02	6.0E-03	2.6E-04
13	1.610E+02	218.2	2.572E+02	1.8E-03	3.0E-04
14	1.378E+02	217.7	2.206E+02	1.0E-03	3.2E-04
15	1.178E+02	217.2	1.890E+02	7.6E-04	3.4E-04
16	1.007E+02	216.7	1.620E+02	6.4E-04	3.6E-04
17	8.610E+01	216.2	1.388E+02	5.6E-04	3.9E-04
18	7.350E+01	215.7	1.188E+02	5.0E-04	4.1E-04
19	6.280E+01	215.2	1.017E+02	4.9E-04	4.3E-04
20	5.370E+01	215.2	8.690E+01	4.5E-04	4.5E-04
21	4.580E+01	215.2	7.421E+01	5.1E-04	4.3E-04
22	3.910E+01	215.2	6.338E+01	5.1E-04	4.3E-04
23	3.340E+01	215.2	5.415E+01	5.4E-04	3.9E-04
24	2.860E+01	215.2	4.624E+01	6.0E-04	3.6E-04
25	2.430E+01	215.2	3.950E+01	6.7E-04	3.4E-04
30	1.110E+01	217.4	1.783E+01	3.6E-04	1.9E-04
35	5.180E+00	227.8	7.924E+00	1.1E-04	9.2E-05
40	2.530E+00	243.2	3.625E+00	4.3E-05	4.1E-05
45	1.290E+00	258.5	1.741E+00	1.9E-05	1.3E-05
50	6.820E-01	265.7	8.954E-01	6.3E-06	4.3E-06
70	4.670E-02	230.7	7.051E-02	1.4E-07	8.6E-08
100	3.000E-04	210.2	5.000E-04	1.0E-09	4.3E-11

TABLE V. SUBARCTIC SUMMER ( $60^{\circ}\text{N}$ , JULY) MODEL ATMOSPHERE

SUBARCTIC SUMMER					
Ht. (km)	Pressure (mb)	Temp. ( $^{\circ}\text{K}$ )	Density ( $\text{g}/\text{m}^3$ )	Water Vapor ( $\text{g}/\text{m}^3$ )	Ozone ( $\text{g}/\text{m}^3$ )
0	1.010E+03	287.0	1.220E+03	9.1E+00	4.9E-05
1	8.960E+02	282.0	1.110E+03	6.0E+00	5.4E-05
2	7.929E+02	276.0	9.971E+02	4.2E+00	5.6E-05
3	7.000E+02	271.0	8.985E+02	2.7E+00	5.8E-05
4	6.160E+02	266.0	8.077E+02	1.7E+00	6.0E-05
5	5.410E+02	260.0	7.244E+02	1.0E+00	6.4E-05
6	4.730E+02	253.0	6.519E+02	5.4E-01	7.1E-05
7	4.130E+02	246.0	5.849E+02	2.9E-01	7.5E-05
8	3.590E+02	239.0	5.231E+02	1.3E-02	7.9E-05
9	3.107E+02	232.0	4.663E+02	4.2E-02	1.1E-04
10	2.677E+02	225.0	4.142E+02	1.5E-02	1.3E-04
11	2.300E+02	225.0	3.559E+02	9.4E-03	1.8E-04
12	1.977E+02	225.0	3.059E+02	6.0E-03	2.1E-04
13	1.700E+02	225.0	2.630E+02	1.8E-03	2.6E-04
14	1.460E+02	225.0	2.260E+02	1.0E-03	2.8E-04
15	1.250E+02	225.0	1.943E+02	7.6E-04	3.2E-04
16	1.080E+02	225.0	1.671E+02	6.4E-04	3.4E-04
17	9.280E+01	225.0	1.436E+02	5.6E-04	3.9E-04
18	7.980E+01	225.0	1.235E+02	5.0E-04	4.1E-04
19	6.860E+01	225.0	1.062E+02	4.9E-04	4.1E-04
20	5.890E+01	225.0	9.128E+01	4.5E-04	3.9E-04
21	5.070E+01	225.0	7.849E+01	5.1E-04	3.6E-04
22	4.360E+01	225.0	6.750E+01	5.1E-04	3.2E-04
23	3.750E+01	225.0	5.805E+01	5.4E-04	3.0E-04
24	3.227E+01	226.0	4.963E+01	6.0E-04	2.8E-04
25	2.780E+01	228.0	4.247E+01	6.7E-04	2.6E-04
30	1.340E+01	235.0	1.338E+01	3.6E-04	1.4E-04
35	6.610E+00	247.0	6.614E+00	1.1E-04	9.2E-05
40	3.400E+00	262.0	3.404E+00	4.3E-05	4.1E-05
45	1.810E+00	274.0	1.817E+00	1.9E-05	1.3E-05
50	9.870E-01	277.0	9.868E-01	6.3E-06	4.3E-06
70	7.070E-02	216.0	7.071E-02	1.4E-07	8.6E-08
100	3.000E-04	210.0	5.000E-04	1.0E-09	4.3E-11

TABLE VI. SUBARCTIC WINTER ( $60^{\circ}\text{N}$ , JANUARY) MODEL ATMOSPHERE

SUBARCTIC WINTER					
Ht. (km)	Pressure (mb)	Temp. ( $^{\circ}\text{K}$ )	Density ( $\text{g}/\text{m}^3$ )	Water Vapor ( $\text{g}/\text{m}^3$ )	Ozone ( $\text{g}/\text{m}^3$ )
0	1.013E+03	257.1	1.372E+03	1.2E+00	4.1E-05
1	8.878E+02	259.1	1.193E+03	1.2E+00	4.1E-05
2	7.775E+02	255.9	1.058E+03	9.4E-01	4.1E-05
3	6.798E+02	252.7	9.366E+02	6.8E-01	4.3E-05
4	5.932E+02	247.7	8.339E+02	4.1E-01	4.5E-05
5	5.158E+02	240.9	7.457E+02	2.0E-01	4.7E-05
6	4.467E+02	234.1	6.646E+02	9.8E-02	4.9E-05
7	3.853E+02	227.3	5.904E+02	5.4E-02	7.1E-05
8	3.308E+02	220.6	5.226E+02	1.1E-02	9.0E-05
9	2.829E+02	217.2	4.538E+02	8.4E-03	1.6E-04
10	2.418E+02	217.2	3.879E+02	5.5E-03	2.4E-04
11	2.067E+02	217.2	3.315E+02	3.8E-03	3.2E-04
12	1.766E+02	217.2	2.834E+02	2.6E-03	4.3E-04
13	1.510E+02	217.2	2.422E+02	1.8E-03	4.7E-04
14	1.291E+02	217.2	2.071E+02	1.0E-03	4.9E-04
15	1.103E+02	217.2	1.770E+02	7.6E-04	5.6E-04
16	9.431E+01	216.6	1.517E+02	6.4E-04	6.2E-04
17	8.058E+01	216.0	1.300E+02	5.6E-04	6.2E-04
18	6.882E+01	215.4	1.113E+02	5.0E-04	6.2E-04
19	5.875E+01	214.8	9.529E+01	4.9E-04	6.0E-04
20	5.014E+01	214.1	8.155E+01	4.5E-04	5.6E-04
21	4.277E+01	213.6	6.976E+01	5.1E-04	5.1E-04
22	3.647E+01	213.0	5.966E+01	5.1E-04	4.7E-04
23	3.109E+01	212.4	5.100E+01	5.4E-04	4.3E-04
24	2.649E+01	211.8	4.358E+01	6.0E-04	3.6E-04
25	2.256E+01	211.2	3.722E+01	6.7E-04	3.2E-04
30	1.020E+01	216.0	1.645E+01	3.6E-04	1.5E-04
35	4.701E+00	222.2	7.368E+00	1.1E-04	9.2E-05
40	2.243E+00	234.7	3.330E+00	4.3E-05	4.1E-05
45	1.113E+00	247.0	1.569E+00	1.9E-05	1.3E-05
50	5.719E-01	259.3	7.682E-01	6.3E-06	4.3E-06
70	4.016E-02	245.7	5.695E-02	1.4E-07	8.6E-08
100	3.000E-04	210.0	5.000E-04	1.0E-09	4.3E-11

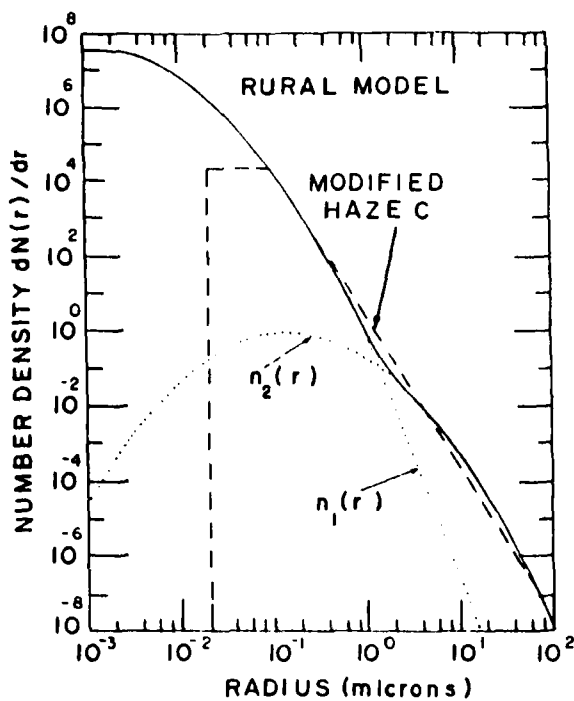


Fig. 7. Size Distribution for the Rural Aerosol Model (solid line) used in LOWTRAN 4. Also shown are the Modified Haze C Model (dashed line) and the Individual Log Normal Distribution (dotted lines) which make up the Rural Model.

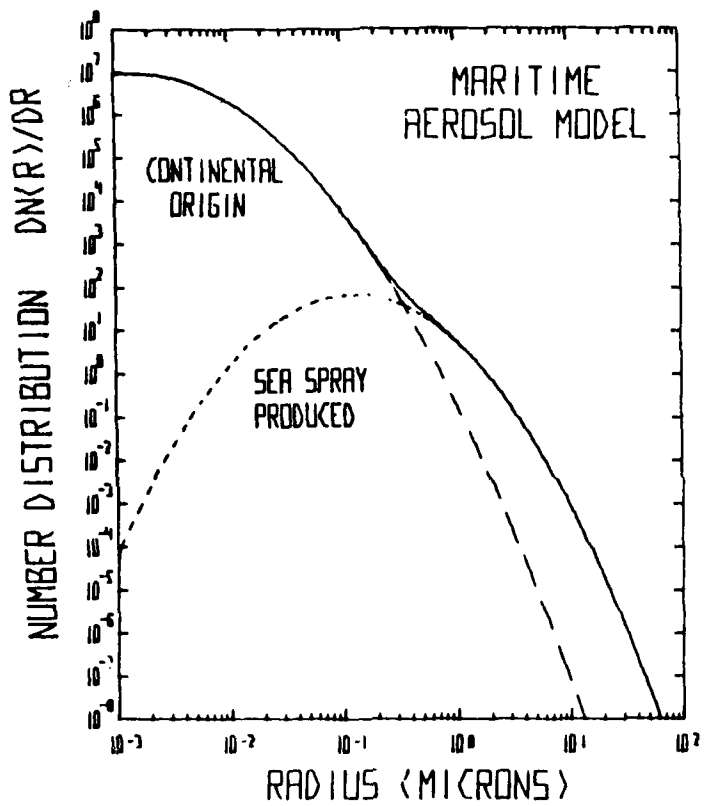


Fig. 8. Size Distribution for the Maritime Aerosol Model (solid line) used in LOWTRAN 4. Also shown are the Individual Distributions for the Aerosols of Continental Origin (long dashes) and the Sea Spray Produced Aerosols (short dashes).

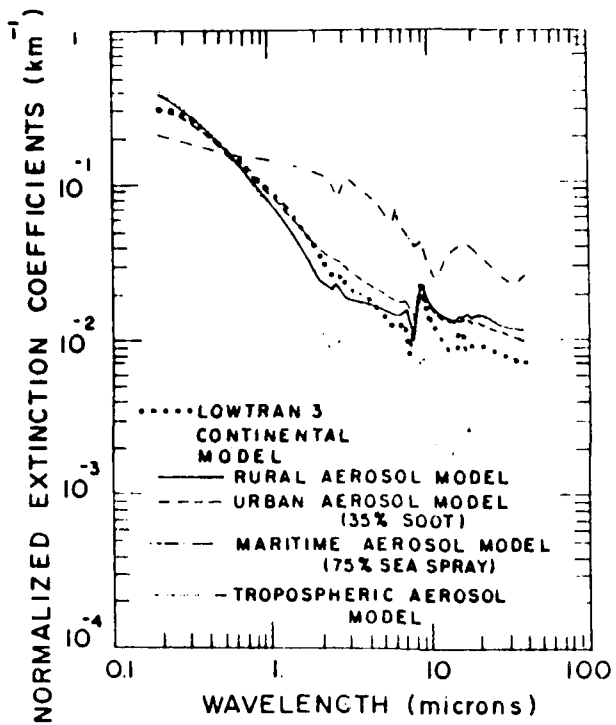


Fig. 9. Extinction Coefficients for the Four Aerosol Models used in LOWTRAN 4 as a Function of Wavelength. The Extinction at 0.55 microns corresponds to a Meteorological Range of 23 km.

aerosol models compiled by Shettle and Fenn (Ref. 23, see also Figs. 7 and 8). A comparison with these models reveals that the modified Haze C distribution (as currently used in SPOT) is very similar to the distributions chosen in LOWTRAN 3B for the rural and urban aerosol models. The extinction coefficients computed for the modified Haze C model (Fig. 10) show, therefore, a wavelength dependence similar to those computed for the urban and rural models in LOWTRAN (Fig. 9); the absorption properties are, however, different from the urban model. In the urban model it is assumed that the aerosols consist of 49 per cent water solubles, 21 per cent dust and 30 per cent highly absorbing soot particles. The chemical properties of the rural model are identical to those chosen for the modified Haze C model.

The indices of refraction, for the aerosol model chosen, are given in Ref. 8 together with the computed attenuation coefficients and other optical parameters. The attenuation coefficients for the model are plotted in Fig. 10 for a total of 59 wavelengths. Fig. 11 shows the dependence of the normalized phase function on wavelength for scattering angles of 0, 30, 90 and 180 degrees. It can be seen that the phase function at  $0^\circ$  varies approximately with  $\lambda^{-2}$ . The phase function at  $30^\circ$  scattering angle is nearly independent of wavelength with an average value of approximately  $0.28 \text{ sr}^{-1}$ . The dependence of the phase function on wavelength for angles of  $90^\circ$  and  $180^\circ$  is highly irregular and fluctuates between  $6.3 \cdot 10^{-3}$  and  $4.2 \cdot 10^{-2} \text{ sr}^{-1}$ .

A comparison of Figs. 10 and 11 reveals that irregularities in the behavior of the phase function with wavelength are reflected in irregularities of the scattering and absorption coefficients. The largest variations occur in regions where the single scattering albedo (ratio of scattering-to-total coefficients) is drastically changing with wavelength, i.e. around 2.7, 6.0, 8.0 and 15  $\mu\text{m}$ . For the creation of the data base used in SPOT (HAZESDATA), the wavelengths for which the phase function are stored had to be chosen such that any interpolation between the phase function data for different wavelengths would not result in sizeable inaccuracies. The wavelengths were, therefore, centered around the absorption bands. Several wavelengths had to be chosen in the visible spectral

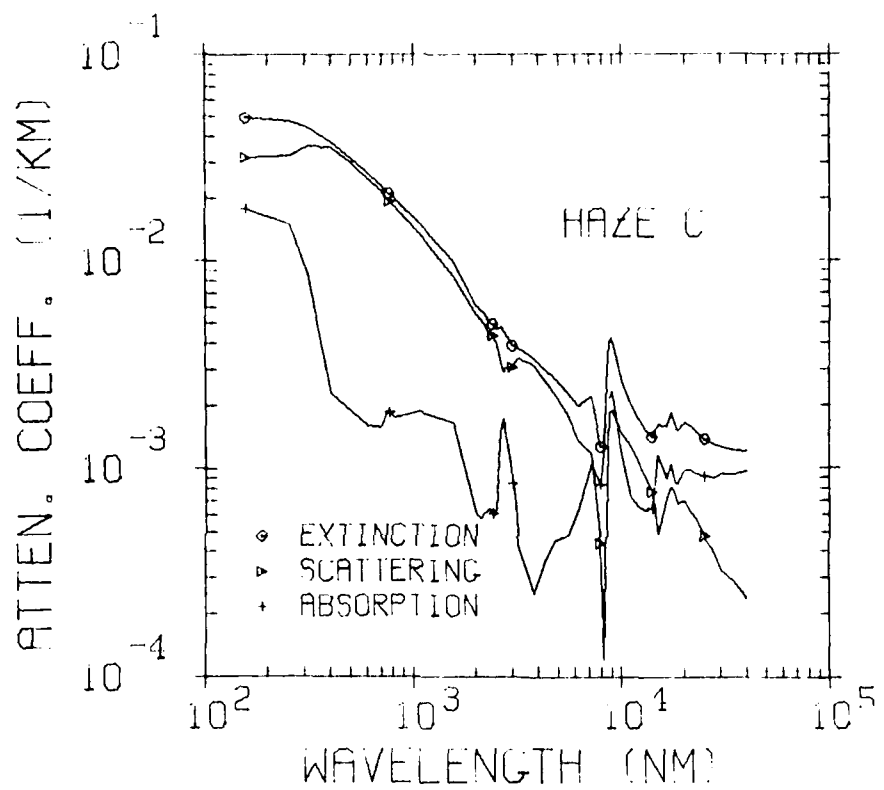


Fig. 10. Attenuation Coefficients for Modified Haze C Aerosol Distribution as a Function of Wavelength

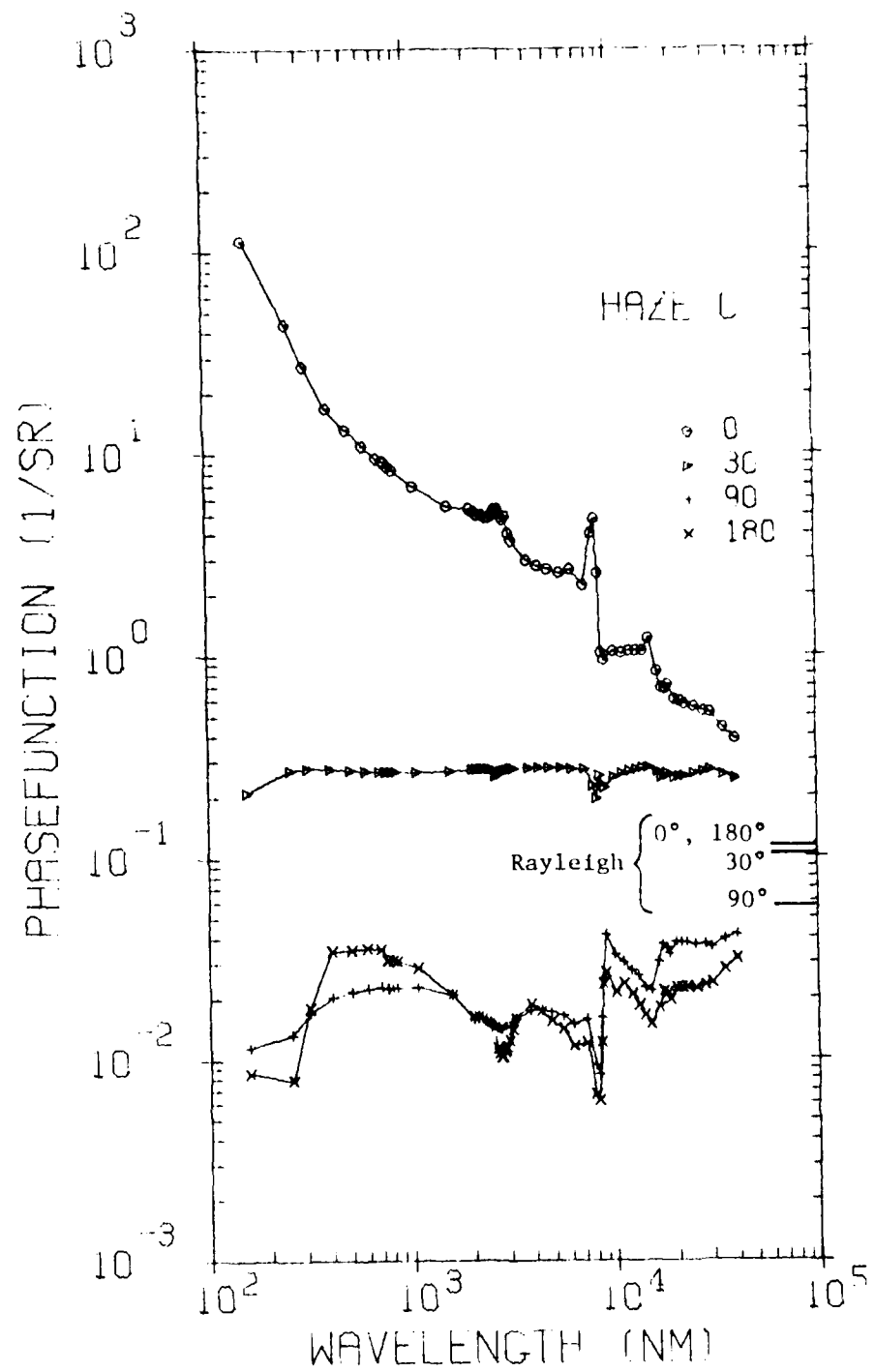


Fig. 11. Phase Function for Modified Haze C Aerosol Distribution as a Function of Wavelength, Scattering Angles of 0, 30, 90 and 180°

region since the phase function in this region varies greatly with wavelength, especially in the forward scattering angles. A total of 38 wavelengths were chosen for the data base, and are given in Table VII.

TABLE VII. WAVELENGTHS ( $\mu\text{m}$ ) CHOSEN FOR DATA BASE HAZESDATA.

0.16, 0.25, 0.31, 0.40, 0.50, 0.60, 0.70, 0.80, 0.84,
1.06, 1.55, 2.00, 2.20, 2.50, 2.75, 3.00, 3.20, 3.80,
4.30, 4.80, 5.50, 6.20, 7.20, 8.20, 8.50, 9.00, 10.0,
11.0, 13.0, 14.0, 15.0, 16.4, 18.0, 20.0, 25.0, 30.0, 35.0, 40.0

The scattering data for the aerosol model were originally computed for 116 different scattering angles for  $\lambda < 5\mu\text{m}$  and for 100 angles for  $\lambda > 5\mu\text{m}$ . A reduction of the number of angles for which the phase function is given must be accomplished such that an interpolation of the phase function with respect to scattering angle does not result in serious errors. The angles at which the phase function is defined, therefore, must be closely spaced in those intervals where the scattering data display large fluctuations. As a matter of convenience, for coding and usage, it is best to choose the same set of scattering angles for each wavelength at which the phase function is defined. The basic data (Ref. 8) were compiled to give the complete scattering matrix (four elements), however, only the phase function (average of first two elements) is used for the SPOT data. The final data base, HAZESDATA, was compiled for a total of 64 scattering angles with the angular increments varied as  $1^\circ$ ,  $2^\circ$ ,  $4^\circ$  and  $2^\circ$  in the regions between 0-10, 10-20, 20-140 and 140-180 degrees, respectively.

A further reduction of the data base requires a more detailed study of the angular and wavelength-dependent behavior of aerosol scattering. It is anticipated that the HAZESDATA data base will suffice for most atmospheric conditions. Advanced versions of SPOT would require similar data bases for other aerosol types such as maritime aerosol, fog, smoke, etc.

### 3.3 Program Logic

SPOT was designed as a preliminary version of an engineering-type predictive users code developed to simulate the radiative energy (signal) reaching a detector viewing any combination of natural and/or man-made features on the ground under illumination conditions resulting from sunlight, moonlight, and the thermal radiation emitted by the atmosphere, the ground, and any man-made features either on the ground or within the atmosphere. It was the intent of the authors to provide a computer code that offered the user flexibility through a number of computational options.

#### 3.3.1 Input

Basically, SPOT allows for the definition of a point monodirectional receiver located within a plane parallel atmosphere at an altitude ALT defined by the user. The sensor's line-of-sight is specified by the standard polar angles THETA and PHI ( $\theta, \phi$ ). The user establishes the radiative environment within which the sensor is to function via two input parameters, ISORC and ITARG. The first variable specifies the radiative source as

- ISORC = 0 sunlight only
- 1 moonlight only
- 2 thermal emission only
- 3 sunlight and thermal emission
- 4 moonlight and thermal emission

while the second parameter indicates the reflective/emissive components to be calculated by the program as

- ITARG = 0 background only
- 1 ground reflectance/emission
- 2 target and background reflectance/emmission.

Atmospheric conditions are specified through various input parameters. The input parameter MODEL identifies the atmospheric model to be used

- MODEL = 1 Tropical ( $15^{\circ}$ N)
- 2 Midlatitude Summer ( $45^{\circ}$ N, July)
- 3 Midlatitude Winter ( $45^{\circ}$ N, January)

- 4 Subarctic Summer ( $60^{\circ}$ N, July)
- 5 Subarctic Winter ( $60^{\circ}$ N, January)
- 6 1962 U. S. Standard Atmosphere .

If aerosol attenuation is to be included in the transmittance calculations performed by LOWTRAN 4, the parameter IHAZE is specified according to,

- IHAZE = 0 No aerosol attenuation included
- 1 Aerosol attenuation (visibility = 25 km if VIS not specified)
- 2 Aerosol attenuation (visibility = 5 km if VIS not specified).

Ground level meteorological range (visibility) is defined by VIS. As indicated above, if VIS is not specified (i.e., VIS = 0.0), LOWTRAN 4 will assume a visibility of either 25 or 5 km depending upon the value of IHAZE.

If ITARG = 0, the ground surface must not lie within the sensor's line-of-sight (i.e.,  $\text{THETA} \leq 90^{\circ}$ ). For this configuration, SPOT will calculate the uncollided components as outlined in sections 3.1.2 and 3.1.5, plus the single-scattered path radiance, described in section 3.1.3, between the sensor and the top of the atmosphere. If  $\text{THETA} = 90^{\circ}$ , the horizontal atmospheric path considered is 1000 km in extent. Note, the source of radiation is determined by the ISORC parameter. Hence, for ISORC = 2, the uncollided radiance due to atmospheric emission along the sensor's line-of-sight is the only component calculated. For ITARG = 1, the ground surface must lie within the sensor's line-of-sight (i.e.,  $\text{THETA} > 90^{\circ}$ ). SPOT will calculate the radiative components described in sections 3.1.3 - 3.1.6 where ground reflectance/emission is considered. And for ITARG = 2, SPOT will consider each of the radiative components discussed in sections 3.1.2 - 3.1.6.

The selection of ITARG = 2 requires the definition of a target at a distance RTARG along the sensor's line-of-sight. A unit vector, normal to the target, is defined by inputting its three directional cosines COSX, COSY, and COSZ (with respect to the X, Y, Z axes respectively). This program option (ITARG = 2) provides the user with the maximum degree of flexibility

and optimization in evaluating target/background signal recognition capabilities for electro-optical sensors operating within the atmosphere.

If the source option chosen includes extraterrestrial radiation (ISORC = 0,1,3,4), SPOT will calculate the single-scattered path radiance between the target and the sensor utilizing the computational procedures outlined in section 3.1.3. This component is referred to as the "partial path radiance". In addition, the program will calculate the "total path radiance" between the sensor and either: (a) the top of the atmosphere ( $\text{THETA} < 90^\circ$ ), (b) a distance of 1000 km ( $\text{THETA} = 90^\circ$ ), or (c) the ground surface ( $\text{THETA} > 90^\circ$ ).

An input parameter, SANG2, which defines the half-angle of the sensor's field-of-view, is used to determine whether or not direct sunlight (or moonlight) is incident upon the sensor. In particular, the angle of incidence is calculated for the direct extraterrestrial radiation with respect to the sensor's line-of-sight (defined by THETA,PHI). The inclination angle of the radiation incident at the top of the atmosphere, with respect to the zenith, is defined by the input parameter ZENITH. The extraterrestrial irradiance is assumed to lie within the azimuthal plane defined by  $\phi = 0$ . If the angle of incidence is less than or equal to the half-angle SANG2, an estimate of the uncollided solar (or lunar) radiation incident at the detector is made using the procedure outlined in section 3.1.2. An additional parameter PHASE, indicating the phase angle of the moon, is required if the extraterrestrial radiation to be considered is moonlight.

If the sensor is oriented such that  $\text{THETA} > 90^\circ$ , the spectral radiance due to ground reflection of the uncollided solar (or lunar) radiation will be calculated as described in section 3.1.4. Target reflection of the uncollided extraterrestrial radiation is calculated if the angle of incidence defined by the unit vector normal to the target and the direction of the uncollided radiation (defined by ZENITH and  $\phi = 0$ ) is less than  $90^\circ$ .

If atmospheric emission is to be considered (ISORC = 2,3,4), SPOT will utilize LOWTRAN 4 to calculate the uncollided atmospheric emission along the detector's line-of-sight, between the sensor and the target (i.e., "partial atmospheric emission"), and from the sensor to either: (a) the top of the atmosphere ( $\text{THETA} < 90^\circ$ ), (b) a distance of 1000 km ( $\text{THETA} = 90^\circ$ ), or (c) the ground surface ( $\text{THETA} > 90^\circ$ ), (i.e., "total atmospheric emission"). Atmospheric emission is calculated as discussed in section 3.1.5. The uncollided thermal emission, emitted by the target, incident at the sensor is calculated as described in section 3.1.6, and if  $\text{THETA} > 90^\circ$ , the uncollided ground emission is also indicated.

In order to provide the user with a multispectral representation of the radiant energy incident upon the detector, SPOT will calculate each of the radiative components for several wavelengths. Currently a maximum of twenty-five wavelengths may be considered. The band of interest is defined by the minimum and maximum frequency to be considered, WAVN1 and WAVN2 respectively, in wavenumbers ( $\text{cm}^{-1}$ ). Note that  $\nu = 10^4/\lambda$  where  $\nu$  is the frequency in wavenumbers ( $\text{cm}^{-1}$ ) and  $\lambda$  is the corresponding wavelength in microns ( $\mu\text{m}$ ). LOWTRAN 4 requires that the spectral step size be a multiple of five wavenumbers ( $5 \text{ cm}^{-1}$ ). Therefore, the SPOT input parameter IWAVE is an integer which specifies the spectral increment in units of  $5 \text{ cm}^{-1}$ , that is

$$\Delta\nu = \text{IWAVE} \cdot 5 \text{ (cm}^{-1}\text{)} \quad . \quad (41)$$

It should be remembered that the various data bases utilized by the SPOT program apply to specific spectral regions. These regions of applicability are summarized in TABLE VIII.

TABLE VIII. SPECTRAL APPLICABILITY OF SPOT DATA BASES

Data Base	Description	Applicable Spectral Region ( $\mu\text{m}$ )
SOLARS	Extraterrestrial Solar Spectrum	.115 - 1000.
SMOON	Extraterrestrial Lunar Spectrum	.200 - 2.8
LT4DATA	LOWTRAN 4 data base	.200 - 28.57
HAZESDATA	MIE scattering matrices	.158 - 40.

For values of ISORC = 0, 1, 3 or 4, SPOT will calculate path-radiance due to first order scattering by molecules and atmospheric aerosols, if the input parameter NLAM is non-zero. If NLAM > 0, SPOT reads the wavelength-dependent single scattering phase function for the thirty-eight wavelengths outlined in section 3.2.4 from the data base HAZESDATA. The input parameter IUNIT indicates the logical unit number on which HAZESDATA resides. For NLAM > 0, the input parameter NANG need not be defined (an internal value of 64 is used). If the user chooses to insert his own phase function, he may do so by defining NLAM < 0, where the absolute value of NLAM specifies the number of wavelength-dependent data sets to be read. The number of discrete angle intervals for which the single scattering phase function is defined is given by the value of NANG. The logical unit number on which the user-defined phase functions reside is given by IUNIT.

It should be noted that the user-defined data base must follow the same format as HAZESDATA. In particular, the SPOT program reads a set of scattering angles PCOS at which the phase function is to be defined. Then follows the wavelength WLAM and the normalized single scattering phase function PDC0, defined at the specified wavelength, given for each of the scattering angles defined. Currently, a maximum of sixty-four scattering angles and phase functions for up to thirty-eight wavelengths are allowed.

For cases in which thermal emission from the ground surface and/or target surface is to be considered (i.e., ITARG = 1, 2 and ISORC = 2, 3, 4), SPOT requires the specification EM(1) and EM(2) of the emissivity, plus TM(1) and TM(2) the absolute temperature, of the ground and target respectively. If the temperature of the ground surface is omitted (i.e., TM(1) = 0.0), SPOT will use the temperature of the lowest atmospheric layer defined for the atmospheric model chosen (MODEL) as the ground surface temperature.

Reflection properties of the ground and/or target are required input if ITARG = 1 or 2. An albedo is defined for the surface of interest by the equation

$$ALB = AO + AI \cdot COSBT$$

(42)

where  $A_0$  and  $A_1$  are coefficients defined by the user and  $\text{COSBT}$  is a quantity calculated internally which represents the cosine of the radiation's incident angle with respect to the surface normal. In addition, the reflection surface may be defined as isotropic ( $\text{IALB} = 1$ ) or Lambertian ( $\text{IALB} = 0$ ), in which case the normalized albedo is given as

$$\text{ALBEDO} = \frac{\text{ALB}}{2\pi} \quad (43)$$

or,

$$\text{ALBEDO} = \frac{\text{ALB} \cdot \text{COSGM}}{\pi} \quad (44)$$

respectively, where  $\text{COSGM}$  is the cosine of the reflection angle calculated internally.

The input parameter  $\text{NNPROB}$  is an integer which designates the problem number and will appear on each page of the printed output for purposes of documentation. A summary of the input data required by SPOT is given in TABLE IX. The major arteries of the SPOT program are indicated by the flow chart shown in Fig. 12.

### 3.3.2 Output

The usefulness of any detector system is marked by the sensor's ability to distinguish between that portion of the signal which is attributable to the target and that portion which results from natural (background) sources. Signal recognition is the vital by-product of the SPOT computer code. In order to provide the user with a quantitative measure of a detector's ability to "recognize" objects within its line-of-sight, SPOT calculates a quantity referred to as a "contrast ratio". The contrast ratio, defined at each wavelength of the multispectral analysis, is given by

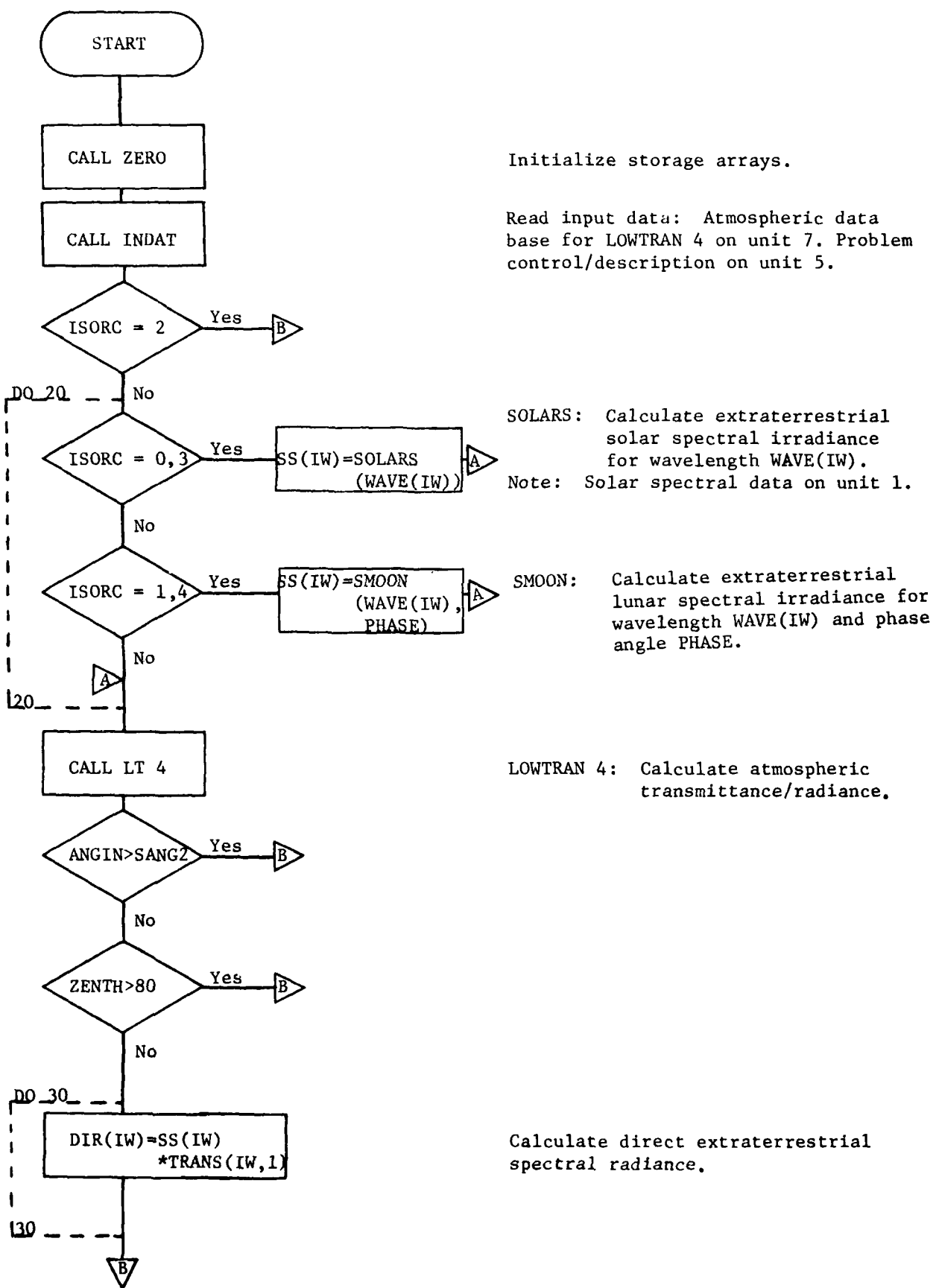
$$\text{CNTRST}(\text{IW}) = \frac{(\text{TTR}(\text{IW}) - \text{TBR}(\text{IW}))}{\text{TBR}(\text{IW})} \quad (45)$$

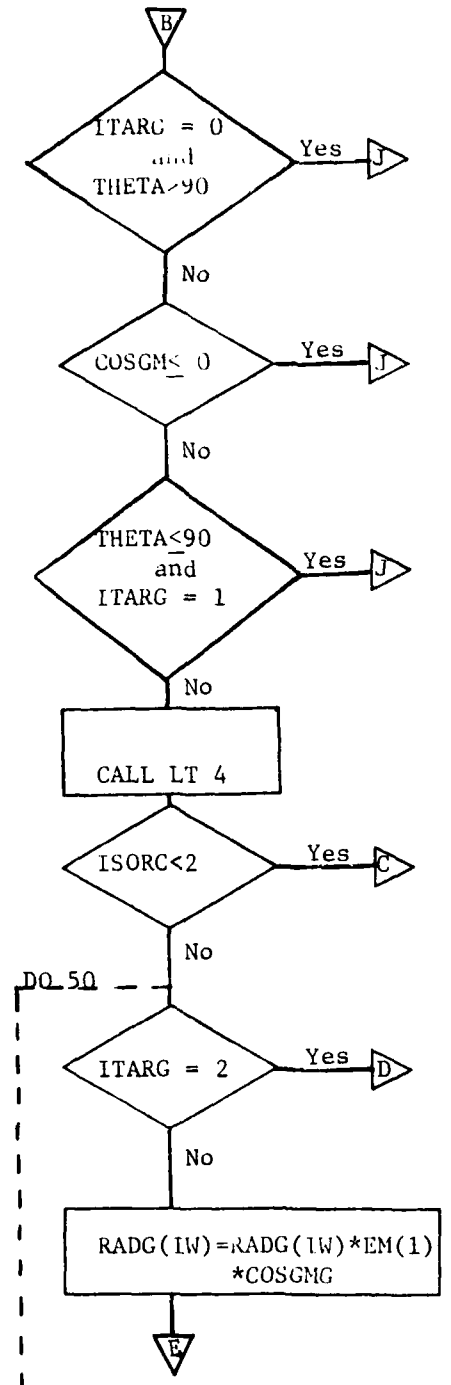
where  $\text{TTR}$  and  $\text{TBR}$  indicate the "total target radiance", and "total background radiance", respectively, at each of the wavelengths specified. Total target

TABLE IX. SUMMARY OF PROBLEM DESCRIPTION INPUT DATA FOR THE SPOT COMPUTER CODE

ISORC = 0 SUNLIGHT ONLY  
 1 MOONLIGHT ONLY  
 2 EMISSION ONLY  
 3 SUNLIGHT AND EMISSION  
 4 MOONLIGHT AND EMISSION  
 ITARG = 0 BACKGROUND ONLY  
 1 GROUND REFLECTANCE/EMISSION  
 2 TARGET REFLECTANCE/EMISSION  
 MODEL = 1 TROPICAL MODEL ATMOSPHERE  
 2 MIDLATITUDE SUMMER  
 3 MIDLATITUDE WINTER  
 4 SUBARCTIC SUMMER  
 5 SUBARCTIC WINTER  
 6 1962 US STANDARD  
 IHAZE = 0 NO AEROSOL ATTENUATION INCLUDED IN THE UNCOLLIDED CALCULATIONS  
 1 AEROSOL ATTENUATION IS INCLUDED (VIS=23KM IF NOT SPECIFIED)  
 2 AEROSOL ATTENUATION IS INCLUDED (VIS= 5KM IF NOT SPECIFIED)  
 NLAM = OPTION FOR AEROSOL SINGLE-SCATTERING PHASE MATRIX  
 NLAM = 0 NO AEROSOL ATTENUATION  
 < 0 READ AVERAGE PHASE MATRIX, NLAM SETS-USER DEFINED  
 > 0 READ AVERAGE PHASE MATRIX FROM R.R.A. DATA SET  
 NANG NUMBER OF ANGLE INTERVALS USED FOR PHASE MATRIX DEFINITION  
 IUNIT UNIT NUMBER ON WHICH PHASE MATRIX DATA RESIDES  
 EM(1) EMISSIVITY OF GROUND  
 EM(2) EMISSIVITY OF TARGET  
 TM(1) TEMPERATURE OF GROUND (KELVIN)  
 TM(2) TMEPERATURE OF TARGET (KELVIN)  
 ZENTH INCIDENT ANGLE OF SUNLIGHT OR MOONLIGHT (DEGREES)  
 A0(1) ALBEDO COEFFICIENT FOR GROUND  
 A1(1) ALBEDO COEFFICIENT FOR GROUND  
 A0(2) ALBEDO COEFFICIENT FOR TARGET  
 A1(2) ALBEDO COEFFICIENT FOR TARGET  
 IALB(1) TYPE OF REFLECTION DISTRIBUTION FOR GROUND  
 IALB(2) TYPE OF REFLECTION DISTRIBUTION FOR TARGET  
 IALB = 0 LAMBERTIAN REFLECTION SURFACE  
 1 ISOTROPIC  
 RTARG SLANT RANGE FROM RECEIVER TO TARGET (KM)  
 COSX X-DIRECTIONAL ANGLE OF TARGET NORMAL (DEGREES)  
 COSY Y-DIRECTIONAL ANGLE OF TARGET NORMAL (DEGREES)  
 COSZ Z-DIRECTIONAL ANGLE OF TARGET NORMAL (DEGREES)  
 ALT ALTITUDE OF RECEIVER (KM)  
 THETA POLAR DIRECTION OF LOOK ANGLE (DEGREES)  
 PHI AZMITH DIRECTION OF LOOK ANGLE (DEGREES)  
 SANG2 HALF ANGLE DEFINING RECEIVER FIELD-OF-VIEW (DEGREES)  
 WAVN1 INITIAL WAVENUMBER FOR BAND OF INTEREST (CM-1)  
 WAVN2 FINAL WAVENUMBER FOR BAND OF INTEREST (CM-1)  
 IWAVE WIDTH OF WAVENUMBER INCREMENT (5 CM-1)  
 VIS METEOROLOGICAL RANGE (KM)  
 PHASE PHASE ANGLE FOR MOONLIGHT (DEGREES)  
 PCOS ANGLES AT WHICH PHASE MATRIX IS DEFINED, NLAM VALUES  
 WLAM WAVELENGTH AT WHICH PHASE MATRIX DATA IS DEFINED  
 PDCO AVERAGE PROBABILITY FOR PHASE MATRIX DEFINITION  
 NPROB PROBLEM NUMBER

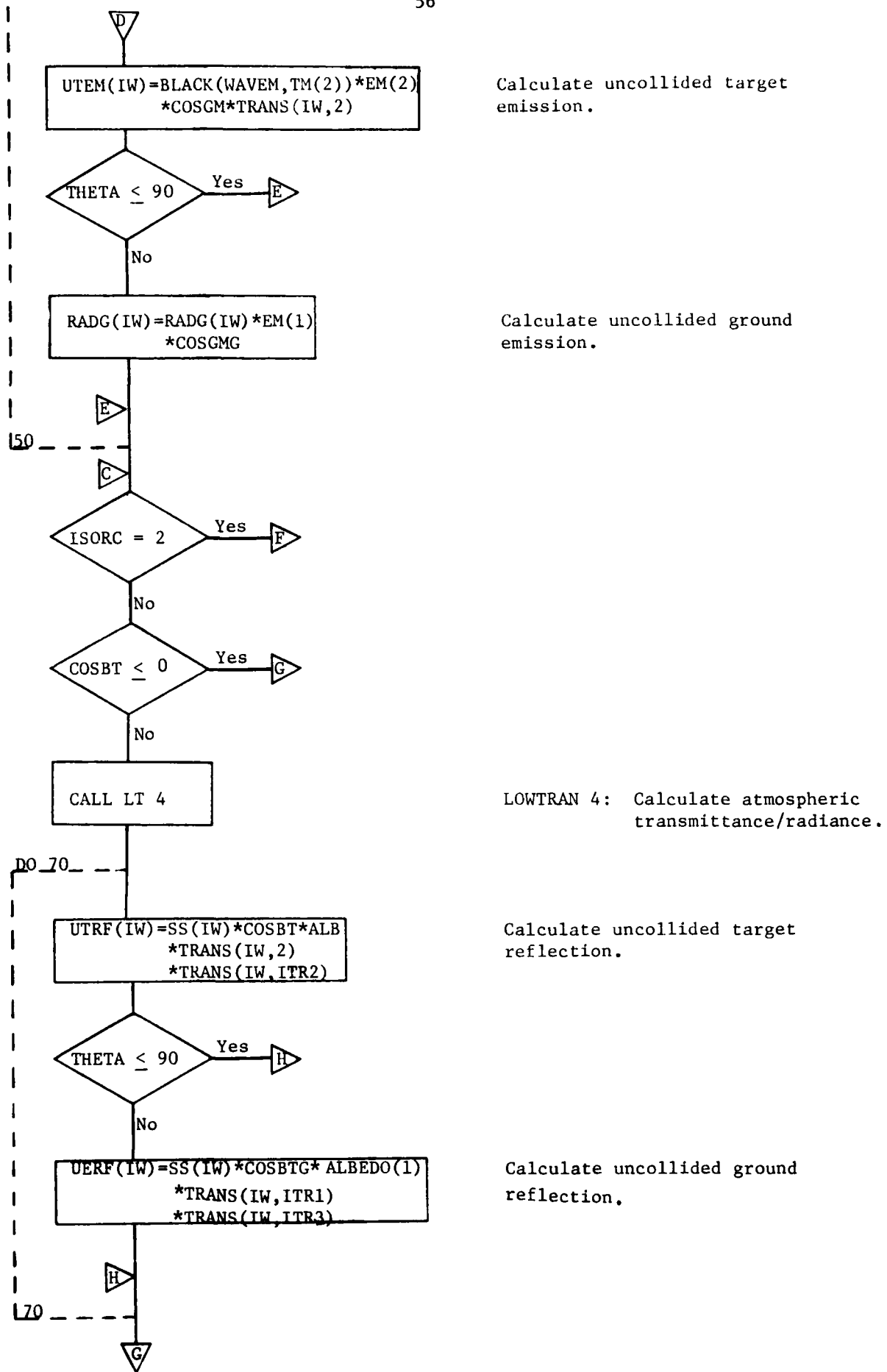
Fig. 12. FLOWCHART for the SPOT Computer Code

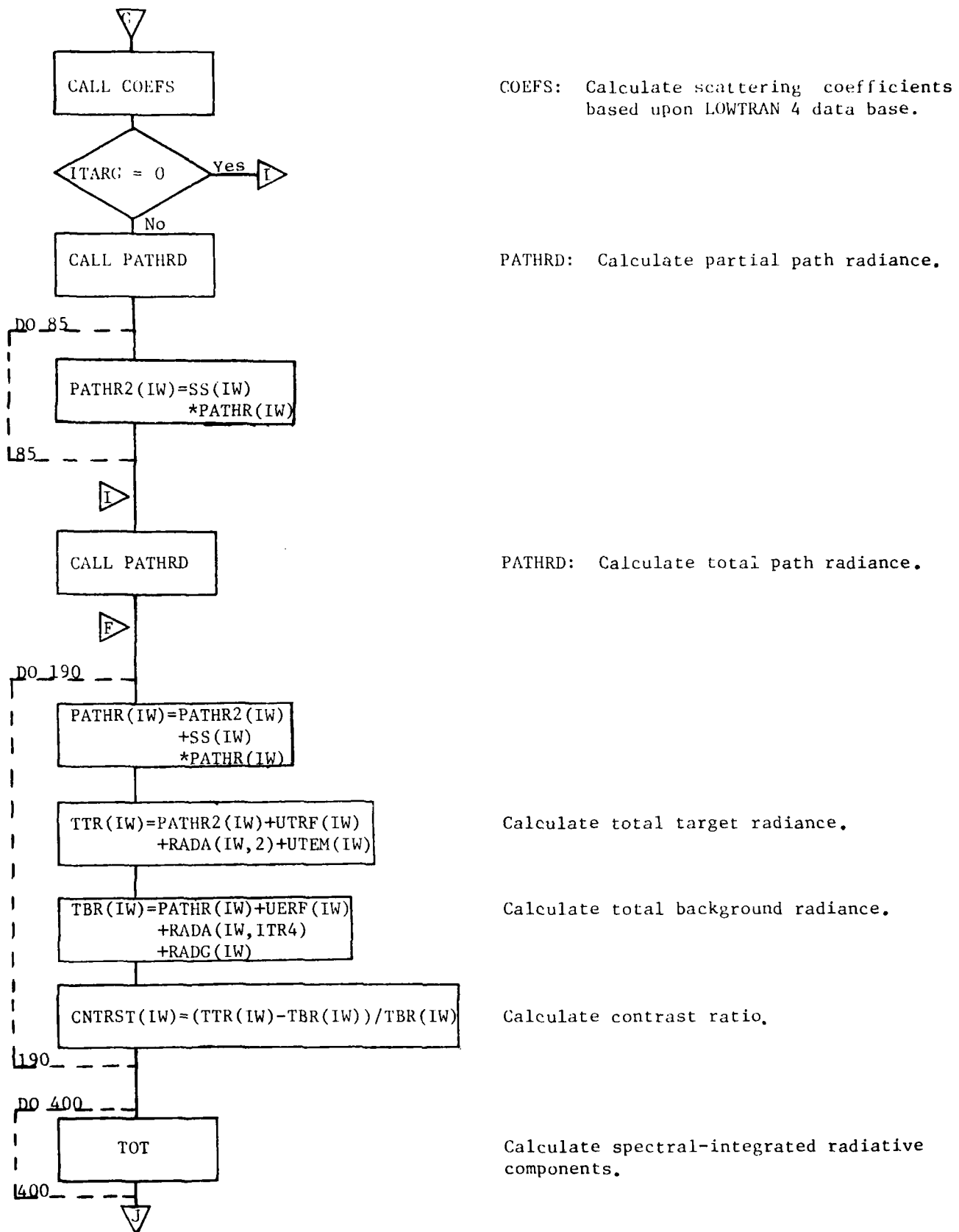


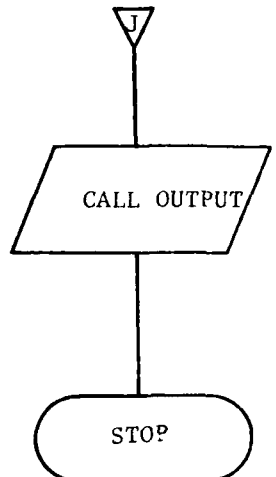


LOWTRAN 4: Calculate atmospheric transmittance/radiance.

Calculate uncollided ground emission.







OUTPUT: Printed output on unit 6.

radiance may include each of the following components (depending upon the choice of options),

- 1) partial path radiance
- 2) target-reflected direct sunlight (or moonlight)
- 3) partial atmospheric emission
- 4) uncollided target emission.

Total background radiance may include,

- 1) total path radiance
- 2) ground-reflected direct sunlight (or moonlight)
- 3) total atmospheric emission
- 4) uncollided ground emission.

If the quantities TTR and TBR, as calculated by SPOT, are equal, the contrast ratio is defined to be zero. On the other hand, if TBR is zero and TTR is non-zero, the contrast ratio is set equal to a large number ( $10^{30}$ ). If ITARG = 1, the ground surface is treated as a target such that the contrast ratio is equal to one. As described herein, the contrast ratio measures the target's effect upon the radiant energy incident upon the detector system.

As a further indication of the sensor's capability to recognize objects within its line-of-sight, SPOT integrates each of the radiative components evaluated over the spectral region defined. This includes the individual components as well as the totals, contrast ratio, and direct flux (sunlight or moonlight incident with the field-of-view). An example of the printed output produced by SPOT is presented in section IV.

### 3.4 Validation

Several sample problems were executed by the SPOT computer code in order to validate the computational methods employed within the program. Hand calculations, utilizing the necessary atmospheric transmittances as calculated by LOWTRAN 4, were used to substantiate the target and ground reflected components as well as the uncollided flux due to incident sunlight. Validation of the wavelength-integrated results, as well as various other parameters provided by the code, was also accomplished through the use of hand calculations.

Results from an earlier study (Ref. 4) provide a comparison of the uncollided thermal radiation (ground and atmospheric emission) as calculated by the FLASH Monte Carlo radiation transport code and LOWTRAN 4 in the 3.0 - 5.0  $\mu\text{m}$  spectral region for a receiver at a 3 km altitude viewing the ground surface ( $\theta = 180^\circ$ ). These results are shown in Fig. 13 along with the results from SPOT calculations performed for the same problem configuration. LOWTRAN 4 data are shown as solid lines, whereas the FLASH and SPOT data are as indicated in the figure. It is obvious that SPOT reproduced the results from LOWTRAN 4, as would be expected. The FLASH results are, similar to LOWTRAN 4 and SPOT, averaged over 20 wavenumbers. Generally, the data computed by both calculational methods, FLASH and LOWTRAN 4 (SPOT), are in good agreement. Some differences occur, particularly around 3.3, 3.6, 4.6 and 5.1  $\mu\text{m}$ . These differences reflect slight variations in the atmospheric models used in FLASH and LOWTRAN 4 as well as a basic difference in their methods used to calculate absorption. Absorption computations in FLASH are based upon the basic absorption line parameter tape that has been compiled by McClatchey (Ref. 13). As previously discussed (section 3.1.1), LOWTRAN 4 employs the band model technique.

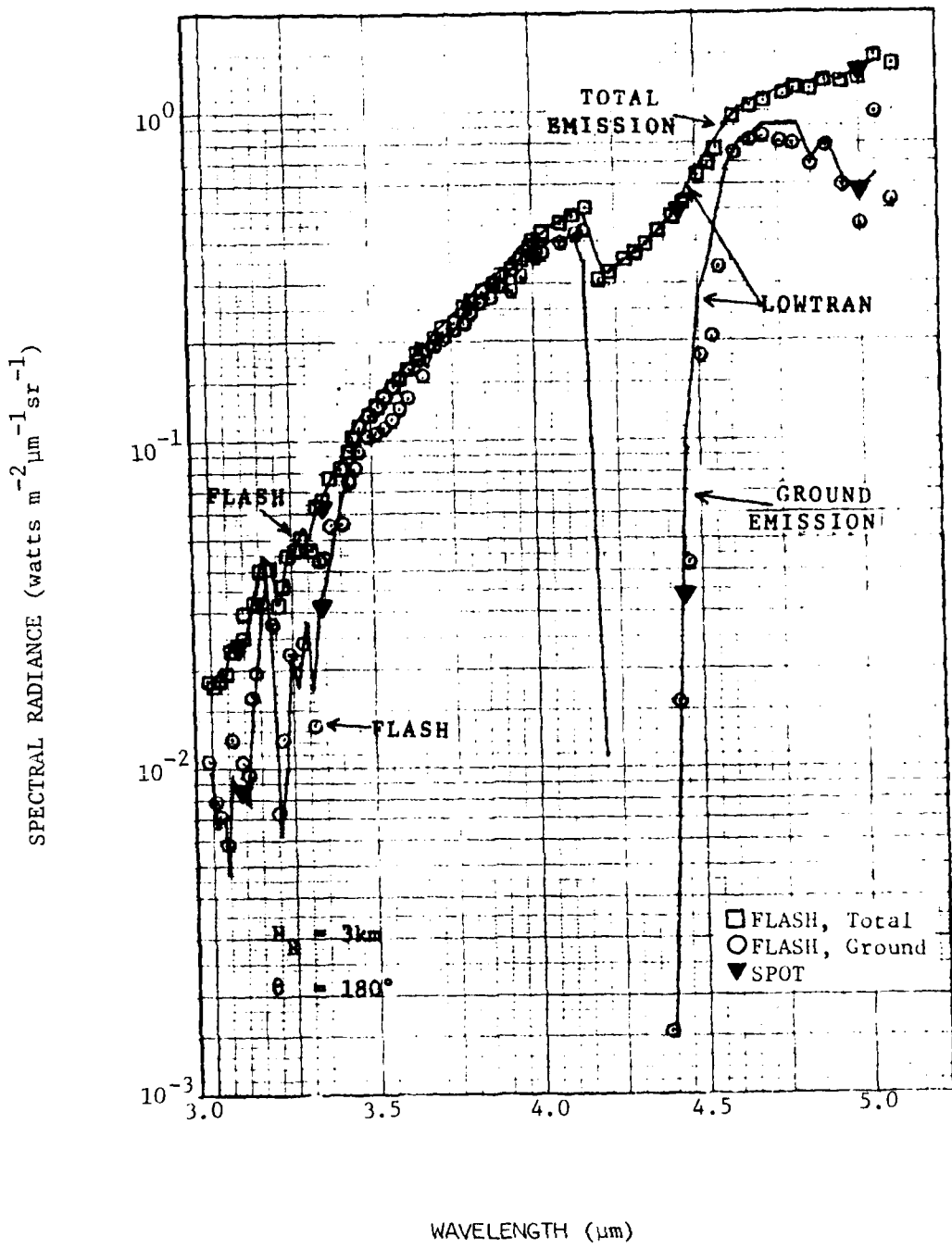


Fig. 13. Comparison of Results from FLASH, LOWTRAN 4, and SPOT Spectral Calculations of Ground Emission and Total Emission (including Uncollided Atmospheric Emission): Ground Emissivity = 1.0

### 3.5 Future Improvements

At its present state of development, the SPOT computer code provides the user the capability of evaluating the primary effects of the radiative environment within which an electro-optical sensor might be expected to function. However, there are many refinements necessary to the program in order to achieve the degree of flexibility and precision required of a use-oriented code applicable to the E-O Sensor community.

The most important modification to be made to the SPOT program is the inclusion of additional radiative components. In particular, multiple scattering of extraterrestrial radiation and the scattering of atmospheric emission must be accounted for in the calculation of path radiance. Multiple scattering of electromagnetic radiation propagating through the atmosphere is a complicated phenomena, often requiring the most advanced computational techniques and computer systems in order to provide an adequate evaluation. It is not the purpose of the SPOT code to perform an exhaustive analysis of the effects of multiple scattering upon the electromagnetic signal received by a sensor located within the atmosphere. Instead, a more empirical approach to the problem is intended, the details of which were outlined in Ref. 1. In addition, preliminary investigations into the multiple scattering problem are discussed in Ref. 5 along with a description of a new Monte Carlo program THARTL (Time-dependent Homogeneous Atmosphere Radiation Transport - Line beam source), written especially for this task.

In addition to the influence of multiple scattering upon the path radiance, target (or ground) reflection of multiple scattered radiation should be included. A computational procedure similar to that described in section 3.1.4 could be used in which the spectral radiance incident at the sensor is given by

$$CTRF(\lambda) = \int_0^{2\pi} \int_0^{\pi/2} RAD(\lambda, \beta, \phi) \cdot (\alpha_t / \pi) \cos(\gamma) \cdot \cos(\beta) \cdot TRANS_1(\lambda) \sin\beta d\beta d\phi \quad (46)$$

where  $RAD(\lambda, \beta, \phi)$  is the spectral radiance due to scattered radiation that is incident upon the target. The radiative field described by

$\text{RAD}(\lambda, \beta, \phi)$  could include the scattered sunlight (or moonlight), scattered atmospheric emission, and direct (uncollided) atmospheric emission which illuminate the target surface.

All of the radiative components discussed in this report which pertain to the reflection or emission of radiation from a surface lying within the sensor's line-of-sight neglect any further interactions which the radiation might undergo during its transmission from the surface to the sensor. Depending upon the problem configuration, multiple scattering of this radiation by the atmospheric constituents present might produce an important effect upon the signal received by the sensor. The THARTL Monte Carlo program mentioned earlier could be used to determine the spectral regions and the atmospheric conditions for which the effects of multiple scattering must be included in the evaluation performed by SPOT.

Another problem which requires additional investigative calculations involves the transmittance for a photon path undergoing single or multiple interactions, either scattering or reflection. Consider the radiance due to target reflection of direct sunlight given by Eq. 34 as

$$\text{UTRF}(\lambda) = \text{SS}(\lambda) \cdot \alpha_t \cdot \frac{\cos(\gamma)}{\pi} \cdot \cos(\beta) \cdot \text{TRANS}_1(\lambda) \cdot \text{TRANS}_2(\lambda) \quad .$$

The total transmittance along the reflected path is given by the product of the transmittances which describe the two path segments individually. LOWTRAN 4 utilizes transmission functions which are dependent upon the total absorber amount found along the atmospheric path of interest. These functions use absorption coefficients which are averaged over 20 wavenumbers. The result of this is that the total transmittance expressed as the product

$$\text{TRANS}_1(\lambda) \cdot \text{TRANS}_2(\lambda)$$

may not be the same as that obtained by summing the total absorber amounts found along both segments of the path and then employing the transmission functions in order to effect a total transmittance characteristic of the photon's true path. This computational inconsistency should be examined in order to determine the magnitude of the deviation incurred. If the

deviation is sufficiently large, the computational methods employed by SPOT would have to be modified so as to eliminate the inaccuracy. As stated above, the modification would consist of summing the total absorber amounts found along each leg of a multiple segment path and then employing the transmission functions used by LOWTRAN 4 in order to obtain a total transmission.

As stated earlier in this report, the SPOT computer code utilizes a plane parallel geometry model; LOWTRAN 4, however, makes use of a spherical shell model. The difference in the two geometrical models will be most evident in atmospheric transmittance/radiance calculations involving long path lengths. This is particularly true for problem configurations in which the sensor's line-of-sight is defined such that its polar angle ( $\theta$ ) approaches, or lies within, the region bounded by  $\theta = 90^{\circ}$  and the true horizon. In such cases, the computational methods used to evaluate the radiative components of the background, due to extraterrestrial sources, are based upon a plane parallel geometry. Atmospheric transmission factors and the integrated total atmospheric emission, provided by LOWTRAN 4, are representative of a spherical shell atmosphere. The atmospheric parameters provided by LOWTRAN 4 may not be strictly compatible with the plane parallel model. However, it is hard to categorize the conditions for which the difference in the models would cause substantial errors in the predicted signals incident at the sensor. Hence, it would be advantageous to perform a sensitivity analysis with respect to this problem in order to determine the atmospheric conditions and spectral regions for which coupling of the two models produces unsatisfactory results.

The most time consuming calculation in SPOT is the path radiance. This is due to the fact that the path radiance evaluation involves a numerical integration (see section 3.1.3) along the sensor's line-of-sight which utilizes LOWTRAN 4 transmittances for each integration step. For the calculation of the total path radiance, this procedure may result in several calls to LOWTRAN 4. Therefore, a refinement in the computational technique used to determine the path radiance would result in a considerable reduction in the execution time necessary to run a SPOT problem.

Another modification to the program which would result in increased user flexibility involves the single scattering phase function required for the path radiance. Presently, SPOT utilizes a data base (see section 3.2.4) which contains single scattering phase functions, based upon MIE theory, at thirty-eight wavelengths characterized by a HAZE C aerosol model. These data are not applicable to atmospheric conditions characterized by extremely low visibility (less than 1 km). Therefore, the data base needs to be modified in order to account for low visibility fogs. In addition to natural atmospheric conditions, various man-made obscurants (i.e. smoke, etc.) should be treated in order to provide the user a full range of atmospheric conditions from which to chose.

An additional expansion to the SPOT code encompasses the inclusion of wavelength-dependent albedos and emissivities for the ground surface and target. In order to produce a more accurate simulation of the electro-optical sensor operating within the atmosphere, a wavelength-dependent response function indicative of the detector system under consideration would be another necessary modification to the SPOT program.

## IV. AN EXAMPLE PROBLEM: E-O SENSOR SCAN

In order to demonstrate the versatility of the SPOT program, a series of problems were executed in which a point monodirectional detector positioned at an altitude of 3 km scanned the atmosphere from the zenith to the nadir. The atmospheric model was chosen to be the 1962 U. S. Standard Atmosphere, characterized by a ground level meteorological range (visibility) of 3 km. Aerosol attenuation, including scattering, was included and the applicable phase matrices were drawn from the RRA data file HAZESDATA. The radiative environment included thermal emission and sunlight defined at an inclination angle of  $60^{\circ}$ . A target was positioned 1 km from the receiver along the receiver's line-of-sight. The unit vector normal to the target's surface was oriented directly toward the receiver. The target was characterized by an emissivity of .95, an absolute temperature of  $295^{\circ}\text{K}$ , and it was treated as a Lambertian reflector with an albedo coefficient (Eq. 42) specified by the expression

$$\text{ALB} = .05 + 0.0 \cdot \text{COSBT} .$$

The ground surface was assumed to be a perfect blackbody, that is, an emissivity of 1.0 and an albedo of zero. In addition, the temperature of the ground was taken as the temperature of the lowest atmospheric layer in the model chosen ( $288.1^{\circ}\text{K}$  for the 1962 U. S. Standard Atmosphere). The azimuthal direction of the sensor's line-of-sight was defined to be zero, while the polar direction was varied between the zenith and nadir, in ten degree increments. The spectral region of definition was from 2000 to 3200 wavenumbers ( $\text{cm}^{-1}$ ), or from 3.125 to 5.0 ( $\mu\text{m}$ ), with increments of 50 wavenumbers ( $\text{cm}^{-1}$ ).

Wavelength-integrated results are shown in Figs. 14-17 as a function of the sensor's polar angle. An angle of  $0^{\circ}$  orients the sensor's line-of-sight toward the zenith, while a value of  $180^{\circ}$  points toward the nadir. In Fig. 14, the total target and total background radiance is shown. The target radiance remains essentially constant throughout the scan. However, the background radiance displays some unusual features particularly at  $60^{\circ}$  and between  $90^{\circ}$  and  $100^{\circ}$ . A comparison with the results shown in Figs. 15-16

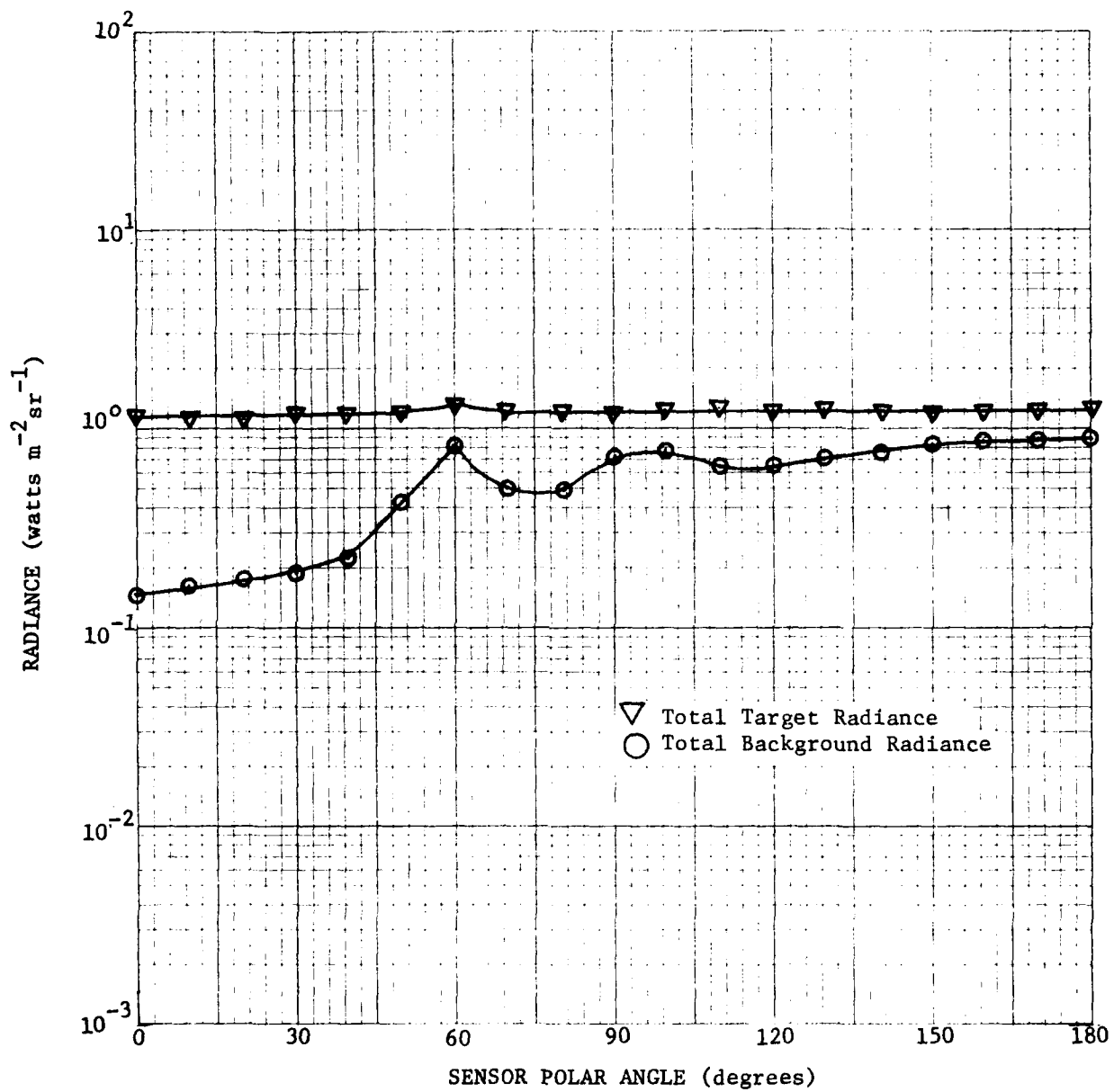


Fig. 14. Total Target and Background Radiance (wavelength-integrated) versus Sensor Polar Angle

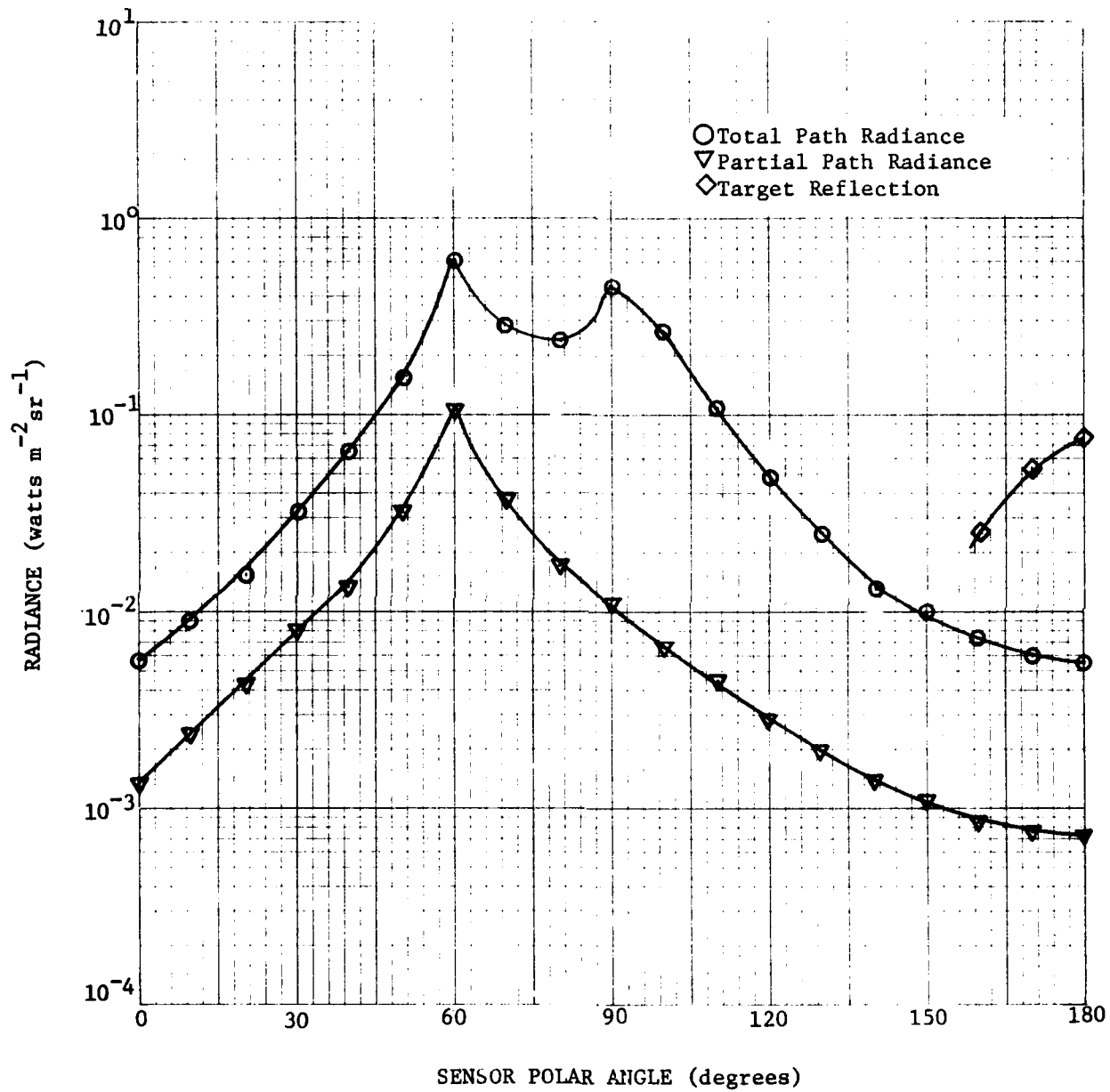


Fig. 15. Target and Background Radiance Components (wavelength-integrated) due to Sunlight versus Sensor Polar Angle

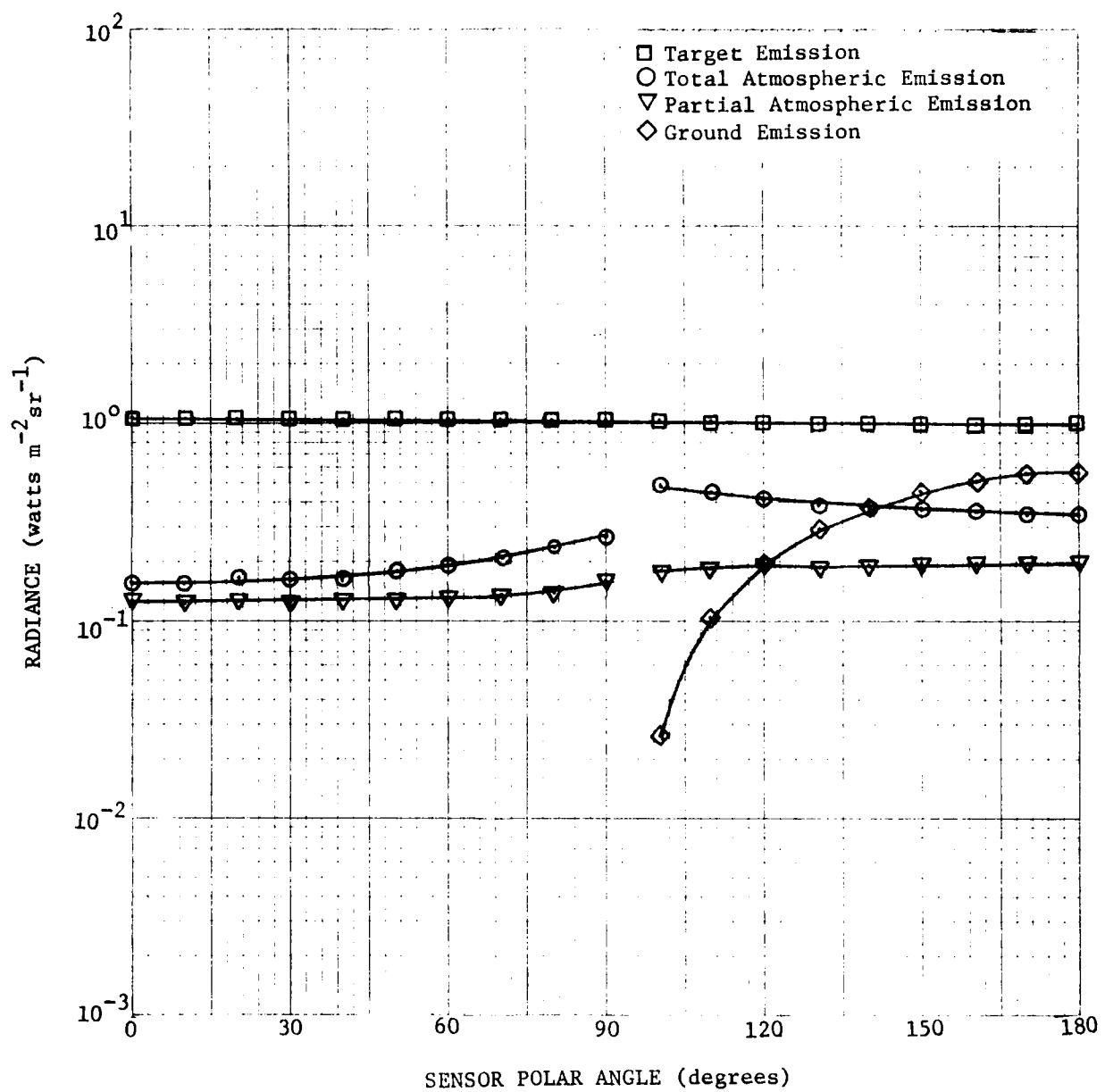


Fig. 16. Target and Background Radiance Components (wavelength-integrated) due to Thermal Emission vs Sensor Polar Angle

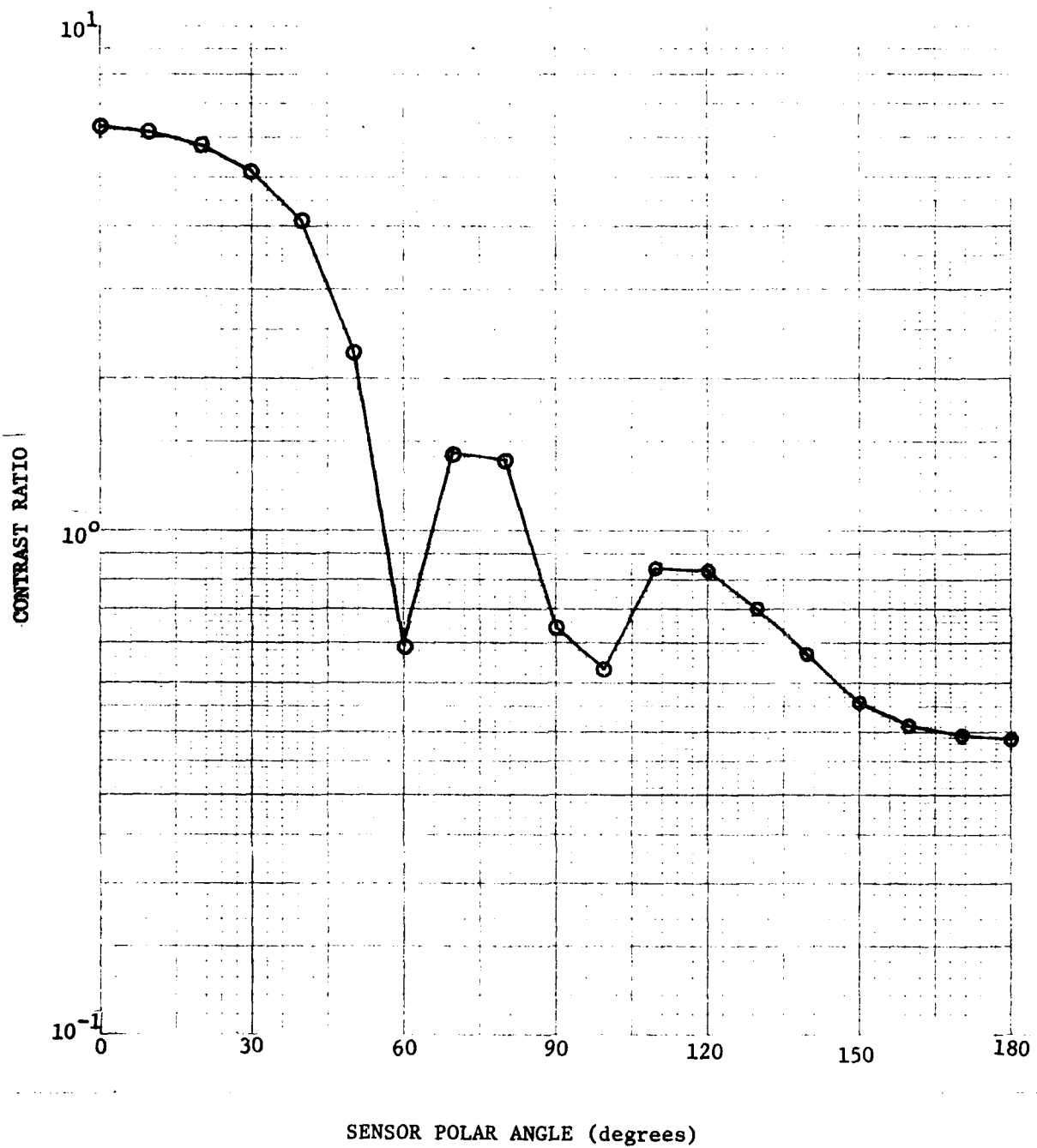


Fig. 17. Contrast Ratio (wavelength-integrated) versus Sensor Polar Angle

provides some insight into the cause of these peculiarities.

Shown in Fig. 15 are the corresponding total and partial path radiance components, integrated over the spectral band of interest. Path radiance, as calculated by SPOT, is the result of single-scattered sunlight, where the scattering particulates consist of the molecules and aerosols suspended in the atmosphere. Phase functions describing aerosol scattering of electromagnetic radiation in the visible and near infrared portions of the spectrum are highly peaked in the forward scattering angles. Hence, the peak recorded at  $60^\circ$  in both components is the result of the forward aerosol-scattered sunlight, whose inclination angle was defined to be  $60^\circ$ . Extraterrestrial irradiance in SPOT is assumed to be incident along an azimuthal angle of zero (section 3.3.1). Therefore, for a polar angle of  $60^\circ$ , the sensor's line-of-sight was directed toward the incident sunlight. An additional peak at  $90^\circ$  is evident in the total path radiance. This is due to the infinite path length viewed through the atmosphere in the horizontal direction.

A slight digression at this point may be of interest. In viewing the total path radiance shown in Fig. 15, it should be emphasized that the first peak, at  $60^\circ$ , is due to the forward scattering of sunlight by aerosols. The second peak, at  $90^\circ$ , is the result of an infinite path length indicative of viewing horizontally. For cases in which the scattering phase function is not highly peaked in any given direction, the initial peak in the total path radiance will disappear. Such is the case for atmospheres characterized by molecular scattering or a small density of aerosol particulates. In addition, this phenomena will display a direct relationship to the wavelength region in which the calculations are performed, since aerosol phase functions at long wavelengths do not exhibit strong forward scattering.

In addition to the path radiance described herein, Fig. 15 also shows the target-reflected direct sunlight. Target reflection occurs only when the uncollided sunlight illuminates the face of the target, i.e. the angle of incidence measured between the target normal vector and the inclination of the uncollided sunlight is less than  $90^\circ$  (section 3.3.1). For

the problem configuration defined, this situation occurred only for sensor polar angles of  $160^{\circ}$ ,  $170^{\circ}$ , and  $180^{\circ}$ . The increase in the target reflected radiance with increasing polar angle is due to the corresponding increase in the cosine term of the incident angle (section 3.1.4).

Contributions to the radiative energy incident at the sensor due to thermal emission are shown in Fig. 16. Uncollided target emission remains virtually constant throughout the scan, as did the total target radiance (Fig. 14). Uncollided thermal emission by the ground occurs only if the sensor's polar angle of orientation is greater than  $90^{\circ}$ . The increase in ground emission with increasing polar angle is attributable to two factors: 1) decreasing optical thickness with a subsequent increase in atmospheric transmittance, and 2) an increase in the cosine term (emission angle) used to characterize emission by a Lambertian surface (Eq. 39).

The total and partial atmospheric emission shown in Fig. 16 display some interesting features. Atmospheric emission is a quantity calculated by LOWTRAN 4, which utilizes atmospheric models characterized by isothermal layers. Since the atmosphere is cooler above 3 km than below (Ref. 11), the total and partial thermal emission for polar angles below  $90^{\circ}$  will be less than that emanating from the atmosphere viewed by a polar angle greater than  $90^{\circ}$ . In addition thermal emission occurs along the full extent of the atmospheric path considered, therefore, as the path length increases so will the radiance due to atmospheric emission. This phenomena is exemplified in Fig. 16 where the total atmospheric emission increases as the path approaches the horizontal polar angle of  $90^{\circ}$ . In the 1962 U. S. Standard Atmosphere used for this example problem, the 3 km altitude of the detector positions the sensor directly on a layer boundary (Ref. 11). Therefore, a discontinuity occurs in the total and partial atmospheric emission between  $90^{\circ}$  and  $100^{\circ}$  degrees, as shown by the broken curves in Fig. 16.

The contrast ratio, integrated over the wavelength interval defined, is shown in Fig. 17 as a function of the sensor's polar angle. As discussed in section 3.3.2, this quantity provides an indication of the magnitude of

the target radiance relative to that of the background. In effect, the contrast ratio displays the variation in the two curves shown in Fig. 14. An analysis of Fig. 17 reveals the significant influx of the total path radiance at  $60^\circ$  and again between  $90^\circ$  and  $100^\circ$ , shown previously in Fig. 15. For polar angles greater than  $90^\circ$ , uncollided ground emission begins to contribute (Fig. 16), as evidenced by the gradual decline in the contrast ratio from  $110^\circ$  to  $180^\circ$  (Fig. 17). Note, at  $100^\circ$  the increase in the total path radiance discussed earlier overshadows the effect of the ground emission.

Wavelength-dependent results obtained from SPOT are discussed in the following text for two specific problem configurations. These configurations relate to sensor polar angles of  $60^\circ$  and  $140^\circ$ . All other descriptive problem parameters are as previously defined in this section. It should be noted, that the results obtained from SPOT are averaged over 20 wavenumbers, due to the use of LOWTRAN 4 - computed transmittances and atmospheric emission. The data presented herein are spaced at intervals of 50 wavenumbers. Curves have been drawn through the data points in order to transform them into a cohesive state which the reader may find easier to comprehend. In no way are these curves intended to describe, predict, or simulate SPOT results obtained at wavenumbers other than the twenty-five values presented. Large fluctuation in the atmospheric transmittance, with respect to wavelength, present in some of the spectral regions examined, prohibit the interpolation or extrapolation of results at additional points within the spectrum.

The results for a sensor polar angle of  $60^\circ$  are shown in Figs. 18 and 19. Each of the radiative components contributing to the target radiance are shown in Fig. 18. In particular, this includes the uncollided target emission and partial atmospheric emission, and the single-scattered partial path radiance. There is no contribution from the target reflection of the direct sunlight because, for this configuration, sunlight illuminates the back side of the target. Also shown in Fig. 18 is the total

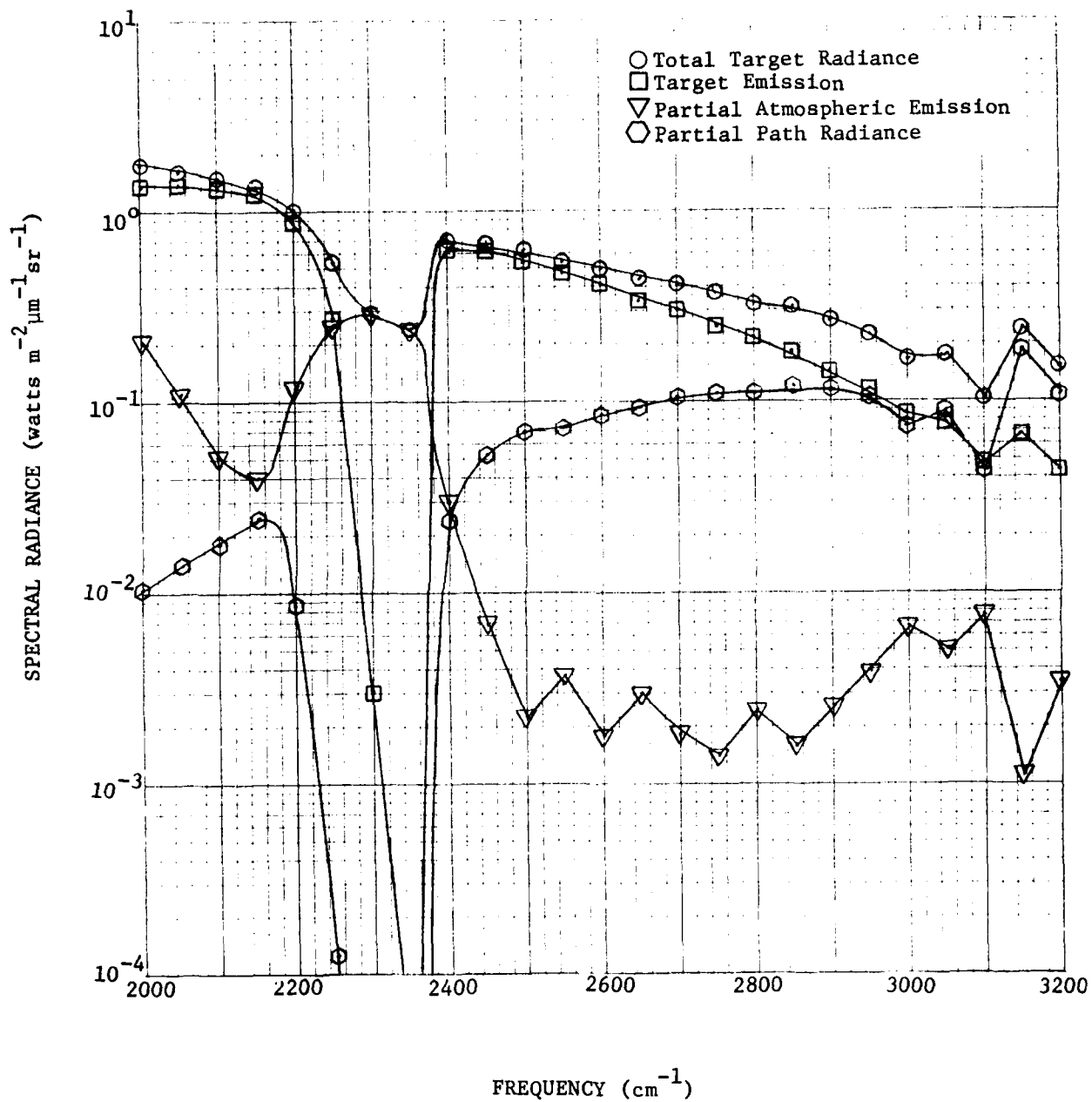


Fig. 18. Target Radiance Components versus Frequency for Sensor Polar Angle of 60°

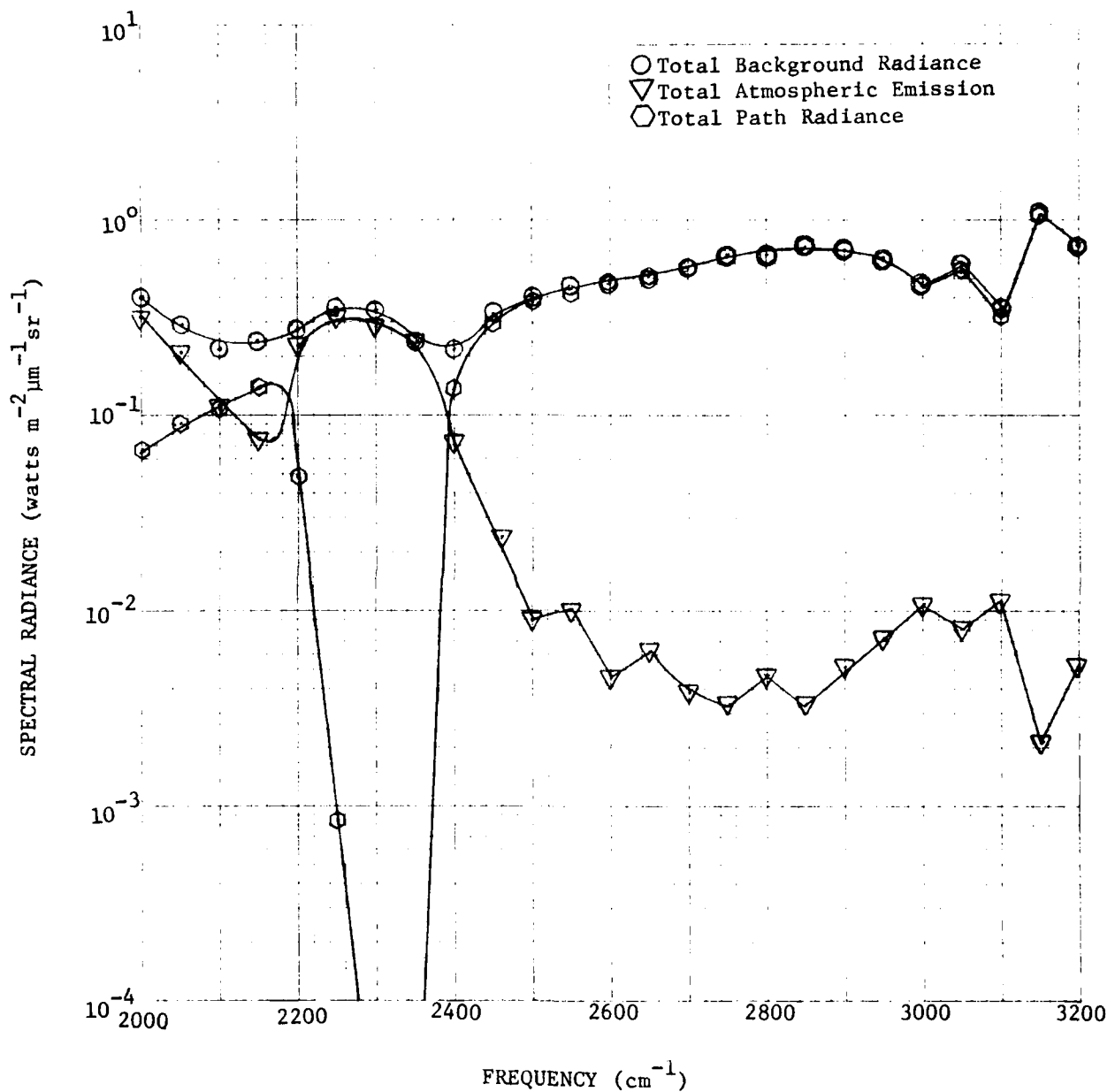


Fig. 19. Background Radiance Components versus Frequency for Sensor Polar Angle of 60°

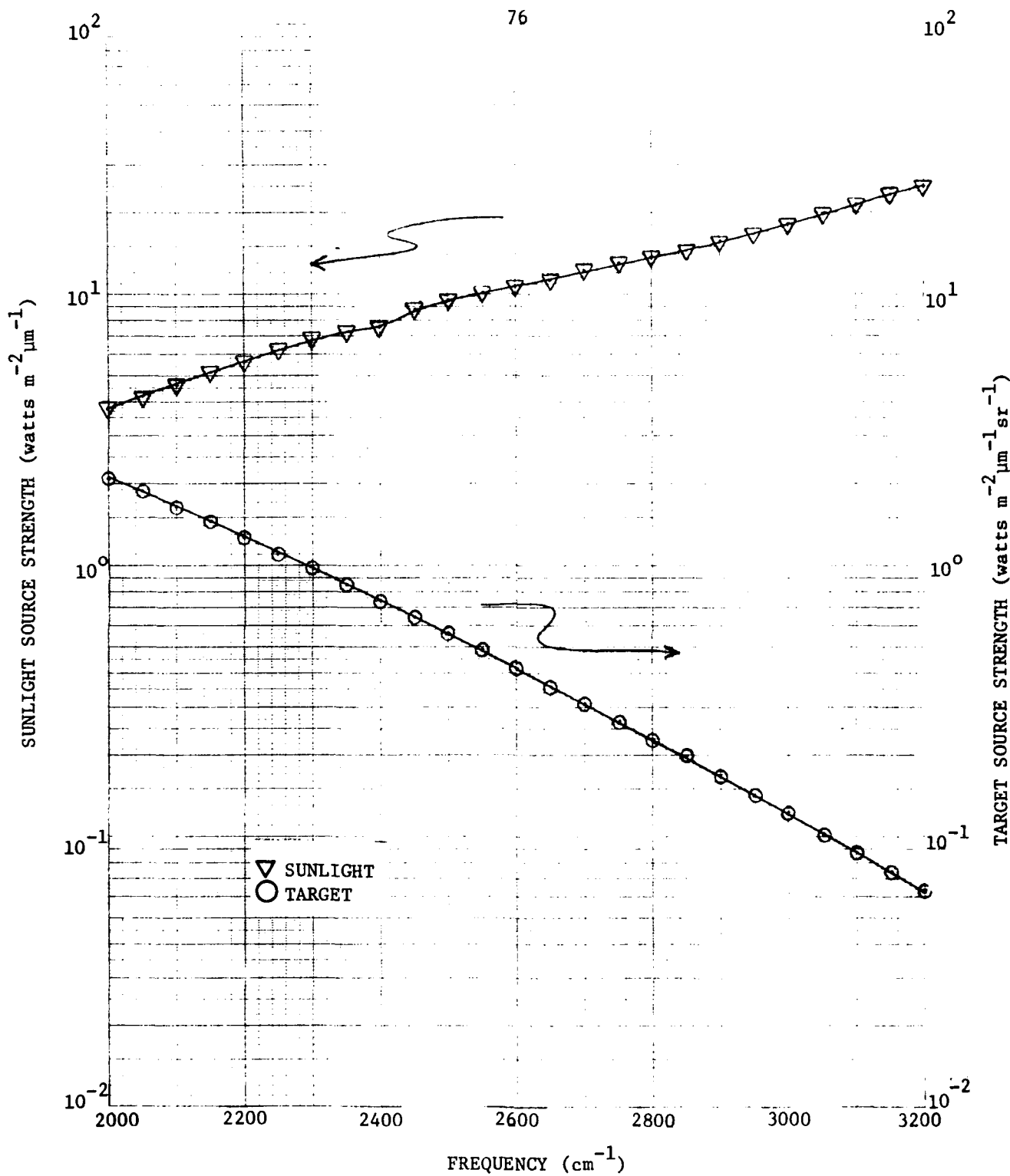


Fig. 20. Spectral Source Strength for Sunlight and Target Emission:  
Target Temperature = 295°K, Emissivity = .95

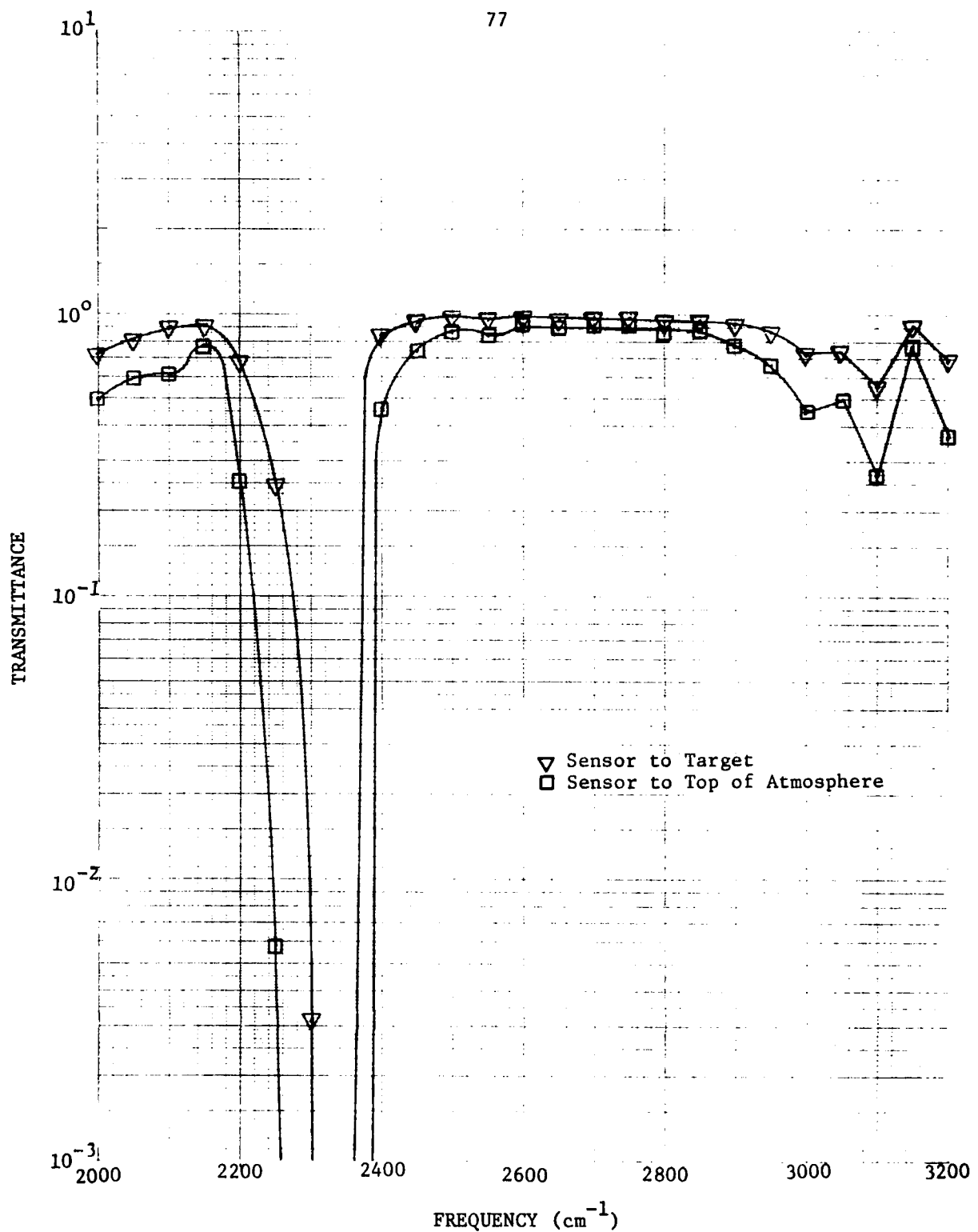


Fig. 21. Atmospheric Transmittance from Sensor to Target and from Sensor to Top of Atmosphere, for Sensor Polar Angle of  $60^\circ$

target radiance, representing the sum of each of the components discussed above. The radiative components describing the background radiance are shown in Fig. 19 along with the total background radiance. Since the sensor's line-of-sight does not intersect the ground surface, there is no contribution from uncollided ground emission nor from the ground reflection of direct sunlight. Hence, the background is due solely to the uncollided total atmospheric emission and the total single-scattered path radiance.

In order to assist in the analysis of Figs. 18 and 19, the extraterrestrial solar spectral irradiance is shown in Fig. 20 along with the target source strength. The source strength for sunlight and the target, as shown in Fig. 20, is not dependent upon the sensor's orientation. Extraterrestrial solar irradiance is obtained from the data base described in section 3.2.1, whereas the target source strength is that of a graybody defined by the product of the blackbody function (Eq. 15) and the target's emissivity. In addition, the atmospheric transmittance, as calculated by LOWTRAN 4, is shown in Fig. 21 for two atmospheric paths of interest. The first path length is that described between the sensor and target, along the sensor's line-of-sight. The second path length is the total path from the sensor to the top of the atmosphere.

A comparison of the results shown in Figs. 18-21 reveals the relationship of the various atmospheric processes involved in the sensor signal recognition problem. An inverse relation is shown between the atmospheric transmittance and radiance. This is particularly evident when comparing the uncollided target emission and partial atmospheric emission in the spectral region between 2150 and  $2400\text{ cm}^{-1}$  shown in Fig. 18. A strong absorption band is located within this spectral region as indicated by the transmittance shown in Fig. 21. As the atmospheric transmittance between the sensor and target decreases, so does the uncollided target emission. However, the partial atmospheric emission displays an increase. This interesting phenomena can be explained by the second law of thermodynamics. As discussed in section 2.2, a blackbody is not only a perfect absorber of thermal radiation, it is a perfect emitter too. LOWTRAN 4 considers the atmosphere as a blackbody when calculating atmospheric

emission. Therefore, an increase in atmospheric absorption (i.e. a decrease in transmittance) must result in a corresponding increase in emission. This same effect is displayed between the atmospheric emission and path radiance shown in Fig. 19.

Uncollided target emission is the primary component of the target radiance, as shown in Fig. 18, except for the absorption band found between 2150 and 2400  $\text{cm}^{-1}$ , and for wavenumbers greater than 3000  $\text{cm}^{-1}$ . A steady decrease in the source strength of the target's surface (Fig. 20), coupled with a decline in atmospheric transmittance (Fig. 21), is responsible for the diminishing response to the target emission displayed between 2600 and 3200  $\text{cm}^{-1}$ . Conversely, a steady increase in the partial path radiance is attributable to the increasing solar spectral irradiance shown in Fig. 20. Fluctuations in the data, shown in Figs. 18 and 19, between 3000 and 3200  $\text{cm}^{-1}$  reflect the behavior of the atmospheric transmittance (and absorption) shown in Fig. 21.

As mentioned earlier, a polar angle of  $60^\circ$  directs the sensor's line-of-sight toward the incident sunlight. Hence, the direct (uncollided) flux due to sunlight is shown in Fig. 22. This figure represents the product of the extraterrestrial irradiance (Figs. 4,5) and the atmospheric transmission along the sensor's line-of-sight between the sensor and the top of the atmosphere (Fig. 21).

The results obtained for a sensor polar angle of  $140^\circ$  are shown in Figs. 23-26. As with the previous example, there is no target reflection of direct sunlight in the target radiance shown in Fig. 23, because sunlight illuminates the back side of the target. In addition, even though the sensor's line-of-sight does intersect the ground surface, since the ground was defined to be a perfect blackbody, there is no ground reflection of direct sunlight in the background radiance shown in Fig. 24. The extraterrestrial solar spectral irradiance and the target source strength are identical to that shown for the previous problem (Fig. 20). The blackbody source strength representative of the ground surface is

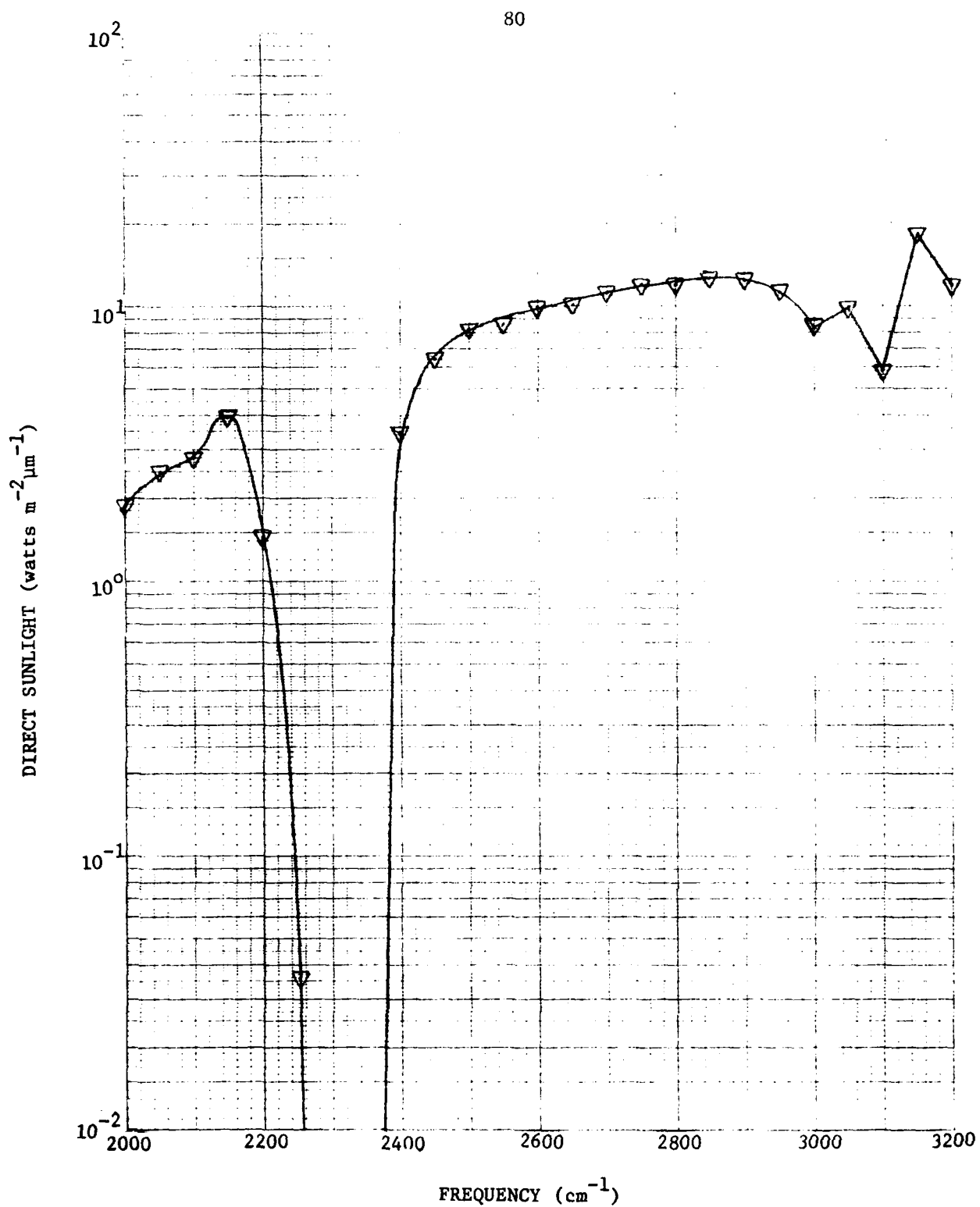


Fig. 22. Uncollided Sunlight Flux versus Frequency for Sensor Polar Angle of 60°

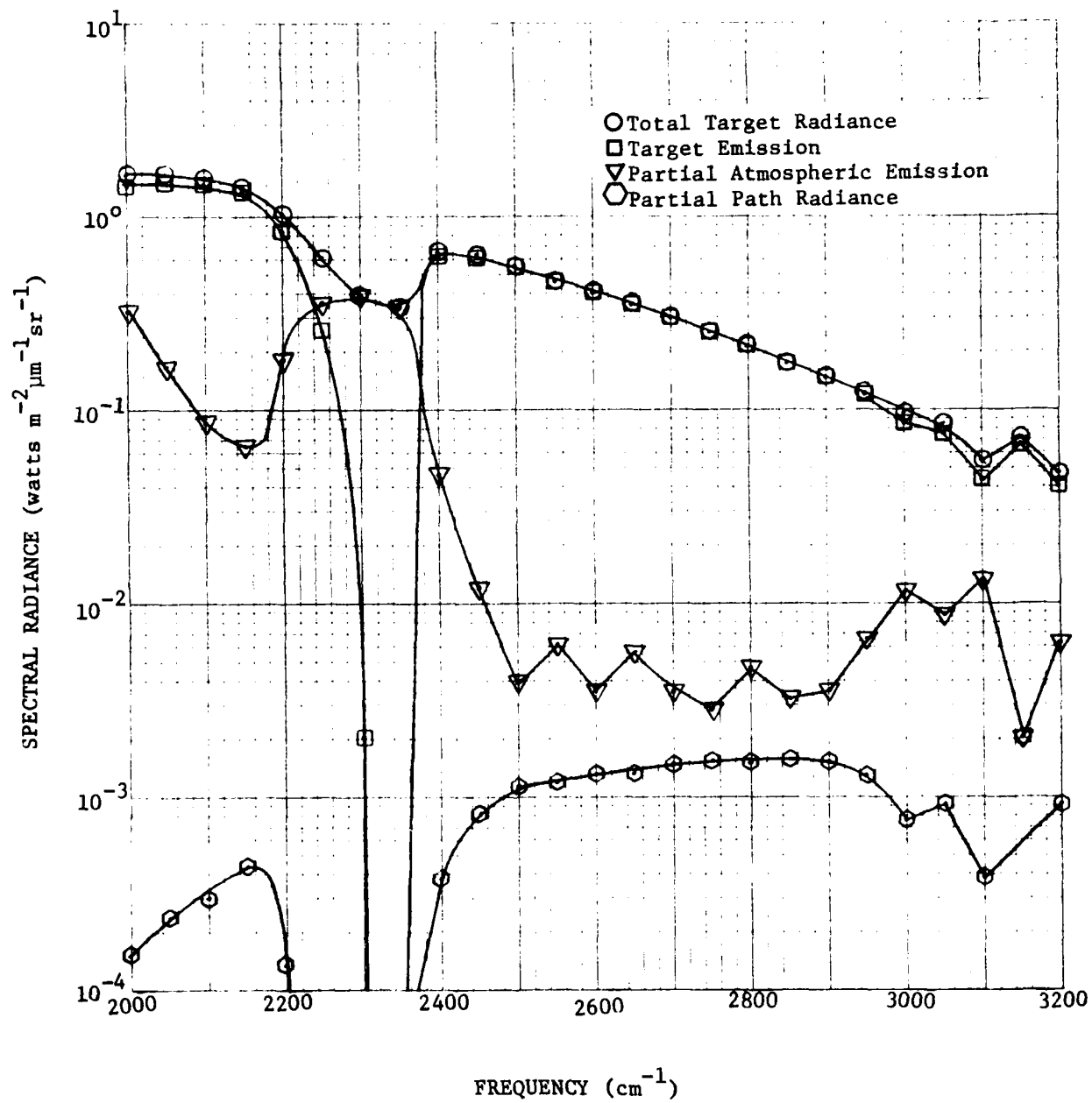


Fig. 23. Target Radiance Components versus Frequency for Sensor Polar Angle of  $140^\circ$

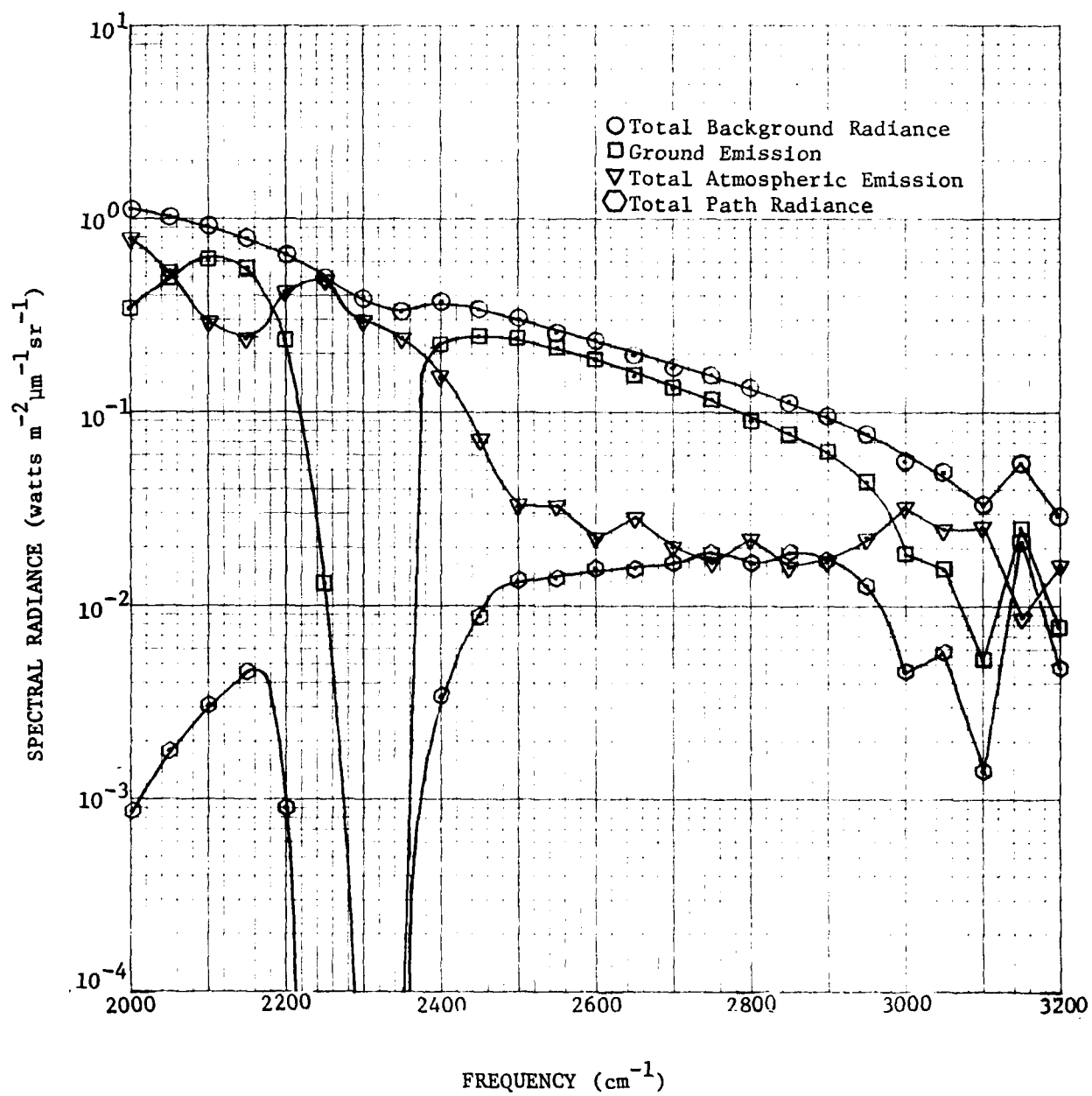


Fig. 24. Background Radiance Components versus Frequency for Sensor Polar Angle of 140°

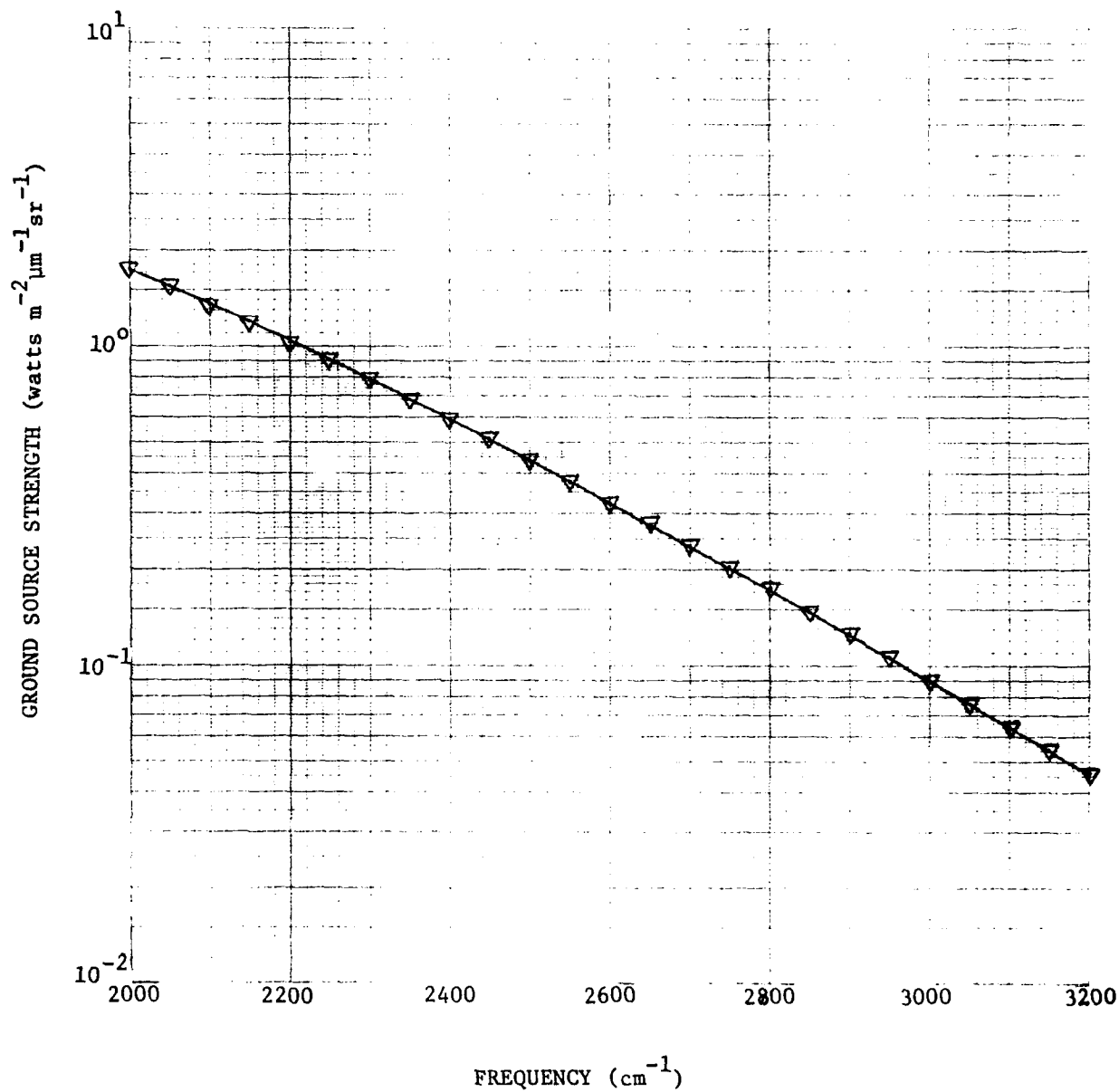


Fig. 25. Spectral Source Strength for Ground Emission: Ground Temperature = 288.1°K, Emissivity = 1.0

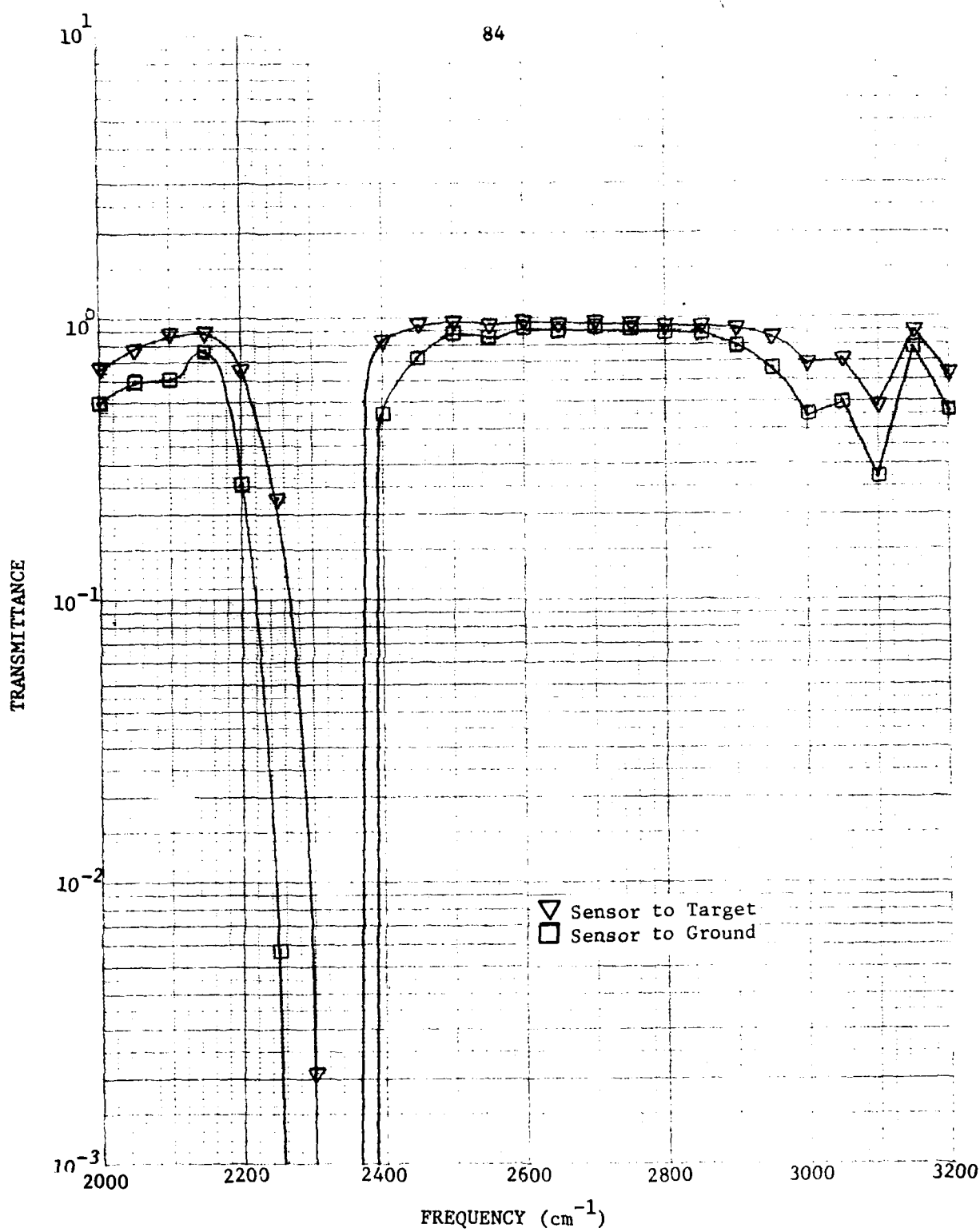


Fig. 26. Atmospheric Transmittance from Sensor to Target and from Sensor to Ground Surface, for Sensor Polar Angle of  $140^\circ$

shown in Fig. 25. For comparative purposes, the atmospheric transmittance, calculated by LOWTRAN 4, along the sensor's line-of-sight between the sensor and target, and between the sensor and ground surface, are shown in Fig. 26.

A comparison of the target radiance obtained for polar angles of  $60^\circ$  and  $140^\circ$  displays many similar features. In fact, the only significant difference between the two is the apparent decrease in the magnitude of the partial path radiance for  $140^\circ$  (Fig. 23). As described earlier, with respect to the path radiance results shown in Fig. 15, this phenomena is attributable to the strong relationship between the single-scattered path radiance and the peaked forward scattering characteristic of atmospheric aerosols. Similar results are found in the total path radiance shown in Figs. 19 and 24. In addition, the significant influence of uncollided ground emission upon the total background radiance is evident when comparing Figs. 19 and 24.

The wavelength-dependent contrast ratio is shown in Fig. 27 for the two specific problem configurations discussed. A positive value for the contrast ratio indicates that the target radiance is greater than the background, while for a negative value, the opposite relation holds. Once again, we must summarize that the contrast ratio is defined as the difference between the target and background radiance divided by the background (Eq. 45). Therefore, it is a quantity indicative of the strength of the target radiance relative to that of the background.

The effect of the absorption band between  $2150$  and  $2400\text{ cm}^{-1}$  is evident in both curves shown in Fig. 27. A ratio of near zero at  $2300$  and  $2350\text{ cm}^{-1}$  indicates that the radiative energy incident at the detector is due primarily to atmospheric emission of thermal radiation within the localized vicinity of the sensor (i.e. target  $\approx$  background). This premise is supported by a comparison of the results shown in Figs. 18-19 and 23-24. Large fluctuations are shown for a polar angle of  $60^\circ$  as the combined effects of target emission, path radiance, and atmospheric emission provide a complex radiative environment. However, the primary contributions by

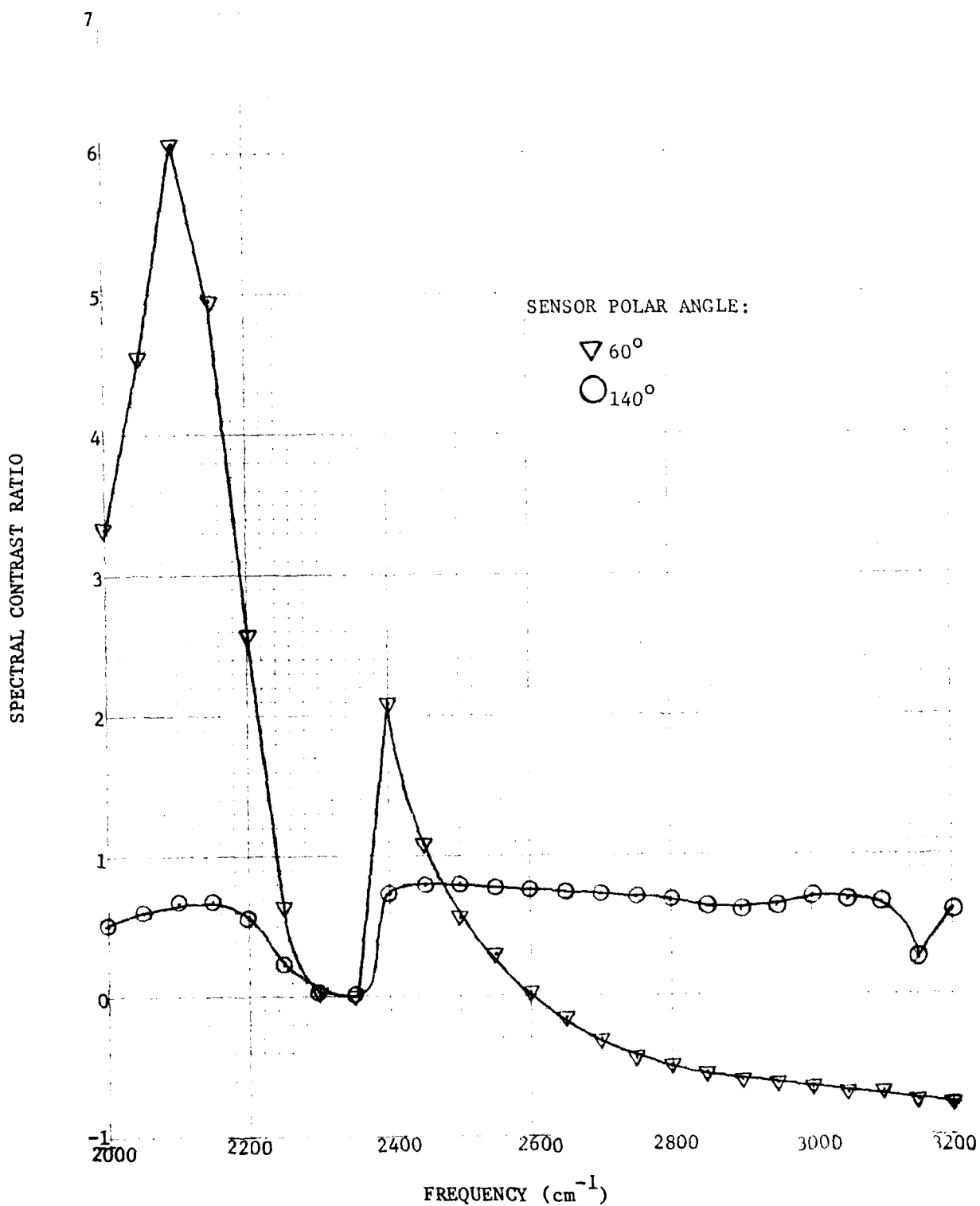


Fig. 27. Spectral Contrast Ratio for Sensor Polar Angles at  $60^\circ$  and  $140^\circ$

D-A101 307 RADIATION RESEARCH ASSOCIATES INC FORT WORTH TEX F/6 20/6  
E-O SENSOR SIGNAL RECOGNITION SIMULATION: COMPUTER CODE SPOT I.(U)  
OCT 78 C M LAMPLEY, W G BLATTNER F08606-77-C-0008  
,UNCLASSIFIED RRA-T7809 NL

202  
2040

END  
DATE  
7-81  
TIME  
DTIC

the uncollided target and ground emission to the radiances obtained for a polar angle of  $140^{\circ}$  result in a somewhat flat contrast ratio, outside of the absorption band.

A sample output from the SPOT computer code is shown in Figs. 28-37 for the example problem discussed in this section for a polar angle of  $60^{\circ}$ . The first page of the printed output (Fig. 28) provides a record of the input data as read by the program. All the parameters are presented, as described in TABLE IX, with the exception of those data which pertain directly to the definition of the single scattering phase function. In keeping with the authors' intention of providing a fast, efficient, user-oriented code, SPOT performs internal checks on several parameters in order to ascertain if the problem configuration defined by the user is consistent with the requirements of the program. The results from these internal checks are provided as diagnostic messages on the second page of the printed output as shown in Fig. 29. Page three of the printed output (Fig. 30) is a recapitulation of the input parameters used to define the basic attributes of the problem to be executed. In accordance with the spectral analysis performed by SPOT, various wavelength-dependent quantities are presented in Figs. 31-35 along with the respective wavelength ( $\mu\text{m}$ ) and corresponding frequency in wavenumbers ( $\text{cm}^{-1}$ ). Source intensities are shown on page four (Fig. 31) for the extraterrestrial source (sunlight or moonlight), target and ground surface. Note, the extraterrestrial source strength is obtained from the data described in section 3.2.1, whereas the target and ground source strength is defined by the product of the temperature-dependent blackbody function (Eq. 15) and the emissivity of the respective surface. Since for a polar angle of  $60^{\circ}$ , the sensor's line-of-sight does not intersect the ground surface, the source strength for the ground is defined to be zero. Each of the radiative components describing the target radiance are shown on page five (Fig. 32) along with the total target radiance. Target reflectance of uncollided sunlight is zero because the incident direct sunlight illuminates the back side of the target (Fig. 2). A similar description of the radiative components

for the background radiance is given on page six of the printed output (Fig. 33). Once again, there are no contributions to the background by the ground surface due to the orientation of the sensor's line-of-sight. The uncollided flux due to sunlight incident upon the detector is shown on page seven (Fig. 34). A recapitulation of the total target and background radiance is given on page eight of the printed output (Fig. 35) along with the contrast ratio. Page nine (Fig. 36) presents the spectral-integrated results for each of the components treated within the SPOT program. The final page of output (Fig. 37) indicates the successful termination of the problem.

$.100+01$	$.000$	$^2$	$.950+00$	$.295+03$	$^2$	$1$	$64$	$3$
$.600+02$								
$.000$	$.000$		$0$					
$.500-01$	$.000$		$0$					
$.100+01$	$.150+03$		$.900+02$	$.120+03$				
$.300+01$	$.600+02$		$.000$	$.200+01$				
$.200+04$	$.320+04$		$10$	$.300+01$				
$6006000$				$,000$				

Fig. 28. Page One of the SPOT Printed Output

RADIATION RESEARCH ASSOCIATES, INC. FORT WORTH, TEXAS  
SPOT -- PROBLEM NUMBER 6006000

90

SPOT DIAGNOSTIC MESSAGES FOLLOW:

1. SUNLIGHT ILLUMINATES BACK SIDE OF TARGET.

Fig. 29. Page Two of the SPOT Printed Output

RADIATION RESEARCH ASSOCIATES, INC. FORT WORTH, TEXAS  
SPOT -- PROBLEM NUMBER 6006000

DEFINITION OF CONTROL PARAMETERS FOLLOWS:

PARAMETER	VALUE	DESCRIPTION
ISORG	3	SUNLIGHT AND EMISSION
ITARG	2	TARGET REFLECTANCE / EMISSION
MODEL	6	1962 U.S. STANDARD
IHAZE	2	AEROSOL ATTENUATION INCLUDED (VIS= 3.0 KM)

Fig. 30. Page Three of the SPOT Printed Output

RADIATION RESEARCH ASSOCIATES, INC. FORT WORTH, TEXAS  
 SPOT -- PROBLEM NUMBER 6006000

WAVELENGTH (MICRONS)	WAVELENGTH (CM-1)	SOURCE INTENSITIES		TARGET SOURCE STRENGTH (WATTS M-2 MICRON-1 SR-1)	GROUND SOURCE STRENGTH (WATTS M-2 MICRON-1 SR-1)
		SOURCE	INTENSITIES		
5.0	0.0	0.0	0.0	0.0	0.0
4.8	0.0	0.0	0.0	0.0	0.0
4.6	0.0	0.0	0.0	0.0	0.0
4.4	0.0	0.0	0.0	0.0	0.0
4.2	0.0	0.0	0.0	0.0	0.0
4.0	0.0	0.0	0.0	0.0	0.0
3.8	0.0	0.0	0.0	0.0	0.0
3.6	0.0	0.0	0.0	0.0	0.0
3.4	0.0	0.0	0.0	0.0	0.0
3.2	0.0	0.0	0.0	0.0	0.0
3.0	0.0	0.0	0.0	0.0	0.0
2.8	0.0	0.0	0.0	0.0	0.0
2.6	0.0	0.0	0.0	0.0	0.0
2.4	0.0	0.0	0.0	0.0	0.0
2.2	0.0	0.0	0.0	0.0	0.0
2.0	0.0	0.0	0.0	0.0	0.0
1.8	0.0	0.0	0.0	0.0	0.0
1.6	0.0	0.0	0.0	0.0	0.0
1.4	0.0	0.0	0.0	0.0	0.0
1.2	0.0	0.0	0.0	0.0	0.0
1.0	0.0	0.0	0.0	0.0	0.0
0.8	0.0	0.0	0.0	0.0	0.0
0.6	0.0	0.0	0.0	0.0	0.0
0.4	0.0	0.0	0.0	0.0	0.0
0.2	0.0	0.0	0.0	0.0	0.0
0.0	0.0	0.0	0.0	0.0	0.0

Fig. 31. Page Four of the SPOT Printed Output

RADIATION RESEARCH ASSOCIATES, INC., FORT WORTH, TEXAS  
SPOT -- PROBLEM NUMBER 6006000

Fig. 32. Page Five of the SPOT Printed Output

RADIATION RESEARCH ASSOCIATES, INC. FORT WORTH, TEXAS  
SPOT -- PROBLEM NUMBER 60006000

COMPONENTS FOR BACKGROUND RADIANC

(WATTS M-2 MICRON-1 SR-1)

WAVELENGTH (MICRONS)	WAVENUMBER (CM <sup>-1</sup> )
-------------------------	-----------------------------------

WAVELLENGTH (MICRONS)	WAVENUMBER (CM <sup>-1</sup> )	GROUND EMISSION	GROUND REFLECTANCE	ATMOSPHERIC EMISSION	TOTAL PATH RADIANC	TOTAL BACKGROUND RADIANC
0.3	3333	0.0000	0.0000	0.0000	0.0000	0.0000
0.4	2500	0.0000	0.0000	0.0000	0.0000	0.0000
0.5	2000	0.0000	0.0000	0.0000	0.0000	0.0000
0.6	1667	0.0000	0.0000	0.0000	0.0000	0.0000
0.7	1429	0.0000	0.0000	0.0000	0.0000	0.0000
0.8	1176	0.0000	0.0000	0.0000	0.0000	0.0000
0.9	964	0.0000	0.0000	0.0000	0.0000	0.0000
1.0	800	0.0000	0.0000	0.0000	0.0000	0.0000
1.1	682	0.0000	0.0000	0.0000	0.0000	0.0000
1.2	583	0.0000	0.0000	0.0000	0.0000	0.0000
1.3	500	0.0000	0.0000	0.0000	0.0000	0.0000
1.4	433	0.0000	0.0000	0.0000	0.0000	0.0000
1.5	375	0.0000	0.0000	0.0000	0.0000	0.0000
1.6	324	0.0000	0.0000	0.0000	0.0000	0.0000
1.7	283	0.0000	0.0000	0.0000	0.0000	0.0000
1.8	250	0.0000	0.0000	0.0000	0.0000	0.0000
1.9	223	0.0000	0.0000	0.0000	0.0000	0.0000
2.0	200	0.0000	0.0000	0.0000	0.0000	0.0000
2.1	180	0.0000	0.0000	0.0000	0.0000	0.0000
2.2	162	0.0000	0.0000	0.0000	0.0000	0.0000
2.3	146	0.0000	0.0000	0.0000	0.0000	0.0000
2.4	132	0.0000	0.0000	0.0000	0.0000	0.0000
2.5	120	0.0000	0.0000	0.0000	0.0000	0.0000
2.6	109	0.0000	0.0000	0.0000	0.0000	0.0000
2.7	100	0.0000	0.0000	0.0000	0.0000	0.0000
2.8	92	0.0000	0.0000	0.0000	0.0000	0.0000
2.9	85	0.0000	0.0000	0.0000	0.0000	0.0000
3.0	79	0.0000	0.0000	0.0000	0.0000	0.0000
3.1	74	0.0000	0.0000	0.0000	0.0000	0.0000
3.2	70	0.0000	0.0000	0.0000	0.0000	0.0000
3.3	66	0.0000	0.0000	0.0000	0.0000	0.0000
3.4	63	0.0000	0.0000	0.0000	0.0000	0.0000
3.5	60	0.0000	0.0000	0.0000	0.0000	0.0000
3.6	57	0.0000	0.0000	0.0000	0.0000	0.0000
3.7	54	0.0000	0.0000	0.0000	0.0000	0.0000
3.8	51	0.0000	0.0000	0.0000	0.0000	0.0000
3.9	48	0.0000	0.0000	0.0000	0.0000	0.0000
4.0	45	0.0000	0.0000	0.0000	0.0000	0.0000
4.1	42	0.0000	0.0000	0.0000	0.0000	0.0000
4.2	40	0.0000	0.0000	0.0000	0.0000	0.0000
4.3	38	0.0000	0.0000	0.0000	0.0000	0.0000
4.4	36	0.0000	0.0000	0.0000	0.0000	0.0000
4.5	34	0.0000	0.0000	0.0000	0.0000	0.0000
4.6	32	0.0000	0.0000	0.0000	0.0000	0.0000
4.7	30	0.0000	0.0000	0.0000	0.0000	0.0000
4.8	28	0.0000	0.0000	0.0000	0.0000	0.0000
4.9	26	0.0000	0.0000	0.0000	0.0000	0.0000
5.0	25	0.0000	0.0000	0.0000	0.0000	0.0000
5.1	24	0.0000	0.0000	0.0000	0.0000	0.0000
5.2	23	0.0000	0.0000	0.0000	0.0000	0.0000
5.3	22	0.0000	0.0000	0.0000	0.0000	0.0000
5.4	21	0.0000	0.0000	0.0000	0.0000	0.0000
5.5	20	0.0000	0.0000	0.0000	0.0000	0.0000
5.6	19	0.0000	0.0000	0.0000	0.0000	0.0000
5.7	18	0.0000	0.0000	0.0000	0.0000	0.0000
5.8	17	0.0000	0.0000	0.0000	0.0000	0.0000
5.9	16	0.0000	0.0000	0.0000	0.0000	0.0000
6.0	15	0.0000	0.0000	0.0000	0.0000	0.0000
6.1	14	0.0000	0.0000	0.0000	0.0000	0.0000
6.2	13	0.0000	0.0000	0.0000	0.0000	0.0000
6.3	12	0.0000	0.0000	0.0000	0.0000	0.0000
6.4	11	0.0000	0.0000	0.0000	0.0000	0.0000
6.5	10	0.0000	0.0000	0.0000	0.0000	0.0000
6.6	9	0.0000	0.0000	0.0000	0.0000	0.0000
6.7	8	0.0000	0.0000	0.0000	0.0000	0.0000
6.8	7	0.0000	0.0000	0.0000	0.0000	0.0000
6.9	6	0.0000	0.0000	0.0000	0.0000	0.0000
7.0	5	0.0000	0.0000	0.0000	0.0000	0.0000
7.1	4	0.0000	0.0000	0.0000	0.0000	0.0000
7.2	3	0.0000	0.0000	0.0000	0.0000	0.0000
7.3	2	0.0000	0.0000	0.0000	0.0000	0.0000
7.4	1	0.0000	0.0000	0.0000	0.0000	0.0000
7.5	0	0.0000	0.0000	0.0000	0.0000	0.0000

Fig. 33. Page Six of the SPOT Printed Output

RADIATION RESEARCH ASSOCIATES, INC., FORT WORTH, TEXAS  
SPOT -- PROBLEM NUMBER 6006000

Fig. 34. Page Seven of the SPOT Printed Output

RADIATION RESEARCH ASSOCIATES, INC. FORT WORTH, TEXAS  
SPOT -- PROBLEM NUMBER 6006000

Fig. 35. Page Eight of the SPOT Printed Output

RADIATION RESEARCH ASSOCIATES, INC. FORT WORTH, TEXAS  
SPOT -- PROBLEM NUMBER 6006000

DETECTOR-RESPONSE WAVELENGTH-INTEGRATED

(WATTS M-2 SR-1)

TARGET EMISSION	1.0410+00
TARGET REFLECTANCE	0.0000
PARTIAL ATMOSPHERIC EMISSION	1.3223-01
PARTIAL PATH RADIANCE	1.0590-01
TOTAL PATH RADIANCE	1.2792+00
GROUND EMISSION	1.0000
GROUND REFLECTANCE	0.0000
TOTAL ATMOSPHERIC EMISSION	1.8738-01
TOTAL PATH RADIANCE	1.4954-01
TOTAL BACKGROUND RADIANCE	6.0234-01

\*\*\*\*\*

CONTRAST

5.9435-01

DIRECT SUNLIGHT

1.1923+01

(WATTS M-2)

Fig. 36. Page Nine of the SPOT Printed Output

RADIATION RESEARCH ASSOCIATES, INC. FORT WORTH, TEXAS  
SPOT -- PROBLEM NUMBER 6006000

\*\*\* END OF JOB \*\*\*

Fig. 37. Page Ten of the SPOT Printed Output

## V. UTILIZATION INSTRUCTIONS FOR THE SPOT COMPUTER CODE

In this section, information is presented which is pertinent to the utilization of the SPOT computer code on the UNIVAC-1108 computer system located at the White Sands Missile Range (WSMR). TABLE X provides the format of the problem control/description input data, which is to be read from logical unit number 5 (normally assigned to the card reader). The successful execution of a SPOT run requires the use of three external data files which reside on mass storage on the WSMR UNIVAC-1108 computer. These files contain, respectively, the atmospheric data base required by LOWTRAN 4, the refined extraterrestrial solar spectral irradiance, and the R.R.A. compilation of aerosol single-scattering phase functions. The data file 8206RRA\*LT4DATA consists of the input data for LOWTRAN 4, as described in Ref. 11, with the exception of the last four cards (referred to as CARD 1, 2, 3 and 4, respectively, in Ref. 11). This file must be assigned to logical unit number 7. The data file 8206RRA\*SOLARS contains the refined extraterrestrial solar spectral irradiance data base (section 3.2.1), and must be assigned to logical unit number 1. If the single scattered path radiance due to aerosol scattering is to be included (ISORC#2 and NLAM#0), wavelength-dependent sets of normalized phase functions are required input. The data file 8206RRA\*HAZESDATA contains the R.R.A. compilation of normalized aerosol phase functions (section 3.2.4). If the user chooses to insert his own set of phase functions, these data must adhere to the format of the R.R.A. set, which is given in TABLE XI.

The SPOT computer code resides on mass storage as the program file 8206RRA\*SPOT. Included in the program file are the symbolic Fortran elements and the relocatable (binary) elements for each routine. In addition, the absolute element 8206RRA\*SPOT.LOAD consists of the load module necessary to execute a SPOT problem. A sample run stream is shown in Fig. 38 for the batch execution of a typical SPOT problem on the WSMR UNIVAC-1108 computer system. For this problem, the R.R.A. data base (HAZESDATA) was included via logical unit number 3 (i.e., IUNIT=3 on card 1 of TABLE X). A temporary

file (LT4OUT.) has been assigned to logical unit number 2. During execution of a SPOT problem, calls to LOWTRAN 4 produce large amounts of intermediate output. This information is stored on unit 2 in a temporary file which will be discarded at the completion of the job. If the user requires the context of this information, the file could be assigned so that it would be catalogued and subsequently retained after the job termination. However, if single scattered path radiance is included in the SPOT calculations, caution should be exercised when retaining this file, because the amount of LOWTRAN 4 output may be excessive.

TABLE X. FORMAT OF THE INPUT DATA FOR THE SPOT COMPUTER CODE

Card	Format	Variable	Definition	Limit
1	7I10	ISORC	Source definition parameter: = 0 sunlight only 1 moonlight only 2 emission only 3 sunlight and emission 4 moonlight and emission	
		ITARG	Reflectance/emission definition parameter: = 0 background only 1 ground 2 target and ground	
		MODEL	Atmospheric model definition parameter: = 1 Tropical ( $15^{\circ}$ N) 2 Midlatitude Summer ( $45^{\circ}$ N, July) 3 Midlatitude Winter ( $45^{\circ}$ N, January) 4 Subarctic Summer ( $60^{\circ}$ N, July) 5 Subarctic Winter ( $60^{\circ}$ N, January) 6 1962 U.S. Standard Atmosphere	
		IHAZE	Option for defining aerosol attenuation: = 0 no aerosol attenuation included in the uncollided calculations 1 aerosol attenuation is included (VIS = 23 km if not specified) 2 aerosol attenuation is included (VIS = 5 km if not specified)	
		NLAM	Option for defining aerosol single scattering phase function: = 0 no aerosol attenuation included in the path radiance calculations < 0 read $ NLAM $ sets of wavelength-dependent user-defined average phase functions > 0 use the R.R.A.-defined data base of 38 wavelength-dependent average phase functions (HAZESDATA)	$\leq  38 $

TABLE X. (Continued)

Card	Format	Variable	Definition	Limit
		NANG	Number of angles for which the aerosol phase functions are to be input	$\leq 64$
		IUNIT	Logical unit number on which the aerosol phase functions reside	#1,2,5, 6,or 7
			If ISORC = 2 omit NLAM, NANG and IUNIT from card 1. If NLAM = 0 omit NANG and IUNIT from card 1. <u>If NLAM &gt; 0 omit NANG from card 1.</u>	
2	4E10.1	EM(1)	Emissivity of the ground surface	$0 \leq EM(1) \leq 1.0$
		TM(1)	Temperature of the ground surface (Kelvin)	
		EM(2)	Emissivity of the target surface	$0 \leq EM(2) \leq 1.0$
		TM(2)	Temperature of the target surface (Kelvin)	
			If ISORC < 2 omit card 2. <u>If ITARG &lt; 1 omit card 2.</u> <u>If ITARG = 1 omit EM(2) and TM(2) from card 2.</u>	
3	E10.1	ZENTH	Incident angle of sunlight or moonlight (degrees)	$\leq 90^{\circ}$
			<u>If ISORC = 2 omit card 3.</u>	
4	2E10.1, I10	A0(1)	Albedo coefficients for the ground surface, where $ALB = A0(1) + A1(1) \cdot COSBT$	
		A1(1)	Option for defining type of reflection distribution for the ground surface: = 0 Lambertian (cosine)	
		IALB(1)	1 isotropic	
			If ITARG < 1 omit card 4. <u>If ITARG = 2 repeat card 4 for the target surface.</u>	
5	4E10.1	RTARG	Slant range from receiver to target (KM)	
		COSX	Angle corresponding to the directional cosine of the target normal vector, with respect to the X-axis (degrees)	
		COSY	Angle corresponding to the directional cosine of the target normal vector, with respect to the Y-axis (degrees)	

TABLE X. (Continued)

Card	Format	Variable	Description	Limit
		COSZ	Angle corresponding to the directional cosine of the target normal vector, with respect to the Z-axis (degrees)	
<u>If ITARG ≤ 1 omit card 5.</u>				
6	4E10.1	ALT	Altitude of the receiver (KM)	
		THETA	Polar direction of the receiver's line-of-sight (degrees)	
		PHI	Azimuthal direction of the receiver's line-of-sight (degrees)	
		SANG2	Half-angle which defines the receiver's field-of-view for inclusion of uncollided sunlight or moonlight (degrees)	
<u>If ISORC = 2 omit SANG2 from card 6.</u>				
7	2E10.1, I10, 2E10.1	WAVN1	Initial frequency for spectral band of interest in wavenumbers (cm <sup>-1</sup> )	
		WAVN2	Final frequency for spectral band of interest in wavenumbers (cm <sup>-1</sup> )	
		IWAVE	Width of frequency increment (or step size) in units of five wavenumbers (5 cm <sup>-1</sup> )	
		VIS	Ground level meteorological range (KM)	
		PHASE	Phase angle for moonlight (degrees)	
<u>If ISORC = 0, 2 or 3 omit PHASE from card 7.</u>				
8	3X, I7	NPROB	Problem number	

TABLE XI. FORMAT OF THE AEROSOL PHASE FUNCTION DATA BASE

Card	Format	Variable	Definition	Limit
1	8E10.1	PCOS(I)	Scattering angles at which the aerosol single-scattering phase functions are to be defined, listed in ascending order with PCOS(1) = 0.0 and PCOS(NANG) = 180.0 (degrees)	I=1, NANG
2	E10.1	WLAM(N)	Wavelength at which the aerosol single-scattering phase function set is defined (microns)	
3	8E10.1	PDCO(N,I)	Average probability for aerosol scattering, i.e. the single-scattering phase function, defined for the wavelength WLAM(N) and scattering angle PCOS(I) in units of (sr <sup>-1</sup> )	I=1, NANG

Note: the card sequence 2 and 3 is repeated for each set of the wavelength-dependent aerosol single-scattering phase functions, i.e. N = 1, |NLAM|. If NLAM > 0, internal values of NANG = 64 and NLAM = 38, respectively, are used, indicative of the data contained within the R.R.A. data base HAZESDATA.

```
@ASG,A      8206RRA*SOLARS.  
@ASG,A      8206RRA*HAZESDATA.  
@ASG,A      8206RRA*LT4DATA.  
@USE       1.,8206RRA*SOLARS.  
@USE       3.,8206RRA*HAZESDATA.  
@USE       7.,8206RRA*LT4DATA.  
@ASG,T      LT4OUT.  
@USE       2.,LT4OUT.  
@ASG,A      8206RRA*SPOT.  
@XQT       8206RRA*SPOT.LOAD  
problem control/description input data  
(see Table X)  
@FIN
```

Fig. 38. Sample Run Stream for Execution of the SPOT Program  
on the WSMR UNIVAC-1108

## REFERENCES

1. Wells, M. B., D. G. Collins and W. G. M. Blättner, Optical Signature Simulation Studies, Radiation Research Associates, Inc., Technical Report RRA-T7801, 1977.
2. Collins, D. G., W. G. Blättner, M. B. Wells, and H. G. Horak, "Backward Monte Carlo Calculation of the Polarization Characteristics of the Radiation Emerging from Spherical Shell Atmospheres," Applied Optics 11, 2684, 1972.
3. Blättner, W. G. M., Utilization Instructions for BRITE, Radiation Research Associates, Inc., Research Note RRA-N7804, 1978.
4. Blättner, W. G. M., Multiple Scattering Effects on Radiation Signatures, paper presented at the First CSL Scientific Conference on Obscuration and Aerosol Research, Radiation Research Associates, Inc., Technical Memo RRA-M7802, 1978.
5. Blättner, W. G. M., C. M. Lampley and M. B. Wells, Scattering Effects on Radiation Signatures, Radiation Research Associates, Inc., Technical Report RRA-T7810, 1978.
6. Blättner, W. G. M., D. G. Collins and M. B. Wells, Computer Procedure for Calculating Light Scattering from Lasers, Radiation Research Associates, Inc., Final Report RRA-T7708, 1977.
7. Blättner, W. G. M. and J. A. Guinn, Jr., "A Generalized Geometry Monte Carlo Code," paper presented at the First CSL Scientific Conference on Obscuration and Aerosol Research, Radiation Research Associates, Inc., Technical Memo RRA-M7804, 1978.
8. Blättner, W. G. M., MIE Calculations for Aerosol Models, Radiation Research Associates, Inc., Report RRA-T7811, 1978.
9. Deirmendjian, D., "Scattering and Polarization Properties of Water Clouds and Hazes in the Visible and Infrared," Applied Optics 3, No. 2, 187-196, 1964.
10. Blättner, W.G.M., Utilization Instructions for Operation of the MIE-2 Program on IBM and UNIVAC Computers, Radiation Research Associates, Inc., Research Note RRA-N7703, 1977.
11. Selby, J. E. A., F. X. Kneizys, J. H. Chetwynd, Jr. and R. A. McClatchey, Atmospheric Transmittance/Radiance: Computer Code LOWTRAN 4, Air Force Geophysics Laboratory, Technical Report AFGL-TR-78-0053, 1978.

## REFERENCES (continued)

12. Siegel, R. and J. R. Howell, Thermal Radiation Heat Transfer, Volume 1, National Aeronautics and Space Administration, NASASP-164, 1968.
13. McClatchey, R. A., et. al., AFCRL Atmospheric Absorption Line Parameter Compilation, Air Force Cambridge Research Laboratories, Technical Report AFCRL-TR-73-0096, 1973.
14. Kasten, F., "Rayleigh-Cabannes Streuung in trockener Luft unter Berücksichtigung neuer Depolarisations-Messungen," Optik 27, 155-166, 1968.
15. Blättner, W. G. and M. B. Wells, Monte Carlo Studies of Sky Radiation, Radiation Research Associates, Inc., Report RRA-T7311, 1973.
16. Thekaekara, M. P., "Extraterrestrial Solar Spectrum, 3000-6100 Å at 1-Å Intervals," Applied Optics, Vol. 13, No. 3, 1974.
17. Turner, R. E., et. al., Natural and Artificial Illumination in Optically Thick Atmospheres, Environmental Research Institute of Michigan, Report No. 108300-4-F, 1975.
18. Bullrich, K., Ber. Deutsch. Wetterd., U. S. Zone No. 4, 1948.
19. Condron, T. P., J. J. Lovett, W. H. Barnes, L. Marcotte and R. Nadile, Gemini 7 Lunar Measurements, AFCRL-68-0438, 1948.
20. Lane, A. P. and W. M. Irvine, Astron. J. 78, No. 3, 1973.
21. U. S. Standard Atmosphere (1962), U. S. Government Printing Office, Washington, D. C.
22. McClatchey, R. A., R. W. Fenn, J. E. A. Selby, F. E. Volz and J. S. Garing, Optical Properties of the Atmosphere (Third Edition), Air Force Cambridge Research Laboratories, Technical Report AFCRL-72-0497, 1972.
23. Shettle, E. P. and R. W. Fenn, "Models of the Atmospheric Aerosols and Their Optical Properties," Optical Propagation in the Atmosphere, Advisory Group for Aerospace Research and Development, AGARD-CP-183, 1976.
24. Volz, F. E., "Infrared Refractive Index of Atmospheric Aerosol Substances," Appl. Opt. 11, 755-759, 1972.
25. Selby, J. E. A. and R. A. McClatchey, Atmospheric Transmittance from 0.25 to 28.5 μm: Computer Code LOWTRAN 2, AFCRL-TR-72-0745, 1972.

## REFERENCES (continued)

26. Selby, J. E. A. and R. A. McClatchey, Atmospheric Transmittance from 0.25 to 28.5  $\mu$ m: Computer Code LOWTRAN 3, AFCRL-TR-75-0255, 1975.
27. Selby, J. E. A., E. P. Shettle and R. A. McClatchey, Atmospheric Transmittance from 0.25 to 28.5  $\mu$ m: Supplement LOWTRAN 3B (1976), AFGL-TR-76-0258, 1976.